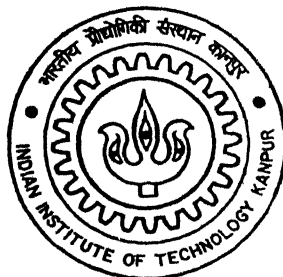# NUMERICAL STUDY OF A TURBULENT PREMIXED FLAME BASED DUMP COMBUSTOR

by

Vishak T

DEPARTMENT OF AEROSPACE ENGINEERING

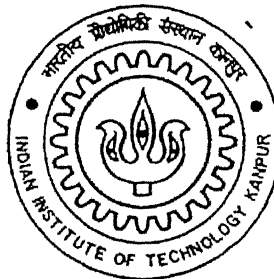## Indian Institute of Technology Kanpur

JANUARY, 2003

NUMERICAL STUDY OF A TURBULENT PREMIXED FLAME BASED DUMP COMBUSTOR

A Thesis Submitted

in Partial Fulfillment of the Requirements

for the Degree of

Master of Technology

by

VISHAK T

to the

DEPARTMENT OF AEROSPACE ENGINEERING
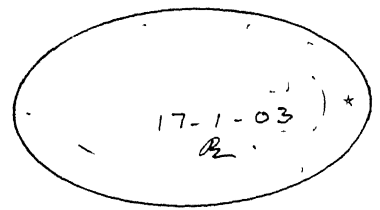
INDIAN INSTITUTE OF TECHNOLOGY, KANPUR

January 2003

CERTIFICATE

It is certified that the work contained in the thesis entitled **"Numerical Study Of A Turbulent Premixed Flame Based Dump Combustor"**, by **Vishak. T,** has been carried out under my supervision and this work has not been submitted elsewhere for a degree.

Dr. D. P. Mishra
Assistant Professor
Department of Aerospace Engineering
Indian Institute of Technology
Kanpur

January 2003

ABSTRACT

The present work is intended to investigate the flowfield inside a dump combustor, typical to Ramjet engine Dump combustors also finds applications in Spacecrafts, Gas turbine burners, Jet-stirred chemical reactors etc Numerical simulation, using the Standard k-ε turbulence model and Eddy Dissipation Concept (EDC) reaction model, of the flowfield inside a Dump combustor, both cold and reacting flow has been made to unravel the physics of sudden expansion flows. Influence of various flow parameters such as inlet Reynolds number, inlet turbulence intensity and geometric parameter such as expansion ratio on important flow quantities like axial velocity, radial velocity, static pressure, static temperature, turbulent kinetic energy and turbulent dissipation rate have been studied extensively. An exclusive study on reattachment length is also carried out. In the reacting flow case the effect of overall equivalence ratio is also investigated.

In the cold flow studies, the effect of inlet turbulence intensity is found to be the dominant parameter determining the flowfield. Flowfield is also dependent on the expansion ratio. In the cold flow case it is found that the inlet Reynolds number has little or no effect on the flow field. It is also found that the effect of turbulence intensity decrease with the increase in the expansion ratio. In the reacting flow case similar trends are observed, but the overall equivalence ratio also plays a vital role. Axial velocities and radial velocities in the reacting flow case are found to be much higher than that of cold flow case. At the end of potential core the reacting flow centerline axial velocity increases rapidly in contrast to the cold flow, where the centerline axial velocity decreases rapidly. In the case of reacting flow the potential core remains relatively cool due to the lack of combustion. The maximum and minimum radial velocities in the reacting flow case are found to be almost twice that of cold flow velocities. A huge reduction in reattachment length, between 40 to 60%, is found in the reacting flow case compared to the cold flow case. The reattachment length is found to be decreasing with the increase in the inlet turbulence intensity and with the decrease in expansion ratio. While predicting the temperature, adiabatic conditions have been assumed, so that adiabatic flame temperature will be the maximum temperature encountered in the flowfield. The flame length is found to be decreasing with the increase in the inlet turbulence level and with the increase in the expansion ratio. From the turbulent kinetic energy study for both the cold and reacting flow, it is found that for the reacting flow, the maximum kinetic energy is in the shear layer region as in the cold flow case. However, in the cold flow case the turbulent kinetic energy almost disappeared halfway through the combustor. But in the reacting flow case, a high value of turbulent kinetic energy is observed through out the length of the combustor. The detailed investigation of turbulent dissipation rate for both the cold and reacting flow reveals that the maximum turbulent diffusion occurs in the shear layer. But a noticeable difference is observed in the reacting flow case as compared to cold flow case is that same amount of significant turbulent dissipation occurs also near the wall, particularly near the exit of the combustor.

Dedicated to

My Parents

&

My Guide

ACKNOWLEDGEMENTS

CONTENTS

LIST OF FIGURES

LIST OF TABLES

NOMENCLATURE

Alphabets

A, B	Empirical constants in reaction modelling
C_p	Specific heat at constant pressure
$C_{1\epsilon}, C_{2\epsilon}, C_\mu$	Constants in k-ε turbulence model
d	Inlet diameter of the combustor
D	Internal diameter of the combustor
D_s	Diffusion coefficient for species s
D_H	Hydraulic diameter
e	Internal energy
E_t	Total energy per unit volume
f	Body force per unit mass
g	Acceleration due to gravity
h	Step height in the combustor
h'	Specific enthalpy
I	Turbulence Intensity
k	Kinetic energy of turbulence
M	Molecular Weight
n	Reaction number
N	Number of chemical species
N_R	Total number of reactions
p	Static pressure
r	Radial coordinate
R_u	Universal gas constant
T	Temperature
u, U	Axial velocity
u'	Instantaneous fluctuation velocity in the z direction
$\bar{u}$	Mean velocity in the z direction
U_0	Inlet axial velocity
v	Radial velocity

$\overset{\cdot}{v}'$	Instantaneous fluctuation velocity in the r direction
$\bar{v}$	Mean velocity in the r direction
V	Fluid velocity
V_s	Relative mass diffusion velocity component
x	Axial distance from the dump plane
Y_s	Mass concentration of species s
z	Axial coordinate

Greek Letters

δ	Kronecker delta function
Δh_f^0	Heat of formation
ε	Dissipation rate of turbulent kinetic energy
λ	Thermal conductivity
μ	Coefficient of viscosity
μ_t	Turbulent or eddy viscosity
ν'	Stoichiometric coefficient for reactant
ν''	Stoichiometric coefficient for product
Π	Stress tensor
ρ	Fluid density
σ_k	Turbulent Prandtl numbers for k
σ_ε	Turbulent Prandtl numbers for ε
τ	Viscous stress tensor
ϕ	Equivalence Ratio
φ	Dissipation function
ω_s	Rate of reaction

Subscripts

0	Inlet condition
i	Component in i direction
j	Component in j direction

k	Component in k direction
p	Constant pressure process
P	Product
r	Component in r direction
R	Reactant
s	Species
t	Turbulent property
z	Component in z direction
θ	Component in θ direction
∞	Ambient condition

Superscript

$'$	Fluctuating quantity

Abbreviation

LDV	Laser Doppler Velocimeter

Overbar

—	Time mean

CHAPTER 1

INTRODUCTION

In recent years, air breathing propulsion technology has been evolving to a mature stage, which can be used for missiles and space applications. The novel concept embodied in this advanced generation of strategic and tactical missiles is the integral rocket ramjet engine (Drewry, 1978). This missile propulsion concept requires the rocket booster and the ramjet engine to operate as a completely integrated system. After the rocket reaches a desirable flying speed, the nozzle and other components can be jettisoned. Then the ramjet engine is ignited to provide the necessary propulsion as the ram pressure achieves its optimal value. Thus, one is required to design a ramjet engine that can operate as a solid propellant rocket in its initial stage of flight. Since the ramjet combustor must initially serve as housing for the rocket propellant, it cannot be ideally configured in terms of fuel injection and combustor geometry for operation in the ramjet mode. The basic ramjet combustor configuration is the so-called sudden expansion dump combustor. In this type of combustor, fuel injection occurs in the air inlet duct upstream of the dump section. Besides this, the dump combustor is a generic configuration, which can be used to investigate and validate the new concept of combustion methodologies.

1.1 Dump Combustor

The dump (sudden expansion) combustor provides a suitable model for both experimental and numerical studies. This configuration models many important characteristics of practical combustion devices, including gas turbine burners and ramjet combustion chambers. A schematic of dump combustor is shown in Fig.1.1. As can be seen in the figure, sudden expansion of flow takes place as the flow enters larger pipe from the smaller pipe, which is important for better mixing of fuel and air and flame stabilization.

1.1.1 Sudden Expansion Flow

The flow through abrupt enlargements in a piping system provides a good example of one of the least explored of all the cases of separated flows, which has common

occurrence in many engineering applications. There have been many analytical and experimental studies reported in open literature. The turbulent flow field downstream of an axisymmetric sudden expansion is of significant importance from both a fundamental and a practical standpoint. As a result such kind of flows have been the focus of numerous analytical and experimental investigations. The configuration used consists of a circular duct having a sudden increase of its diameter. Such kind of flow with sudden expansion is an area of practical importance in various engineering applications such as jet-stirred chemical reactor, combustor and pipe networks. It is important to understand the flow structure as the formation of a recirculation region immediately downstream of the expansion causes the loss of pressure, which must be minimised. Since recirculation is used to ensure better mixing of fuel and oxidizer or to anchor the flame, a sound knowledge of the structure of the recirculation region and the reattachment length is of great importance to the designers of combustors. In the case of high-temperature gas flows the knowledge of the flow reattachment location is important because the peak heat release is found to be in the vicinity of the reattachment region, and this in turn, establishes the kind of heat transfer distribution downstream of reattachment in the redevelopment region and upstream in the separated flow region (Back and Roschke, 1972).
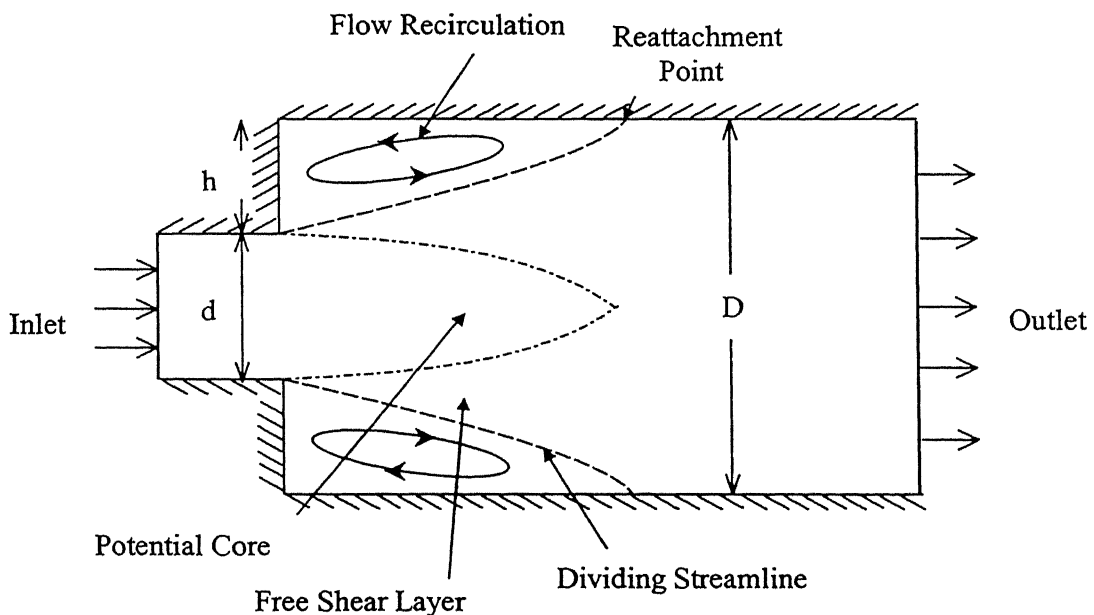
Fig.1.1 Representative schematic of flowfield inside the dump combustor

1.1.2 Combustor Flowfield

The flow field of a dump combustor is a complicated phenomenon characterized by turbulent mixing, flow separation, flow recirculation, shear flow reattachment and various other phenomena as shown in Fig.1.1. The flowfield just downstream of the dump plane can be divided by a dividing streamline (actually a dividing surface) into three main regions namely (i) the *flow recirculation region*, (ii) the *main flow region* (potential core) and (iii) a *free shear layer* in between with high turbulence levels Following reattachment of the shear layer at the wall, the flow proceeds to develop and, in the case of an axisymmetric sudden expansion, a fully developed turbulent pipe flow is eventually achieved.

The *potential core* is defined as a region of the flow where the inlet centerline velocity is maintained (Gabruk and Roe, 1994). The flow recirculation region just downstream of the dump section acts as the main flame holder (without physical interjection) by providing a low-velocity region and recirculation of hot combustion products and radical species into fresh reactants and thus provides primary flame stabilization (Gabruk and Roe, 1994). Additional flame stabilization can be obtained, with mechanical flame holding devices at the air inlet/combustor interface, at the expense of total pressure loss. In the recirculation region, the high adverse pressure gradient results in reverse flow and promotes instability and turbulence. Eddies produced in the recirculation region and in the neighborhood of the reattachment point can be considered as a highly concentrated source of turbulence. The high turbulent intensities in this region increase the mixing of the fuel and air, leading to nearly a complete combustion. Subsequent convection, diffusion, and decay of the flow structures developed in the recirculation zone and the main flow have a significant effect on the overall flow field of the combustor (Gabruk and Roe, 1994). The mean velocity profiles and turbulent parameters associated with the recirculation zone are primary factors governing the development of the overall flow field. The point at which the dividing streamline strikes the wall is called the *reattachment point*. It is the lateral growth or spread of the shear layer that determines the location of flow reattachment and thus the axial extent of the flow separation region (Back and Roschke, 1972).

3

Simple mixing theory provides no information on the details of the reattachment process, but only indicates the position at which the thickening shear layer would intersect the wall. The part of the shear layer that does not have enough momentum to overcome the pressure rise associated with reattachment is then turned rearward to form the reverse flow. Between the main flow and the reverse flow along the wall, a new shear layer starts to grow (Back and Roschke, 1972).

The *dividing streamline* is defined, as the line at which there is zero net flow between it and the wall [Moon and Rudinger (1977), Yang and Yu (1983)]. A mathematical expression for the dividing streamline can be written as

$$\int_{R_1}^{R} U r dr = 0 \qquad (1.1)$$

Where R_1 is the point through which the dividing streamline passes and R is the radius of the combustion chamber. U represents the axial velocity at R. This integration can be performed numerically at many axial locations within the recirculation zone, and the value of R_1 can be determined for which the integral vanishes. The dividing streamline at first runs nearly parallel to the wall and approaches it only in the vicinity of the stagnation point. The stagnation point is, where the dividing streamline reaches the wall of the tube. This dividing streamline is usually considered to be the boundary that separates the recirculation zone from the main flow.

There is very little combustion occurring in the high-speed core near the dump plane. The reaction zone originates at the step and propagates both radially inward and outward to form a hot, accelerated, annular region, which surrounds the potential core. The reacting case has a considerably shortened region of recirculation, associated with higher recirculation velocities (Gabruk and Roe, 1994). The *step height h*, the radius difference of the enlargement, is an important parameter for combustion chamber flow characterization. It determines how far the new shear layer that borders the reverse flow region spreads into the original shear layer. The inlet flow Reynolds number is another interesting parameter, which affects the flow structure in dump combustor (Yang and Yu, 1983). Another important parameter, which affects the flowfield inside the dump combustor is the *Overall Equivalence Ratio*, ϕ, which is defined as the ratio of stoichiometric fuel air ratio to the actual fuel air ratio. Recirculating flows are

4

characterized by the presence of reverse flow, which results in turbulent diffusive transport in all coordinate directions (Moon and Rudinger, 1977).

1.2 Need For Mathematical Modelling

It is quite clear from the previous section that the flowfield inside a dump combustor, in the engineering applications, is highly turbulent and reactive. The practical difficulty in the measurements of all the flow quantities of interest like turbulent kinetic energy, turbulent dissipation rate, and fluctuating temperature necessitate the need for mathematical modelling. Recently, the numerical techniques have been used to model reasonable complex flow situations, which has emerged as a powerful tool to understand the physics of the problem in more detail. While computational models facilitate the simulation of complex problems, it is to be borne in mind, however, that the accuracy of predictions will depend on the use of appropriate mathematical models. Continued improvement and use of suitable mathematical models will significantly reduce the time and cost of finding solutions for practical problems. As a result, the use of CFD codes by the engineering community has increased dramatically in the last few years. Important steps in numerical analysis are method of problem definition, problem solution, and problem analysis.

Successful prediction of unsteady, axisymmetric, turbulent, and recirculating flows in a dump combustor requires knowledge of the physical laws governing the transport, creation, and destruction of turbulence. This knowledge must be cast in mathematical form, and a scheme for solving the resultant differential equations must be written into a computer program. No practical numerical treatment can span all the time and length scales of turbulence, and the time-averaged equations, containing unknown convective correlations, must be solved (Moon and Rudinger, 1977). A solution of these non-linear equations is only possible where a turbulence model can be formulated which prescribes how these correlations are to be found. The accuracy with which turbulence parameters can be predicted is largely dependent upon the accuracy of these models. Calculation of turbulent flow fields involves modelling of the turbulence properties in the form of turbulent kinetic energy, an eddy viscosity, or some other model. Such models are derived on the basis of a hypothesis, such as Prandtl's "mixing length", but ultimately,

5

experimental data for mean velocity and turbulence parameters are needed to develop or test a model (Moon and Rudinger, 1977). Sets of partial differential equations, continuity, axial and transverse momentum, turbulence energy, and turbulence dissipation were simultaneously solved. Predictions made using these equations were brought into good agreement with the data taken from the recirculating flows under investigation by selection of appropriate "constants" in the models. Turbulence model coefficients are a major concern to the model's predictability. Using different model coefficients for free shear and wall shear flows, the existing turbulence model can predict satisfactorily more turbulent flows, including round jet and separation flows (Jaw and Chen, 1998). Although advances in large computers have led to the wide use of higher-order turbulence models to predict turbulent flows, there is still no unique turbulence model that can predict satisfactorily all turbulent flows. Numerical modelling of turbulent flows provides a cost-effective and time saving method of engineering design.

Modelling reacting flow is even more cumbersome process than turbulence modelling and the coupling between these two makes the turbulence reacting flow modelling more tedious one. In the reacting flow, which, we are going to deal with in the later part of this study, has to consider contribution of each species in the mixture. These aspects of turbulent reacting flow are still evolving to predict the flow structures well.

1.3 Concluding Remarks

In the present chapter a brief insight into the basic dump combustor geometry and the basic features of the flowfield is presented. It is quite clear that the flowfield inside a dump combustor, in the engineering applications, is highly turbulent and reactive. Many flow and geometrical parameters that might affect the flowfield is also discussed. The need for mathematical modelling is also addressed. In the following chapter, a brief overview of the works so far been done in this field by the previous researchers is given. The formulation of the governing equations and the modelling of the turbulent flow with and without reaction is described in the chapter following literature survey. The cold flow and the reacting flow studies have been treated separately in the last part of the study.

6

CHAPTER 2

LITERATURE SURVEY

Till mid seventies, the design and development of dump combustors were based on global parameters like chamber volume, mass flow rate, air fuel ratio and inlet temperature and pressure (Natarajan et al, 2000). Empirical correlations were used to develop combustors based on proven design concepts. Often these were found inadequate for arriving at optimal designs. Hence, the need for a more fundamental approach has been recognized and the demand for predictions of the flowfield, temperature and species concentrations in a combustor has been on the increase. The main features of interest in the flowfield of a dump combustor are the turbulent jet mixing, recirculatory flow, separation and reattachment, which play a vital role in determining combustion efficiency and flame stability (Natarajan et al, 2000). The literature survey presented below summarises some of the important findings of research works carried out on practical dump combustors and related aspects. For the sake of clarity, it has been divided into various subsections covering different aspects such as cold flow, reacting flow and numerical studies.

2.1 Cold Flow

In 1944, Kalinske studied experimentally sudden expansion pipe flow and found that within the 'potential core' the velocity profile was flat and the turbulent intensity was no higher than that in the upstream pipe. It was also found that this core rapidly disappeared within a few pipe diameters from the beginning of the enlargement.

In another interesting study, Lipstein (1962) conducted a series of experiments covering a wide range of expansion ratios (*expansion ratio* is defined as the ratio of the larger pipe diameter to the smaller pipe diameter), $\beta = 1.11$-3.33 and for Reynolds number, Re $= 2.6\times10^5$. The most interesting aspect of the study was the axial pressure gradient along the wall, which was initially negative for some distance beyond the enlargement and thereafter became positive. The sudden enlargement was found to have a flat static pressure profile in the radial direction, and an extensive recirculation zone. Along the

edge of the core and the recirculation zone, a region of high turbulent shear stress, with high velocity gradient, was found.

Zemanick and Dougall (1970) found that in the turbulent regime there is a relatively small influence of either Reynolds number or expansion ratio on the reattachment location in terms of step heights as inferred from heat transfer measurements.

Moon and Rudinger (1977) experimentally investigated the behaviour of recirculating flows typical of advanced air-breathing and rocket injectors. The recirculation, which occurred in the separation region behind the sudden expansion (β = 1.43), was investigated using a Laser Doppler Velocimeter (LDV). The flow at the inlet of the dump plane was fully developed. They have used a long pipe after sudden expansion, which, was connected to a vacuum pump. Flow symmetry was evaluated from the flow reattachment length. Their conclusion was that the location of flow reversal is practically independent of the flow velocity over the range from Reynolds number 1.9×10^5 to 4.2×10^5 based on the smaller tube diameter. Detailed measurements of mean axial velocities showed the reattachment length for turbulent flows to be between 6h and 9h (h = step height of the combustor). It is also noted that the velocity in the center of the tube decreases slowly with increasing distance from the step. It has been found that there is no flow reversal for x/h greater than about 8.3. A fully developed turbulent flow is re-established at a distance of about 26.7h from the step. But, since in their set-up the larger tube was connected to a vacuum pump, it is conjectured that the flowfield inside the chamber, might have affected.

Drewry (1978) performed experimentally cold flow studies pertinent to axisymmetric, sudden expansion dump combustor configurations for integral rocket ramjet missiles. His studies included surface flow visualization and measurements of total and static pressure at the wall. He carried out experiments with three interchangeable exhaust nozzles with β = 2.38. He found that it is possible to express the variation of recirculation zone length with step height with two linear relationships, where the reattachment length equals 7.9h and 9.2h for lower inlet flow Mach numbers of about 0.5 and for higher inlet flow Mach number near 0.9 respectively. The slight change in the dependency of recirculation zone length on step height is felt due to the influence of

inlet flow Reynolds number. The inlet Reynolds number (based on the inlet diameter) ranged from approximately 1.3×10^6 up to 2.2×10^6. From the wall static pressure distribution, it is clear that the position of maximum wall static pressure occurs well downstream of the flow reattachment region. From the radial profiles of total pressure, it was clear that there is large radial gradient in total pressure in the viscous shear layer region.

In 1979, flow past a downstream facing annular step was experimentally investigated in the Mach number range of 0.1 to 0.95 (Re = 3 - 20.3×10^5) by Kangovi and Page (1979). The approaching flow was steady and uniform. The maximum recirculation velocity was found to be about 0.2 times the free stream velocity. Their investigation showed that separation and reattachment considerably influence the recovery pressure. They also demonstrated that the full pressure recovery does not occur at the point of reattachment. Downstream of the step, the wall static pressure is practically constant up to a distance of 4h. This is followed by a rise in pressure, which is a characteristic of reattaching flows. The results of their measurements showed the reattachment point to be about 8h downstream of the step. In their experimental set-up inside the large pipe there was a center body, which was extended along the centerline, which certainly might have affected the flowfield inside the larger pipe. They confirmed the presence of a weak secondary separation point and its location was within one step height downstream of the step. This secondary separation region was very weak and appeared to be the result of the inability of the recirculating flow to negotiate a 90^0 turn as it approaches the back step from the downstream side.

Lu (1980) used LDV for the measurement of the turbulent airflow velocity along the centerline and radially, at certain cross sectional areas of a sudden expansion cylindrical tube ($\beta = 2$). In the beginning, the centerline velocity decreases slowly between the inlet and the downstream distance of x/h = 4. At a downstream distance of x/h = 16, the velocity profile becomes a fully developed one. He observed that inside the separation region, the fluid elements move in the opposite direction of the main flow. According to the study, the boundary layer reattachment for a sudden expansion flow should occur between a cross section of x/h = 2.5 and 7.5. In this experiment, the outlet has been connected to the vacuum cleaner, and at the outlet there is a sudden contraction

(terminated with a diameter which is same as the inlet tube diameter), which might have affected the flowfield inside the chamber.

In another study Yang and Yu (1983) experimentally investigated the characteristics and dynamics of an abruptly expanded flow in a model combustion followed by a nozzle for $Re = 6.4 \times 10^4$. From the experimental data of the mean velocities, and wall pressure distribution it was noticed that there is a slight decline in pressure after the enlargement, the relative minimum is located near $x/h = 2.3$, then a rapid rise in pressure follows. The zero crossing of pressure occurred at about 8.5 step heights. The reattachment length reported, 4.5h is shorter than expected, which is argued to be due to the presence of a short rapidly contracted nozzle following the sudden enlargement. The higher back pressure in their study definitely contributed to the shorter reattachment length. The potential core was estimated to be 2.72h in length. It should be noted that the maximum reverse velocity was located at about 2.3h. The magnitude of this maximum reverse velocity was about 10% of the inlet velocity and about 12% of the center velocity at the same location. The maximum radial velocity was found between $x = 4.1$ and $4.5h$, where the reattachment point was located. The radial velocity at these two points was about $0.31U_0$ (U_0 is the inlet centerline velocity).

So and Ahmed [So (1987), So and Ahmed (1988, 1989)] have conducted a series of experiments and argued that inlet turbulence has the greatest effect on decreasing the reattachment length. On the other hand, other parameters, such as inlet flow Reynolds number, expansion ratio etc. have little or no effect on reattachment length. Further, they argued that the effect of inlet geometry on reattachment length is shown to be significant but indirect, since the change of the reattachment length observed can be accounted for only by the change of the turbulence caused by the alteration of the geometry. Their inference was that the increase of the turbulence level decreases the reattachment length due to the energy supply to the separating shear layer from the high turbulence level.

Durret et al (1988) used a LDV to measure radial and axial flow in axisymmetric sudden expansion airflow. They made measurements in a sudden expansion test section with a diameter ratio of 1.9 and 2.7 at a Reynolds number of 8.4×10^4 based on inlet diameter. A convergent nozzle was used at the inlet. The primary objective of their study was to

examine the radial velocity behaviour. Radial velocity was more than an order of magnitude less than the axial velocity, except near the wall. A stream function contour map derived from the mean velocity data indicated that the reattachment occurred at x/h = 8.3 for expansion ratio of 1.9. They have clearly identified the existence of the secondary recirculation zone just below the sudden expansion. The secondary recirculation zone, where, the mean velocities are much lower than in the primary zone is seen to extend from x/h = 0 to 1.2, where the secondary reattachment point occurs

Gould et al (1990) were made simultaneous two-component LDV measurements in the incompressible turbulent flowfield following an axisymmetric sudden expansion. The production, convection, and diffusion of turbulent kinetic energy were computed directly from the experimental data using central differencing method. Velocity measurements on both sides of the centerline at x = 0.2h downstream of the dump plane indicated that the inlet profile was very symmetric. Results including circumferential static pressure measurements, LDV measurements across the entire test section, and integrated mass flux balances at a number of axial planes, all indicated axial symmetry throughout the flowfield.

2.2 Reacting Flow

Many studies have concentrated on isothermal (cold) flows through dump combustors because of the difficulties involved with taking velocity measurements in highly turbulent reacting flow fields.

Gabruk and Roe (1994) used a two-component LDV to measure mean and turbulent velocities in an axisymmetric dump combustor, in both reacting and nonreacting flows. The goal of their research effort was to provide an analysis of the effects of heat release on a turbulent flow field. Significant differences were observed between mean centerline velocities and the extent of the recirculation zones for the cold and reacting flows. They carried out experiments in a combustor using propane–air mixture at ϕ = 0.65 with an expansion ratio of 1.5, where, the inlet Reynolds number was 1.18×10^5. Inlet turbulence intensity was approximately 15%. The combustor terminated with a convergent nozzle, with a 60% area reduction. They found that heat release has little

effect on the mean centerline velocity for axial locations less than approximately 10h from the dump plane. This similarity between the reacting and cold flow velocities is due to the lack of combustion occurring in the high-speed potential core in the center of the flowfield. The end of the potential core is marked by a regional deceleration in the cold flow case and acceleration in the reacting flow case. Downstream of the nonreacting potential core, heat release has a significant effect in the center of the combustor flowfield. After x/h = 10, the mean axial velocities, for the reacting case begin to increase rapidly. The reacting case has a considerably shortened region of recirculation, associated with higher recirculation velocities. There is very little combustion occurring in the high-speed core near the dump plane. At axial locations greater than 10h, however, a rapid acceleration of the flow due to local energy release is evident, marking the propagation of the reaction to the centerline and the end of the potential core flow in the reacting case. At axial locations less than 4h from the dump plane, the high shear region between the potential core and the recirculation region can be clearly identified by the high velocity gradient. For the reacting flow the recirculation length is approximately 3.5h from the dump plane, opposed to 6.75h for the cold.

Gould et al (1994) made experimental measurements of velocity in a low-speed turbulent flow field (Re = 1.15×10^5) following an axisymmetric sudden expansion with and without combustion. They have selected a convergent inlet nozzle to provide a uniform inlet velocity profile. They conducted experiments with an expansion ratio of 2. Velocity measurements on both sides of the centerline and circumferential static pressure measurements indicated that the flow is axisymmetric. They have not mentioned about the inlet turbulence level, which could have resulted in better understanding of the flowfield. Comparisons of mean velocities, temperature distributions, and recirculation zone sizes have been made with and without combustion. A lean, completely premixed propane-air mixture, with an equivalence ratio of 0.5 was used for the reacting flow part of the study. They have used a long pipe after sudden expansion. The central core region (velocity) upstream of x/h = 5.0 in the reacting flow case was virtually unchanged from that of the cold flow case because the temperature in this region was near the inlet temperature. Higher mean axial velocities in the shear layer found in the reacting flow case can attributed partly due to volumetric expansion. At the downstream measurement location (x/h = 12), the reacting flow mean axial

velocity was found to be approximately 1.7 times greater than the cold flow mean velocity across the entire tube diameter. It is interesting to note that the reacting flow centerline velocity does not decay as rapidly as the cold flow centerline velocity does. The relatively low temperature on the centerline at all measurement locations in the reacting flow would suggest that this result is not due to volumetric expansion alone. A comparison of the axial momentum flux ($\int \rho u^2 r \, dr$) at x/h=5 and 12 indicates that the axial centerline pressure gradient in the reacting flow is approximately one-half that which exists in the cold flow, which may be the reason why the centerline velocity does not decay as rapidly in the reacting flow case. The increased velocity in the radially growing shear layer, which is due to heat release, tends to preserve the central core region. Mean temperature measurements show that the core region stays relatively cool and that the maximum temperatures are achieved in the recirculation zone and the developing boundary layer downstream of the reattachment point. These profiles indicate that the mean temperature gradient in the radial direction is positive through most of the shear layer. They summarised as the reacting flow mean axial velocities were higher due to heat release, and the recirculation zone was shorter and thinner than observed in the cold flow case.

2.3 Numerical study

A brief review of numerical studies made in the area of dump combustor and sudden expansion flows are presented in this section. Teyssandier and Wilson (1974) made an integral analysis of the type used to predict the flow of co-flowing jets and applied to the problem of a sudden enlargement in a pipe (Borda-Carnot expansion). This technique successfully predicted all the overall flow parameters of interest like reattachment lengths, pressure profile, etc. The analysis indicated that point of minimum pressure does not coincide with the location of the maximum return-flow velocity. Moving radially outward, a region of high turbulent shear exists which consists of both downstream flow and a portion of the recirculation eddy. They found that for the smaller expansion ratios the potential core might exist well beyond the reattachment point.

Moon and Rudinger (1977) used k-ε model to predict steady, axisymmetric, turbulent, isothermal and recirculating flows. These equations in two dimensions have been

13

written in finite difference form, and solved using a modified version of the SIMPLE (Semi-Implicit Method for Pressure-Linked Equations) computer program. The empirical coefficients contained in the turbulence model equations take the value recommended by Launder and Spalding (1972) based on computations of the free shear flows They concluded that the extent of the recirculation zone is practically independent of Reynolds Number, based on the diameter of the smaller tube, over the range 10^3 to 10^6. The reattachment length for turbulent flows is to be between 6 and 9h.

Gould et al (1990) employed k-ε turbulence model recommended by Launder and Spalding (1972) to compare their own isothermal experimental results (described in section 2.1). Agreement was good for mean axial velocities and turbulent kinetic energy, however the modelled turbulent kinetic energy was underpredicted in the region between the shear layer and the centerline of the flow giving lower values of turbulent kinetic energy downstream of the potential core than measured. Finally, their conclusion was that k-ε model does a very respectable job in modelling this particular flowfield.

The study of Jang (1991) is the first systematic paper on the variation of reattachment length with the variation of different flow parameters such as inlet Reynolds number (Re = 10500-138000), inlet turbulence intensity (I = 0.5-20%) and geometric parameter like expansion ratio (β = 1.47-3.00). He performed numerical calculation on the isothermal sudden expansion flows under axisymmetric geometry. Turbulence is modelled using the high Reynolds number version of the two-equation k-ε model for turbulence (Launder and Spalding, 1972). As recommended by Launder and Spalding (1972), the presence of the near wall viscous sublayer is resolved through the use of wall function. Most calculations performed for the uniform inlet velocity profile clearly showed that the reattachment length can be plotted on a single curve as a function of the turbulence intensity, regardless of the value of the Reynolds number and expansion ratio. This calculated trend confirmed that inlet centerline turbulence stands out as the most important over the Reynolds number and expansion ratio. However, a rather substantial disagreement between calculated and experimental data of reattachment length is observed especially for the region of low turbulence level less than 5%. In general, the calculation compared well with the experimental data for a high turbulence region

14

greater than 10%, in which the reattachment length is observed to be less sensitive to the change of the turbulence level.

The paper by Freitas (1995) summarizes the results of a series of five benchmark simulations, which were completed using commercial CFD codes. The objective was to identify the fundamental predictive capabilities of early CFD codes and turbulence models. The commercial CFD package FLUENT predicted the backward-facing step flow including reattachment length quite satisfactorily.

Gran et al (1997) performed computations of an axisymmetric bluff-body stabilized turbulent diffusion flame. The test case is simulated using standard k-ε turbulence model for high Reynolds number flows along with the use of wall functions near the solid surfaces. The Eddy Dissipation Concept (EDC) by Magnussen and Hjertager (1976), with a fast chemistry assumption has been used in this study. They have used a general-purpose computational fluid dynamics code, which is based on the finite volume concept and uses a nonorthogonal curvilinear computational mesh with collocated variable arrangement. The convective terms are discretized by the second-order upwind scheme and the SIMPLE algorithm finds the pressure field. For the combustion case, the k-ε model predicted blow out.

A calculation method has been developed by De Zilwa et al (2000) and used to represent isothermal flows downstream of plane symmetric expansions with dimensions and velocities encompassing both laminar and turbulent flows. The turbulent flow simulations made use of the k-ε turbulence model and provided a satisfactory representation of measurements, except in regions close to the wall and within the recirculation regions. The conservation equations were discretized by the third-order scheme, a second-order centred difference scheme was adopted for diffusive fluxes and the pressure field was solved with the Pressure Implicit with Splitting of Operators (PISO) algorithm. The turbulence model constants chosen are that suggested by Launder and Spalding (1972). The longer reattachment length was underestimated in their study. The k-ε model over predicted the generation of turbulent kinetic energy inside a separating shear layer and hence, its spreading rate, which results eventually in a shorter reattachment length, as, observed here. The discrepancies were attributed mainly to the

limitations of the k-ε model, particularly in the presence of streamline curvature and anisotropic turbulence

An overview of the second-order closure turbulence models is presented by Jaw and Chen (1998), in which they have studied various turbulence models available at present. It included k-ε -eddy viscosity model. However, their conclusion was that at the present time, there exists no unified turbulence model. Each model applies successfully to some turbulent flows, while it predicts unsatisfactory results for other flows, especially for flows that are very different from those for which the models were calibrated. Jaw and Chen (1998) numerically validated the capability k-ε model on predicting the flow behind a backward facing step. The k-ε model predicted the length of separation zone and the mean velocity profiles satisfactorily.

Reattachment length measurements and predictions made by previous researchers is summarised in Table.2.1. From the table, it can be observed that, even though all the researchers aim was same, i.e., to understand the flowfield inside the dump combustor, there is no systematic study has been carried out to find the influence of all the parameters on the flowfield. Some of the researchers have not taken care of inlet turbulence intensity at all, which is an important parameter governing the flowfield.

2.4 Objective Of Present Study

Although several attempts have been made to investigate the characteristics of dump combustor, there is still an incomplete understanding of the turbulence-combustion interaction process. Turbulent combustion is highly nonhomogeneous, involving large fluctuations in temperature, composition, density, and velocity. There also can be a strong interaction between the aerodynamic and heat release mechanisms. The objective of the present numerical study is to obtain further insight and fundamental understanding of the overall characteristics of this type of flowfield. Emphasis has been placed on the performance of detailed fluid dynamic studies using a basic dump combustor configuration, typical of those of current interest in the development of the integral rocket ramjet propulsion system.

Table.2.1 Summary of Reattachment length by several researchers

Sl. No.	Researchers	Year	Type of Study	Reattachment length, x/h	Expansion Ratio, D/d	Flow Conditions	
						Reynolds number, Re	Turbulence Intensity, I (%)
1	Back, L. H. and Roschke, E. J. [2]	1972	Experimental	8.50	2.6	0.05×10^5	Negligible
2	Moon, L. F. and Roodinger, G. [24]	1977	Experimental	8.31	1.43	$1.9 - 4.2 \times 10^5$	-
3	Drewry, J. E. [5]	1978	Experimental	7.90	1.54	14×10^5	-
				9.20		22×10^5	
4	Kangovi, S. and Page, R. H. [18]	1979	Experimental	8.00	1.3	$30 - 100 \times 10^5$	-
5	Lu, C. C [22]	1980	Experimental	2.50-7.50	2.00	$0.03 - 0.07 \times 10^5$	-
6	Yang, B. T. and Yu, M. H. [33]	1983	Experimental	4.50	2.69	0.64×10^5	14.5
7	So, R. M. C [28]	1987	Experimental	7.40	1.5	0.9×10^5	5.7
				5.40			13.7
				4.00			17.6
8	Durrett, R. P. et al. [6]	1988	Experimental	8.30	1.9	0.84×10^5	2.5
9	Gabruk, R. S. and Roe, L. A. [9]	1994	Experimental	6.75 (cold) 3.50 (hot)	1.50	1.18×10^5	15
10	Jang, D. S. [14]	1991	Numerical (k-ε model)	5.65	1.47	0.46×10^5	5
				4.65			10
				4.20			15
				6.50		0.92×10^5	2.75
				7.00	3.00	0.11×10^5	1
				5.00		0.32×10^5	14.6

17

Most of the numerical studies have concentrated on cold flows through dump combustors because of the difficulties involved with solving turbulent reacting flow fields No systematic calculation has been reported in the open literature to relate the length of reattachment with the important parameters such as inlet turbulence level, particularly for reacting flow case. Attempts have been made to study numerically the turbulent flow field following an axisymmetric sudden expansion with and without combustion Thus the purpose of this study is to understand the effects of important flow and geometrical parameters on the reattachment length by performing numerical calculation on the cold and reacting sudden expansion flows under axisymmetric geometry. Parametric calculations are performed in terms of three important parameters such as inlet turbulence level, Reynolds number and expansion ratio. The flowfield characteristics studied are axial velocity, radial velocity, static pressure, static temperature, turbulent kinetic energy and turbulent dissipation rate, which will be helpful in understanding the complicated flow conditions in a dump combustor.

2.5 Concluding Remarks

An exclusive study on the findings of research works carried out on practical dump combustors and related aspects was made in this chapter. It is found even though several attempts have been made to investigate the characteristics of dump combustor; there is still an incomplete understanding of the flowfield inside the same, particularly for the reacting flow case. There is no systematic study has been carried out to find the influence of all the parameters on the flowfield. In the next chapter cold flow analysis inside the dump combustor is presented.

CHAPTER 3

MATHEMATICAL FORMULATION

In this chapter a brief review of governing equations along with turbulence and reacting flow modelling is given. A close look at the boundary conditions and the solution techniques adopted in using FLUENT code is also made.

3.1 Governing Equations

3.1.1 Continuity Equation

The conservation of mass law applied to a fluid passing through an infinitesimal, fixed control volume yields the following equation of continuity (Anderson et al, 1984)

$$\frac{\partial \rho}{\partial t} + \nabla \cdot (\rho\, V) = 0 \tag{3.1}$$

where ρ is the fluid density and V is the fluid velocity. The first term in this equation represents the rate of increase of the density in the control volume and the second term represents the rate of mass flux passing out of the control surface (which surrounds the control volume) per unit volume. Equation (3.1) is the general form of the mass conservation equation and is valid for incompressible as well as compressible flows.

It is well understood from previous studies that the flow through dump combustors is highly axisymmetric in nature [Drewry (1978), Gould et al (1990, 1994)]. So in the numerical simulation, axisymmetric governing equations are solved.

For axisymmetric geometries, the continuity equation in cylindrical coordinates (r, z) is given by [Bird et al (1994), Ward-Smith (1980), Yuan (1967)]

$$\frac{\partial \rho}{\partial t} + \frac{\partial}{\partial r}(\rho\, v) + \frac{\rho\, v}{r} + \frac{\partial}{\partial z}(\rho\, u) = 0 \tag{3.2}$$

where r is the radial coordinate, z is the axial coordinate, v is the radial velocity and u is the axial velocity. Please note that this equation obeys conservation-law.

3.1.2 Momentum Equations

Newton's second law applied to a fluid passing through an infinitesimal, fixed control volume yields the following momentum equation (Anderson et al, 1984)

$$\rho \frac{DV}{Dt} = \rho \, f - \nabla p + \frac{\partial}{\partial x_j} \left[\mu \left(\frac{\partial u_i}{\partial x_j} + \frac{\partial u_j}{\partial x_i} \right) - \frac{2}{3} \delta_{ij} \mu \frac{\partial u_k}{\partial x_k} \right] \qquad (3.3)$$

or
$$\rho \frac{DV}{Dt} = \rho \, f - \nabla p + \frac{\partial}{\partial x_j} \left[\tau_{ij} \right] \qquad (i, j, k = 1, 2, 3) \qquad (3.4)$$

where τ_{ij} is the viscous stress tensor and δ_{ij} is the Kronecker delta function (δ_{ij} =1 if i = j and δ_{ij} = 0 if i ≠ j); u_1, u_2, u_3 represent the three components of the velocity vector V; x_1, x_2, x_3 represent the three components of the position vector. μ is the coefficient of viscosity and p is the static pressure.

The first term on the right-hand side of Equation (3.3) is the body force per unit volume. Body forces act at a distance and apply to the entire mass of the fluid. The most common body force is the gravitational force. In this case, the force per unit mass, f equals the acceleration due to gravity vector, g

$$\rho f = \rho g \qquad (3.5)$$

and
$$f = f_r \, \hat{r} + f_\theta \, \hat{\theta} + f_z \, \hat{z} \qquad (3.6)$$

where, f_r, f_θ and f_z are body forces in the r, θ and z directions respectively. $\hat{r}$, $\hat{\theta}$ and $\hat{z}$, are unit vectors in the respective directions.

The second and third term on the right-hand side of equation (3.3) represents the surface forces per unit volume. These forces are applied by the external stresses on the fluid element. The stresses consist of normal stresses and shearing stresses.

20

For axisymmetric geometries, neglecting the body forces, the radial and axial momentum conservation equations in cylindrical coordinates (r, z), respectively is given by [Ward-Smith (1980), Yuan (1967)]

$$\frac{\partial}{\partial t}(\rho v) + \frac{1}{r}\frac{\partial}{\partial r}(r\rho v v) + \frac{1}{r}\frac{\partial}{\partial z}(r\rho u v) = -\frac{\partial p}{\partial r}$$
(3.7)

$$+\frac{1}{r}\frac{\partial}{\partial r}\left[r\mu\left(2\frac{\partial v}{\partial r}-\frac{2}{3}\left(\frac{\partial v}{\partial r}+\frac{v}{r}+\frac{\partial u}{\partial z}\right)\right)\right]+\frac{\partial}{\partial z}\left[\mu\left(\frac{\partial u}{\partial r}+\frac{\partial v}{\partial z}\right)\right]$$

and
$$\frac{\partial}{\partial t}(\rho u) + \frac{1}{r}\frac{\partial}{\partial r}(r\rho v u) + \frac{1}{r}\frac{\partial}{\partial z}(r\rho u u) = -\frac{\partial p}{\partial z}$$
(3.8)

$$+\frac{1}{r}\frac{\partial}{\partial r}\left[r\mu\left(\frac{\partial u}{\partial r}+\frac{\partial v}{\partial z}\right)\right]+\frac{\partial}{\partial z}\left[\mu\left(2\frac{\partial u}{\partial z}-\frac{2}{3}\left(\frac{\partial v}{\partial r}+\frac{v}{r}+\frac{\partial u}{\partial z}\right)\right)\right]$$

3.1.3 Energy equation

The first law of thermodynamics applied to a fluid passing through an infinitesimal, fixed control volume yields the following energy equation (Anderson et al, 1984)

$$\frac{\partial E_t}{\partial t} + \nabla \cdot E_t V = \frac{\partial Q}{\partial t} - \nabla \cdot q + \rho f \cdot V + \nabla \cdot \left(\Pi_{ij} \cdot V\right)$$
(3.9)

where E_t is the total energy per unit volume given by

$$E_t = \rho\left(e + \frac{V^2}{2} + \text{potential energy} + \ldots\right)$$
(3.10)

$$V^2 = u^2 + v^2 + w^2$$
(3.11)

and Π_{ij} is the stress tensor given by

$$\Pi_{ij} = -p\delta_{ij} + \left[\mu\left(\frac{\partial u_i}{\partial x_j}+\frac{\partial u_j}{\partial x_i}\right)-\frac{2}{3}\delta_{ij}\mu\frac{\partial u_k}{\partial x_k}\right] \qquad (i, j, k=1, 2, 3) \qquad (3.12)$$

21

The first term on the left-hand side of the energy equation represents the rate of increase of total energy per unit volume in the control volume while the second term represents the rate of total energy lost by convection (per unit volume) through the control surface. The first term on the right-hand side of the equation is the rate of heat, Q, produced per unit volume by external agencies while the second term is the rate of heat lost by conduction (per unit volume) through the control surface The third term represents the work done on the control volume (per unit volume) by the body forces while the fourth term represents the work done on the control volume (per unit volume) by the surface forces.

If only internal energy (e) and kinetic energy are considered significant in equation (3.10), a useful variation of the original energy equation is obtained.

$$\rho \frac{De}{Dt} + p(\nabla.V) = \frac{\partial Q}{\partial t} - \nabla.q + \nabla.(\tau_{ij}.V) - (\nabla.\tau_{ij}).V \qquad (3\,13)$$

The last two terms in this equation can be combined into a single term since

$$\tau_{ij} \frac{\partial u_i}{\partial x_j} = \nabla.(\tau_{ij}.V) - (\nabla.\tau_{ij}).V \qquad (3.14)$$

This term is customarily called the *dissipation function*, φ and represents the heat equivalent of the rate at which mechanical energy is expended in the process of deformation of the fluid due to viscosity. Hence

$$\rho \frac{De}{Dt} + p(\nabla.V) = \frac{\partial Q}{\partial t} - \nabla.q + \varphi \qquad (3.15)$$

Using the definition of enthalpy

$$h' = e + \frac{p}{\rho} \qquad (3.16)$$

$$\rho \frac{Dh'}{Dt} = \frac{Dp}{Dt} + \frac{\partial Q}{\partial t} - \nabla.q + \varphi \qquad (3.17)$$

For axisymmetric geometries, the conservation form energy equations in cylindrical coordinates (r, z) for Newtonian fluids of constant ρ, μ and λ is given by [Bird et al (1994), Kuo (1986)]

$$\rho\, C_p \left(\frac{\partial T}{\partial t} + v \frac{\partial T}{\partial r} + u \frac{\partial T}{\partial z} \right) = \lambda \left[\frac{1}{r} \frac{\partial}{\partial r} \left(r \frac{\partial T}{\partial r} \right) + \frac{\partial^2 T}{\partial z^2} \right] \qquad (3.18)$$

$$+ 2\mu \left[\left(\frac{\partial v}{\partial r} \right)^2 + \left(\frac{v}{r} \right)^2 + \left(\frac{\partial u}{\partial z} \right)^2 \right] + \mu \left[\left(\frac{\partial u}{\partial r} + \frac{\partial v}{\partial z} \right)^2 \right]$$

where C_p is the specific heat at constant pressure, and λ is the thermal conductivity of the fluid.

3.2 Turbulence Modelling

Turbulent flows are characterized by fluctuating velocity fields. These fluctuations mix transported quantities such as momentum, energy, and species concentration, and cause the transported quantities to fluctuate as well. Since these fluctuations can be of small scale and high frequency, they are too computationally expensive to simulate directly in practical engineering calculations. Instead, the instantaneous (exact) governing equations can be time-averaged to remove the small scales, resulting in a modified set of equations that are computationally less expensive to solve.

3.2.1 Turbulent Continuity Equation

In turbulent flow, considering the fluctuations in flow properties, on time averaging, the continuity equation in axisymmetric condition becomes (Ward-Smith, 1980)

$$\frac{\partial \rho}{\partial t} + \frac{\partial}{\partial r} \left(\rho \bar{v} \right) + \frac{\rho \bar{v}}{r} + \frac{\partial}{\partial z} \left(\rho \bar{u} \right) = 0 \qquad (3.19)$$

where velocity component along   r-direction $v = \bar{v} + v'$

z-direction $u = \bar{u} + u'$ (3.20)

$\bar{v}$ and $\bar{u}$ represents time averaged mean velocities in the r and z directions respectively, whereas, v' and u' denotes instantaneous fluctuation velocities in the r and z direction respectively.

3.2.2 Turbulent Momentum Equations

In turbulent flow case, the Navier-Stokes equation becomes,

$$\frac{\partial}{\partial t}\left(\rho\,\overline{v}\right)+\frac{1}{r}\frac{\partial}{\partial r}\left(r\,\rho\left(\overline{v}^2+\overline{v'^2}\right)\right)+\frac{1}{r}\frac{\partial}{\partial z}\left(r\,\rho\left(\overline{uv}+\overline{u'v'}\right)\right)=-\frac{\partial p}{\partial r} \tag{3.21}$$

$$+\frac{1}{r}\frac{\partial}{\partial r}\left[r\,\mu\left(2\frac{\partial\overline{v}}{\partial r}-\frac{2}{3}\left(\frac{\partial\overline{v}}{\partial r}+\frac{\overline{v}}{r}+\frac{\partial\overline{u}}{\partial z}\right)\right)\right]+\frac{\partial}{\partial z}\left[\mu\left(\frac{\partial\overline{u}}{\partial r}+\frac{\partial\overline{v}}{\partial z}\right)\right]$$

and
$$\frac{\partial}{\partial t}\left(\rho\,\overline{u}\right)+\frac{1}{r}\frac{\partial}{\partial r}\left(r\,\rho\left(\overline{vu}+\overline{v'u'}\right)\right)+\frac{1}{r}\frac{\partial}{\partial z}\left(r\,\rho\left(\overline{u}^2+\overline{u'^2}\right)\right)=-\frac{\partial p}{\partial z} \tag{3 22}$$

$$+\frac{1}{r}\frac{\partial}{\partial r}\left[r\,\mu\left(\frac{\partial\overline{u}}{\partial r}+\frac{\partial\overline{v}}{\partial z}\right)\right]+\frac{\partial}{\partial z}\left[\mu\left(2\frac{\partial\overline{u}}{\partial z}-\frac{2}{3}\left(\frac{\partial\overline{v}}{\partial r}+\frac{\overline{v}}{r}+\frac{\partial\overline{u}}{\partial z}\right)\right)\right]$$

These are time smoothed momentum equations in axisymmetric cylindrical coordinates, radial and axial directions respectively, under the conditions unsteady, compressible, variable viscosity and Newtonian fluid. Here $\overline{v'^2}$, $\overline{u'^2}$, $\overline{u'v'}$ and $\overline{v'u'}$ are the components of the turbulent momentum flux and they are generally referred to as the *Reynolds Stresses* [Anderson et al (1984), Yuan (1967)].

However, the modified equations contain additional unknown variables, and turbulence models are needed to determine these variables in terms of known quantities. Addition terms that appear in equation (3.21) and equation (3.22) compared to terms in equation (3.7) and (3.8) represent the effect of turbulence. These Reynolds stresses must be modeled in order to close equations (3.21) and (3.22). A detailed description on turbulence models is made in studies of Jaw and Chen (1998).

A common method employs the Boussinesq (1877) hypothesis (Anderson et al, 1984) to relate the Reynolds stresses to the mean velocity gradients. For the general Reynolds stress tensor, the Boussinesq assumption gives

24

$$-\rho \overline{u_i' u_j'} = \mu_t \left(\frac{\partial u_i}{\partial x_j} + \frac{\partial u_j}{\partial x_i} \right) - \frac{2}{3} \left(\rho k + \mu_t \frac{\partial u_k}{\partial x_k} \right) \delta_{ij} \qquad (3.23)$$

where μ_t is the turbulent or eddy viscosity and k is the kinetic energy of turbulence, expressed as

$$k = \frac{\overline{u_i' u_i'}}{2} \qquad (3.24)$$

Knowing the eddy viscosity allows one to estimate the unknown turbulent stresses in each of the conservation of momentum equations and therefore close the problem. The disadvantage of the Boussinesq hypothesis as presented is that it assumes μ_t is an isotropic scalar quantity, which is not strictly true. At present, one of the most popular models for predicting turbulent flows is the second order closure turbulent model. In general, these models involve two turbulence quantities. One is the turbulent kinetic energy and the other is a quantity related to the dissipation rate of turbulent kinetic energy. Among these models, the k-ε model is the most frequently adopted one mainly because ε itself appears in the k equation and the exact ε equation can be derived from Navier-Stokes equation. Here ε is the dissipation rate of turbulent kinetic energy.

3.2.3 The Standard k-ε Model

The Boussinesq hypothesis is used in the k- ε model. The advantage of this approach is the relatively low computational cost associated with the computation of the turbulent viscosity, μ_t. In the case of the k-ε model, two additional transport equations, one for the turbulence kinetic energy, k, and other one for the turbulence dissipation rate, ε, are solved, and μ_t is computed as a function of k and ε. The k-ε model has become the workhorse of practical engineering flow calculations in the time, since it was proposed by Launder and Spalding (1972). Robustness, economy, and reasonable accuracy for a wide range of turbulent flows explain its popularity in industrial flow and heat transfer simulations. In the derivation of the k-ε model, it was assumed that the flow is fully turbulent, and the effects of molecular viscosity are negligible. The standard k-ε model is therefore valid only for fully turbulent flows.

The turbulence kinetic energy, k, and its rate of dissipation, ε, are obtained from the following transport equations (Launder and Spalding, 1972) respectively

$$\frac{\partial}{\partial t}(\rho k) + \frac{\partial}{\partial x_i}(\rho k u_i) = \frac{\partial}{\partial x_j}\left[\left(\mu + \frac{\mu_t}{\sigma_k}\right)\frac{\partial k}{\partial x_j}\right] - \rho\overline{u_i'u_j'}\frac{\partial u_j}{\partial x_i} - \rho\varepsilon \qquad (3.25)$$

$$\frac{\partial}{\partial t}(\rho\varepsilon) + \frac{\partial}{\partial x_i}(\rho\varepsilon u_i) = \frac{\partial}{\partial x_j}\left[\left(\mu + \frac{\mu_t}{\sigma_\varepsilon}\right)\frac{\partial\varepsilon}{\partial x_j}\right] - C_{1\varepsilon}\frac{\varepsilon}{k}\rho\overline{u_i'u_j'}\frac{\partial u_j}{\partial x_i} - C_{2\varepsilon}\rho\frac{\varepsilon^2}{k} \qquad (3.26)$$

In k equation, the second term on RHS represents the generation of turbulence kinetic energy due to the mean velocity gradients. $C_{1\varepsilon}$ and $C_{2\varepsilon}$ are constants. σ_k and σ_ε are the turbulent Prandtl numbers for k and ε, respectively.

3.2.4 The Turbulent Viscosity

The "eddy" or turbulent viscosity, μ_t, is computed by combining k and ε as follows

$$\mu_t = \rho\, C_\mu \frac{k^2}{\varepsilon} \qquad (3.27)$$

where C_μ is a constant. The model constants $C_{1\varepsilon}$, $C_{2\varepsilon}$, C_μ, σ_k and σ_ε have the following values as recommended by Launder and Spalding (1972).

$$C_{1\varepsilon}=1.44,\; C_{2\varepsilon}=1.92,\; C_\mu=0.09,\; \sigma_k=1.0 \text{ and } \sigma_\varepsilon=1.3$$

3.3 Reacting Flow Modelling

3.3.1 Species Transport Equations

For a multi component system the equation of continuity for each species in the mixture is needed to be solved. The concentration of the various species in a multi component system can be expressed as *Mass Fraction*, $Y_s = \rho_s / \rho$, which is the mass concentration

of species s divided by the total mass density of the solution. Applying Fick's Law of mass diffusion, equation of continuity for the s th species, for axisymmetric geometry, in cylindrical coordinates becomes

$$\left(\frac{\partial(\rho Y_s)}{\partial t} + u\frac{\partial(\rho Y_s)}{\partial z} + v\frac{\partial(\rho Y_s)}{\partial r} \right) - \frac{1}{r}\frac{\partial}{\partial r}\left(rD_s\frac{\partial(\rho Y_s)}{\partial r} \right) - \frac{\partial}{\partial z}\left(D_s\frac{\partial(\rho Y_s)}{\partial z} \right) = \omega_s$$

(3 28)

Here ω_s is the rate at which species s is produced by chemical reaction within the mixture considered. D_s is the diffusion coefficient for species s in the mixture. The second and third terms of the above equation represents diffusion flux terms that arises due to concentration gradient. ω_s is needed to be modelled to solve the individual species continuity equations.

The *Eddy Dissipation Model* suggested by Magnussen and Hjertager (1976) is used to model the rate of reaction ω_s, which for the n th reaction is given by the smaller (i.e., limiting value) of the two expressions below

$$\omega_{s,n} = v'_{s,n} M_s A\rho \frac{\varepsilon}{k} \frac{Y_R}{v'_{R,n}M_R}$$

(3.29)

$$\omega_{s,n} = v'_{s,n} M_s AB\rho \frac{\varepsilon}{k} \frac{\sum_P Y_P}{\sum_s^N v''_{s,n}M_s}$$

(3.30)

The eddy-dissipation model relates the rate of reaction to the rate of dissipation of the reactant- and product- containing eddies. k/ε represents the time scale of the turbulent eddies following the eddy-dissipation model of Spalding (1970). This model is useful for prediction of premixed reacting flows.

Then, the source of chemical species s due to reaction, ω_s, is computed as the sum of the reaction sources over the N_R reactions that the species may participate in

$$\omega_s = M_s \sum_{n=1}^{N_R} \omega_{s,n}$$

(3.31)

where M_s = The molecular weight of species s

27

$\omega_{s,n}$ = The molar rate of creation/destruction of species s for the n th reaction

N   = Number of chemical species

k   = Turbulent kinetic energy

ε   = Turbulent dissipation rate

$\nu'_{s,n}$ = Stoichiometric coefficient for reactant s in n^{th} reaction

$\nu''_{s,n}$ = Stoichiometric coefficient for product s in n^{th} reaction

A   = Empirical constant equal to 4.0

B   = Empirical constant equal to 0.5

Y_P = Mass fraction of any product species, P

Y_R = Mass fraction of a particular reactant, R

The ideal gas equation states that (Kuo, 1986)

$$p = \rho \, R_u \, T \sum_{s=1}^{N} \frac{Y_s}{M_s} \qquad (3.32)$$

where R_u is the universal Gas constant, 8.314 kJ/(kmol.K)

3.3.2 Energy Equation

For a multi component system, considering the body forces, acting on each species, f_s the energy equation becomes (Kuo, 1986)

$$\rho \frac{Dh'}{Dt} - \frac{\partial p}{\partial t} = \frac{\partial(u_i \tau_{ij})}{\partial x_j} + \frac{\partial Q}{\partial t} - \nabla.q + \rho \sum_{s=1}^{N} Y_s \, f_s.(u + V_s) \qquad (3.33)$$

where, the last term in the above equation represents the body force work of s th species. h' is the total enthalpy and V_s is the relative mass diffusion velocity component.

For a multi component system, for axisymmetric geometries, the conservation form energy equations in cylindrical coordinates (r, z) is given by (Kuo, 1986)

$$C_p \left(\frac{\partial(\rho T)}{\partial t} + v\frac{\partial(\rho T)}{\partial r} + u\frac{\partial(\rho T)}{\partial z} \right) - \left(\frac{\partial p}{\partial t} + v\frac{\partial p}{\partial r} + u\frac{\partial p}{\partial z} \right) = \lambda \left[\frac{1}{r}\frac{\partial}{\partial r}\left(r\frac{\partial T}{\partial r} \right) + \frac{\partial^2 T}{\partial z^2} \right]$$

$$-\sum_{s=1}^{N} \omega_s \Delta h_{f,s}^0 - \left[\frac{1}{r}\frac{\partial}{\partial r}\left(r\rho T\sum_{s=1}^{N} C_{p,s} Y_s v_s \right) + \frac{\partial}{\partial z}\left(\rho T\sum_{s=1}^{N} C_{p,s} Y_s u_s \right) \right]$$

$$+2\mu \left[\left(\frac{\partial v}{\partial r} \right)^2 + \left(\frac{v}{r} \right)^2 + \left(\frac{\partial u}{\partial z} \right)^2 \right] + \mu \left[\left(\frac{\partial u}{\partial r} + \frac{\partial v}{\partial z} \right)^2 \right]$$

$$-\frac{2}{3}\mu \left[\left(\frac{1}{r}\frac{\partial}{\partial r}(rv) + \frac{\partial u}{\partial z} \right)^2 \right] + \rho \sum_{s=1}^{N} Y_s \left(f_{s,r} v_s + f_{s,z} u_s \right)$$

$$(3.34)$$

where $\Delta h_{f,s}^0$ is the heat of formation of species s. λ is the thermal conductivity.

For the turbulent reacting flow, energy equation takes the form

$$C_p \left(\frac{\partial(\rho T)}{\partial t} + \bar{v}\frac{\partial(\rho T)}{\partial r} + \bar{u}\frac{\partial(\rho T)}{\partial z} \right) - \left(\frac{\partial p}{\partial t} + \bar{v}\frac{\partial p}{\partial r} + \bar{u}\frac{\partial p}{\partial z} \right) = \lambda \left[\frac{1}{r}\frac{\partial}{\partial r}\left(r\frac{\partial T}{\partial r} \right) + \frac{\partial^2 T}{\partial z^2} \right]$$

$$-\sum_{s=1}^{N} \omega_s \Delta h_{f,s}^0 - \left[\frac{1}{r}\frac{\partial}{\partial r}\left(r\rho T\sum_{s=1}^{N} C_{p,s} Y_s \overline{v_s} \right) + \frac{\partial}{\partial z}\left(\rho T\sum_{s=1}^{N} C_{p,s} Y_s \overline{u_s} \right) \right]$$

$$+2\mu \left[\left(\frac{\partial \bar{v}}{\partial r} \right)^2 + \left(\frac{\bar{v}}{r} \right)^2 + \left(\frac{\overline{v'^2}}{r^2} \right) + \left(\frac{\partial \bar{u}}{\partial z} \right)^2 \right] + \mu \left[\left(\frac{\partial \bar{u}}{\partial r} + \frac{\partial \bar{v}}{\partial z} \right)^2 \right]$$

$$-\frac{2}{3}\mu \left[\left(\frac{1}{r}\frac{\partial}{\partial r}(r\bar{v}) + \frac{\partial \bar{u}}{\partial z} \right)^2 \right] + \rho \sum_{s=1}^{N} Y_s \left(f_{s,r} \overline{v_s} + f_{s,z} \overline{u_s} \right)$$

$$(3.35)$$

Solving an axisymmetric turbulent reacting flow problem needs the solution of, one global continuity equation, two momentum equations, one energy equation, N-1 species transport equations, one equation of state and one equation relating all Y_s.

$$\sum_{s=1}^{N} Y_s = 1 \qquad\qquad (3.36)$$
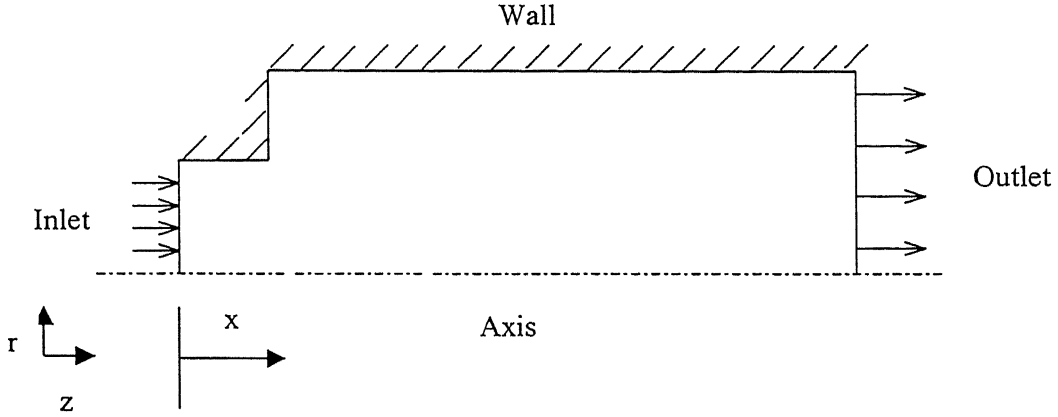
29

3.4 Boundary Conditions

Fig.3.1 Axisymmetric geometry and boundaries

To complete the physical problem specification, boundary conditions must be supplied on each boundary segment of the flow domain. These usually belong to one of the following types (Ghoshdastidar, 1998).

1. The values of the dependent variables are specified at the boundaries (Dirichlet condition).
2. The derivative of the dependent variable is given as a constant or as a function of the independent variable on one boundary (Neumann condition).
3. The derivative of the dependent variable is given as a function of the dependent variable on the boundary (Robbins condition).

The geometry used in this study is shown in Fig.3.1. Axisymmetric configuration is considered. A detailed description of the boundary conditions applied is given below.

1. At the combustor inlet

$$u = U_0$$
$$v = 0$$
$$p = P_\infty \qquad\qquad (3.37)$$
$$T = T_\infty$$

30

2. On the wall, the no-slip condition (u = v = 0) is specified on velocity along with

$$\frac{\partial p}{\partial n} = 0 \qquad (3.38)$$

and adiabatic wall condition

$$\frac{\partial T}{\partial n} = 0 \qquad (3.39)$$

3. Along the axis (Axisymmety),

$$\frac{\partial u}{\partial r} = \frac{\partial p}{\partial r} = 0 \qquad (3.40)$$

$$v = 0$$

4. Outflow boundary condition is applied at the combustor outlet. No boundary condition information is needed at an outflow boundary (Patankar, 1980), where the fluid leaves the calculation domain. The code extrapolates the required information from the interior. The outflow boundary condition is obeyed in fully developed flows where the diffusion fluxes for all flow variables in the exit direction are considered to be zero.

Also at the flow inlet, turbulence level is specified in terms of Percentage Turbulence intensity, I and Hydraulic diameter, D_H. The relationship between the turbulent kinetic energy, k, and turbulence intensity, I, is given by (FLUENT 5 Users Guide, 1998)

$$k = \frac{3}{2}\left(u_{avg}I\right)^2 \quad \text{where} \quad I = \frac{\sqrt{\frac{1}{2}\left(\overline{u'^2} + \overline{v'^2}\right)}}{u_{avg}} \qquad (3.41)$$

where u_{avg} is the mean flow velocity.

The relationship between turbulent dissipation rate, ε and Hydraulic diameter is given by

$$\varepsilon = C_{\mu}^{\frac{3}{4}} \frac{k^{\frac{3}{2}}}{D_H}$$ (3.42)

where C_{μ} is an empirical constant specified in the turbulence model (approximately 0.09). In reacting flow case *mass fractions of each individual species* should be mentioned at the inlet.

3.5 Numerical Simulation

3.5.1 Description of the Solver

The governing equations along with the turbulent-reaction modelling equations have been solved using FLUENT flow solver (Version 5.5, Fluent Inc., 1998). All the calculations were carried out in SUN Ultra Wok Station with UltraSPARC-IIi 360 MHz Processors. FLUENT is a state-of-the-art computer program for modelling fluid flow and heat transfer in complex geometries. The software provides a two level interaction with the user through the pre-processor known as GAMBIT and the main module of FLUENT. The required geometry and the mesh (grid) generation can be done using GAMBIT 2.0. Once a grid has been read into FLUENT, all the remaining operations are performed within the solver. These include setting boundary conditions, setting physical models, defining fluid properties, executing the solution, and viewing and post processing the results.

FLUENT provides comprehensive modelling capabilities for a wide range of incompressible and compressible, laminar and turbulent fluid flow problems. Steady state or transient analysis can be performed. In FLUENT, a broad range of mathematical models for transport phenomena (like heat transfer and chemical reactions) is combined with the ability to model complex geometries. Robust and accurate turbulence models are a vital component of the FLUENT suite of models. Particular care has been devoted to address issues of near-wall accuracy via the use of extended wall functions and zonal

models. A particular strength of FLUENT is its ability to model combustion phenomena using a variety of models, including eddy dissipation concept model (FLUENT 5 Users Guide, 1998) FLEUNT solves the governing conservation equations of fluid dynamics by a finite-volume formulation on a structured, non-orthogonal, curvilinear coordinate grid system using a collocated variable arrangement.

All the results were obtained using segregated implicit solver. Each scalar equation such as momentum, energy, turbulent kinetic energy, turbulent dissipation rate, species transport equations have been discretized using *second order upwind scheme*. The pressure interpolation scheme used is Standard. Pressure-Velocity coupling is achieved by the *SIMPLE* (Semi Implicit Method for Pressure Linked Equations) algorithm (Launder and Spalding, 1972) resulting in a set of algebraic equations, which are solved using a line-by-line tridiagonal matrix algorithm (TDMA). FLUENT models turbulent flows with the Spalart-Allmaras model, k-ε model, and a second-moment closure or Reynolds-stress model (RSM). In the present study *k-ε model* suggested by Launder and Spalding (1972) has been used to model the turbulent flow. Near wall viscous sub layer is solved using *non-equilibrium wall functions*. The *fast rate chemistry Eddy Dissipation Concept (EDC)* suggested by Magnussen (1976) is used for modelling reacting flow.

For all the variables of mass, velocity components u and v, and turbulence quantities k and ε, the convergence criteria are set as the normalised total overall residue value, which is equal to 10^{-5}. The computations were under relaxed for providing stability to the iteration procedure. The under relaxation factors used for cold flow study are 0.3 for p, 0.7 for u and v, 0.8 for k and ε, and 1 for μ and ρ, where as in the reacting flow studies, it is 0.2 for p, 0.5 for u, v, k and ε, 1 for E, 0.8 for μ and ρ, and 0.8 for all species mass fractions. Boundary conditions have been set, as described in the previous section. Constant inlet velocity profile is used in all simulations. Initialisation of the iteration has been made using the inlet values. In the reacting flow case a high initial temperature is given to 'ignite' the combustion process. All simulations in cold flow condition took about 45 minutes machine time and converged in 900 iterations, whereas in reacting flow case it was around 100 minutes and 2400 iterations respectively.

3.5.2 Selection of computational grid

Mid plane axisymmetry has been assumed. The complete flow domain is discretized into a structured grid as shown in Fig.3.2. A finer grid size has been selected in region with steep gradients, for obtaining good accuracy in the predicted solution.
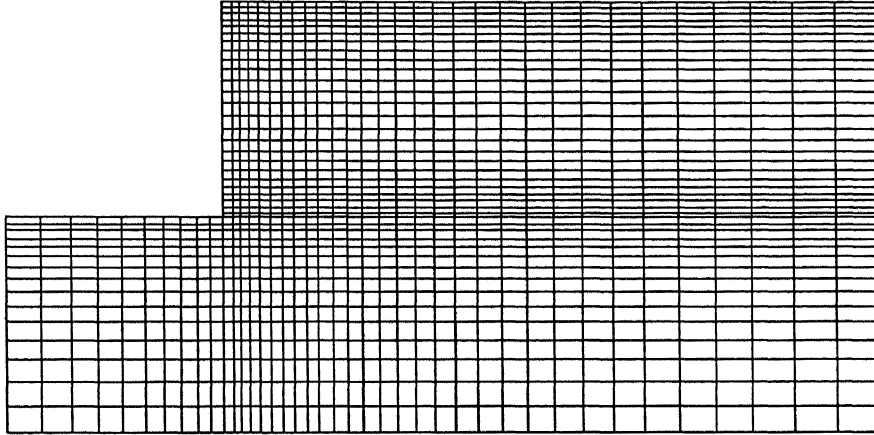

Fig.3.2 Grid pattern in the geometry

3.5.3 Grid Independence Test

A grid independence test has been performed using the grids of 200×50, 200×30, 100×50 and 100×30 cells in the z and r directions respectively for the total geometry. Test was carried out for cold flow case for an expansion ratio of 2, with inlet Reynolds number and turbulence intensity being 1×10^5 and 5% respectively. The discrepancy in the centerline mean axial velocity is found to be very small (maximum of 3.1%) relative to the solution for the 200×50 grid, when the number of grid points are reduced in z and r directions. This can be observed in Fig.3.3.
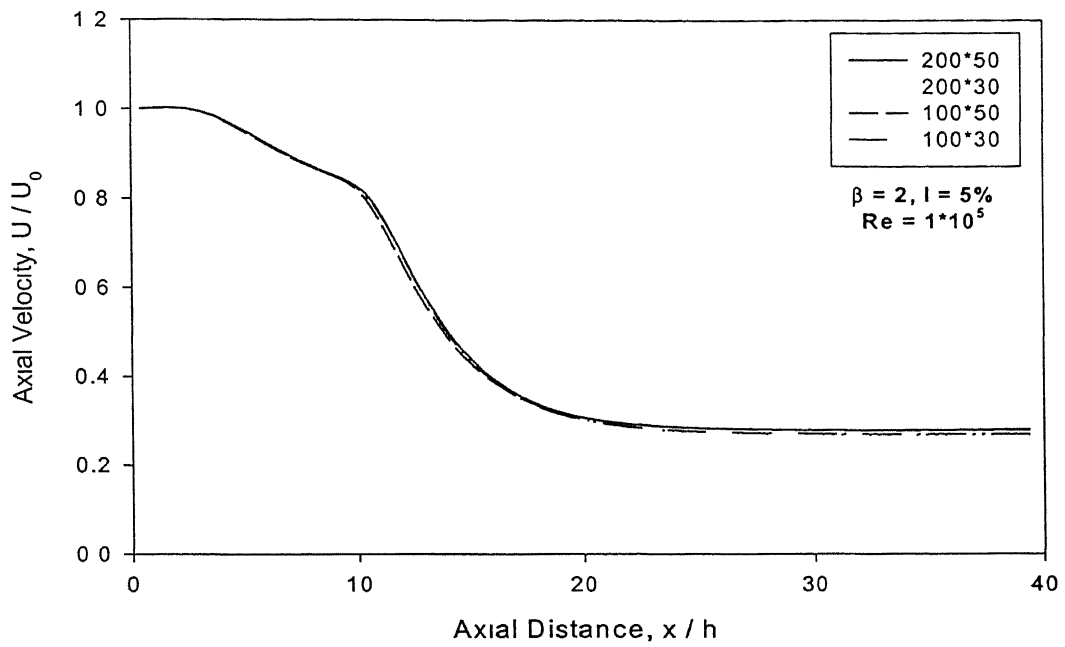
Fig.3.3 Results of Grid Independence study

CHAPTER 4

COLD FLOW

An exclusive study on turbulent cold flow inside the dump combustor has been carried out, which can be divided into two parts. In the first part validation of the numerical code is made, where an experimental test case, available in the literature is exactly simulated and results are compared. In the second part the effects of various geometrical and flow parameters that affect the flowfield are studied. An attempt has been made to understand the physics involved in the flow. In the present study, the effect of Reynolds numbers, turbulence intensities and geometries are explored extensively with air as the working fluid.

4.1 Validation of the Code

Even though, a large number of literature available in this particular topic, a clear presentation that lists all the flow and geometric test conditions, is very rarely found. One such work was experiments conducted by Gabruk and Roe (1994), where, inlet velocity profile is carefully documented to provide a suitable boundary condition, which has been used in the present investigation. The results of mean centerline axial velocity, U_c, normalised with inlet centerline velocity, U_0 for Reynolds number, Re = 1.18×10^5 along with the experimental data of Gabruk and Roe (1994) is plotted in Fig.4.1. It can be noticed that both the experimental data and the numerical prediction matches well, in the flow regime considered with a maximum difference of 6.2% in axial velocity. The recirculation length extends up to 6.85 step height as per prediction, which is consistent with the experimental finding of Gabruk et al., where they got recirculation length as 6.75-step height. Radial profiles of mean axial velocities at axial locations, x=1h, 5h and 10h are presented in Fig.4.2, Fig.4.3 and Fig.4.4 respectively. At axial locations less than 5h from the dump plane, the high shear region between the potential core and the recirculation region can be clearly identified by the high velocity gradient. Observations near the combustor wall show rapid velocity decay and a region of flow reversal in the recirculation zone. Highest negative axial velocities occur at sections between 2 to 4 step heights from the dump plane. After 6h downstream of the dump plane, negative axial velocity vanishes and the flow becomes more or less simple pipe flow.
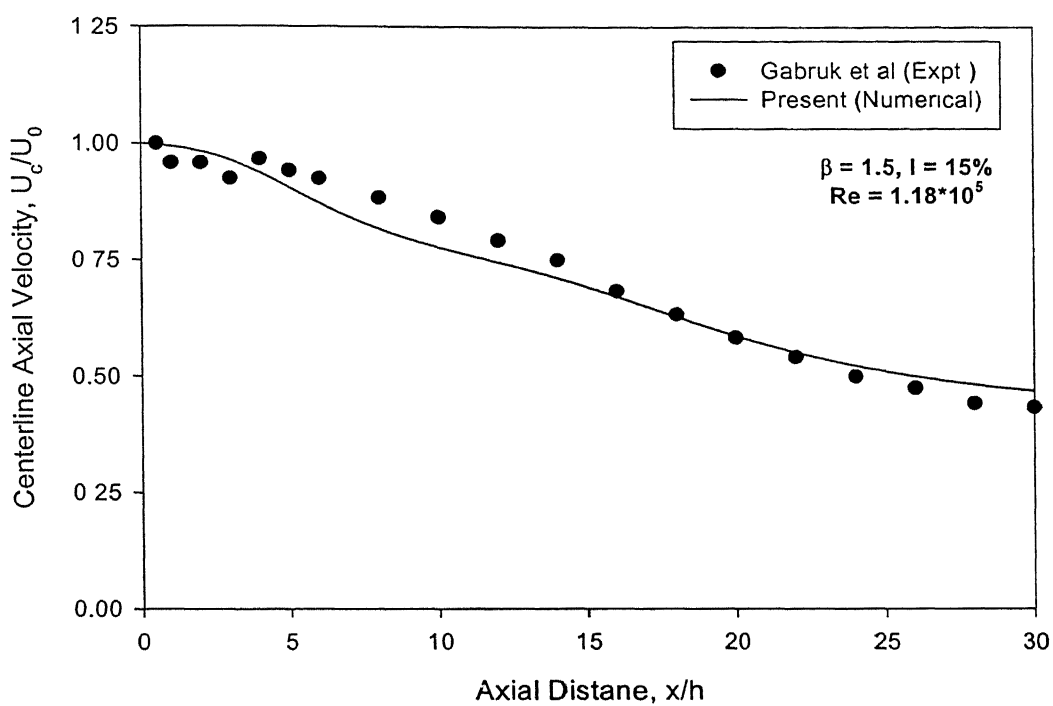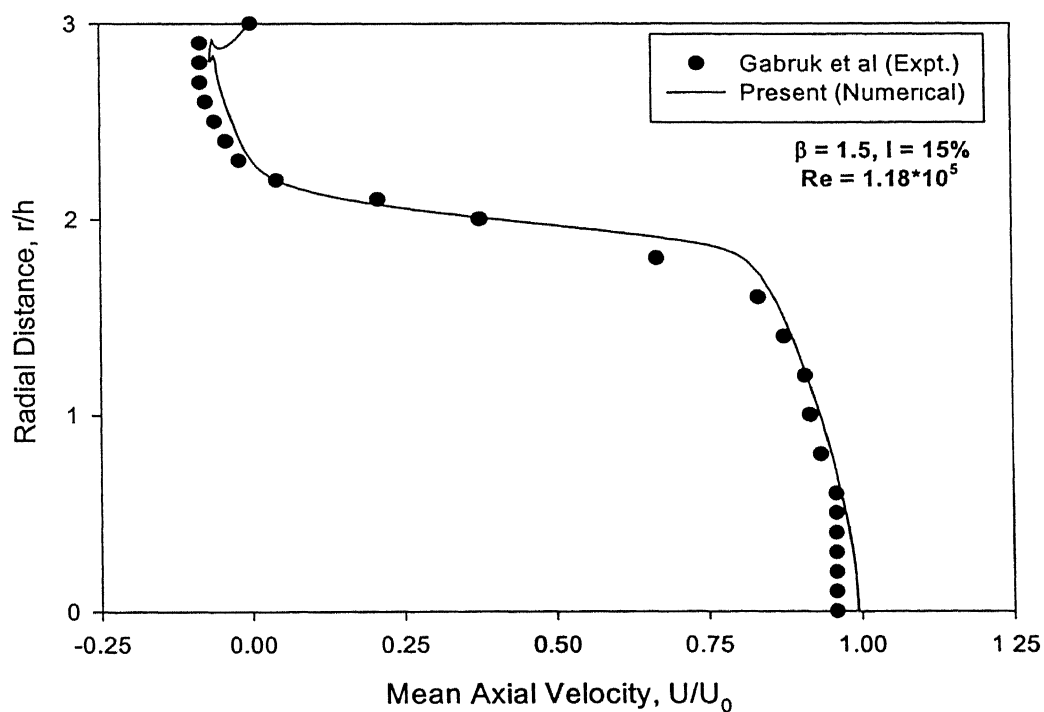
Fig.4.1 Centerline mean Axial Velocity
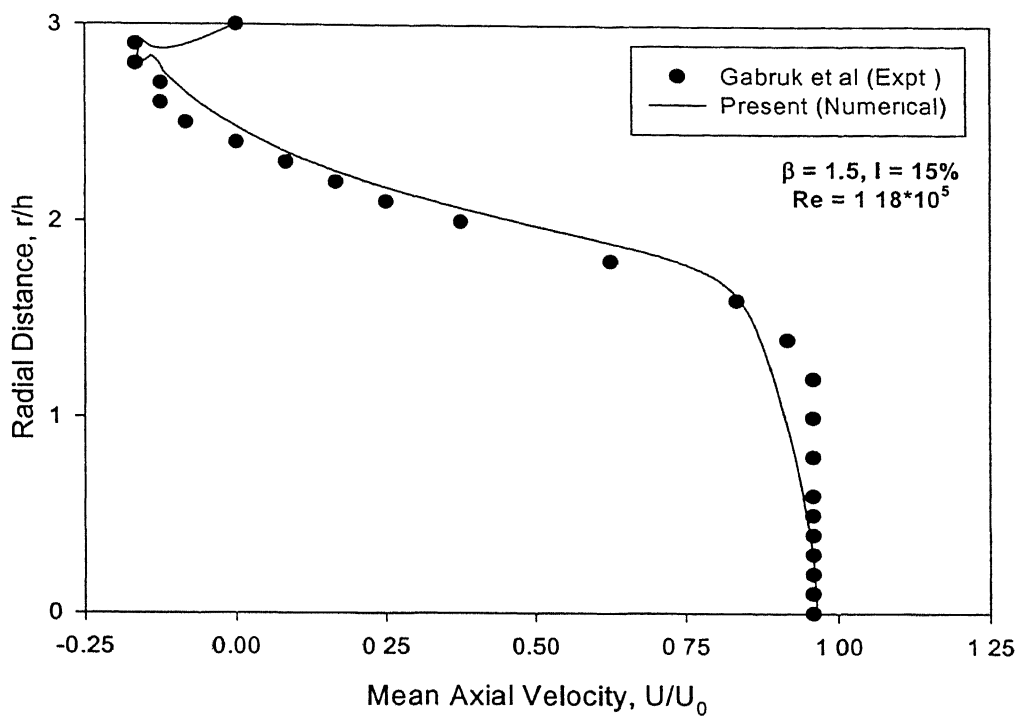

Fig.4.2 Mean Axial Velocity profile at x = 1h

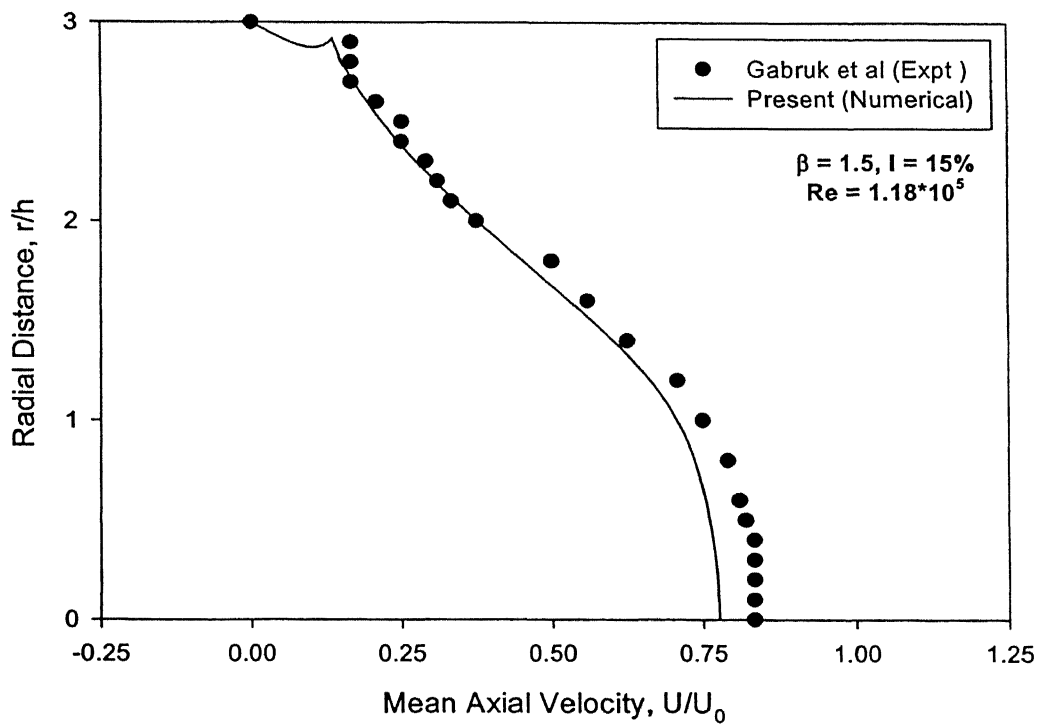**Fig.4.3 Mean Axial Velocity profile at x = 5h**

Fig.4.4 Mean Axial Velocity profile at x = 10h

4.2 Parametric Study

An extensive study on cold flow quantities including axial velocity, radial velocity, static pressure, turbulent kinetic energy and turbulent diffusion rate has been presented in this section. Some important flow parameters such as inlet Reynolds number, turbulence intensity and geometrical parameter like expansion ratios have been varied to find out the effect of each of these parameters on the flowfield.

4.2.1 Mean Centerline Axial Velocity

The mean centerline axial velocity distribution shows how far the potential core or the region where the inlet velocity at the dump plane is maintained exists and at what axial distance the uniform flows is attained. The flow conditions considered are Reynolds number, Re (based on smaller pipe diameter) and inlet turbulence intensity, I. The geometric feature varied is combustor expansion ratio, β (D/d). Fig.4.5, Fig.4.6 and Fig.4.7 depict the distribution of centerline axial velocity, U_c, for three expansion ratios (β) 1.5, 2 and 3 respectively. Velocities have been normalized using inlet centerline velocity, U_0. All lengths have been normalized with step height, h of the combustor. It can be found from Fig.4.5 that uniform flow attains at 35h and 50h downstream of the dump plane for turbulence intensities 15 % and 5% respectively for all considered Reynolds numbers at an expansion ratio of 1.5. And, it is 21h and 25h for turbulence intensities 15% and 5% respectively for expansion ratio 2, as can be seen from Fig.4.6. Fig.4.7 indicates the length of attaining uniform flow as 13h and 16h for turbulence intensities 15% and 5% respectively for expansion ratio 3. These data is summarised in Table.4.1. On analysing the figures it is found that for higher turbulence intensities the length of potential core is considerably reduced. Increase in inlet turbulence level helps to attain uniform flow at much shorter distance irrespective of the expansion ratio and Reynolds number as can be seen from the figures. The variation of Reynolds number while keeping turbulence intensity level constant does not have much influence on the centerline axial velocity profile. Similar observations has also been reported in the work of So and Ahmed (1988, 1989).
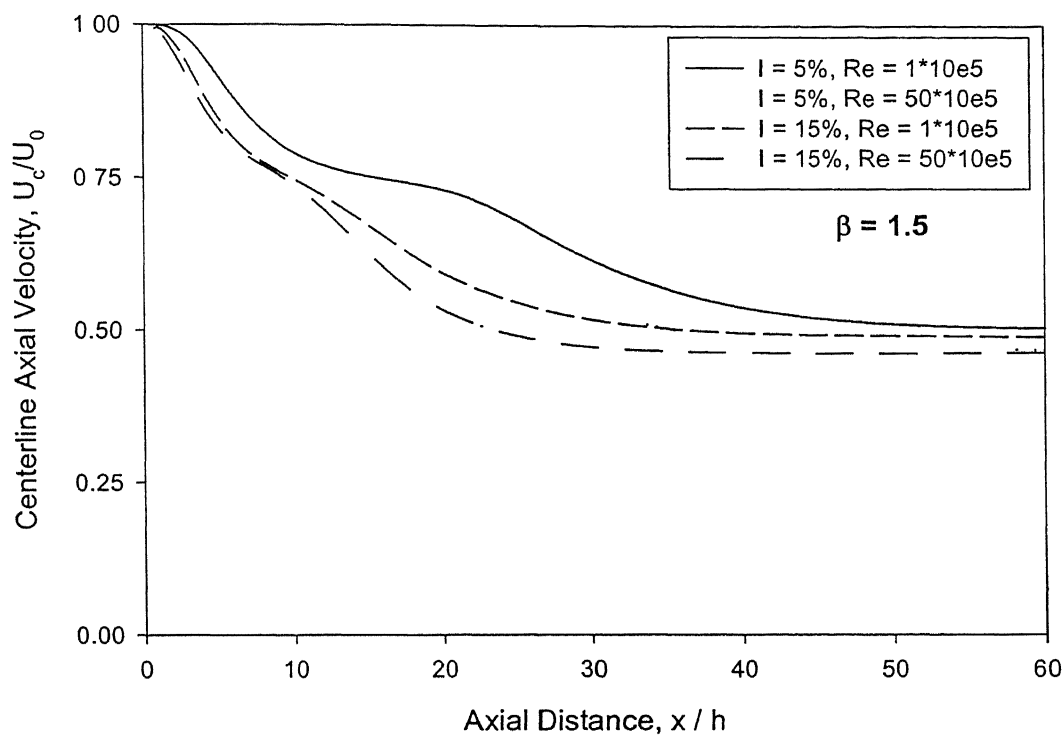
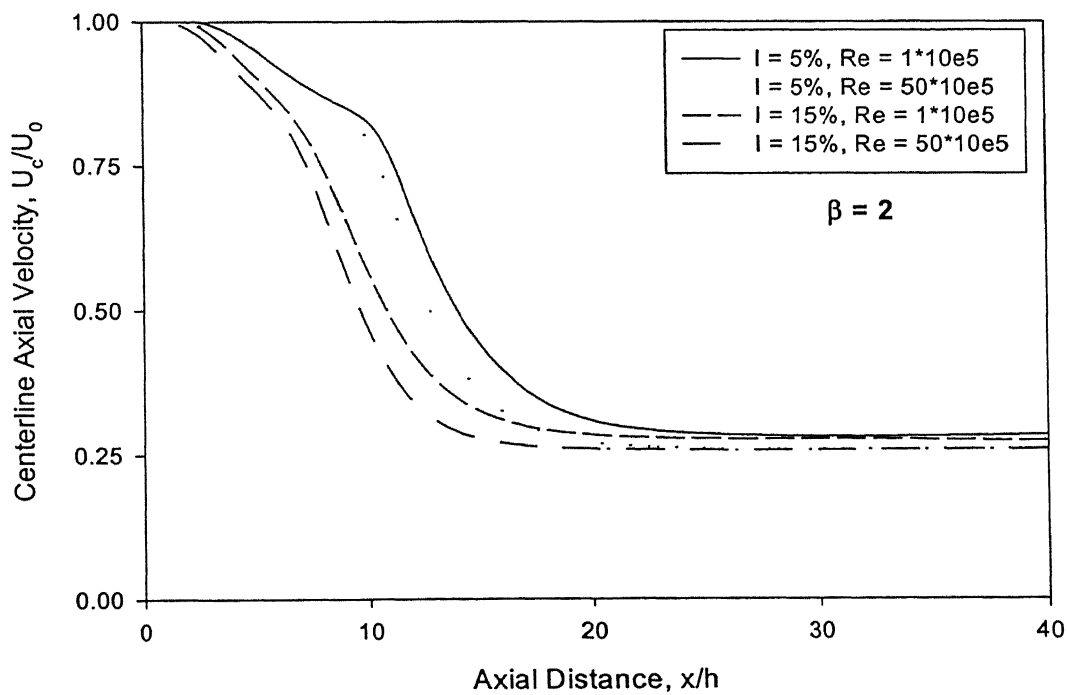**Fig. 4.5 Mean Centerline Axial Velocity distribution for Expansion Ratio = 1.5**

Fig. 4.6 Mean Centerline Axial Velocity distribution for Expansion Ratio = 2
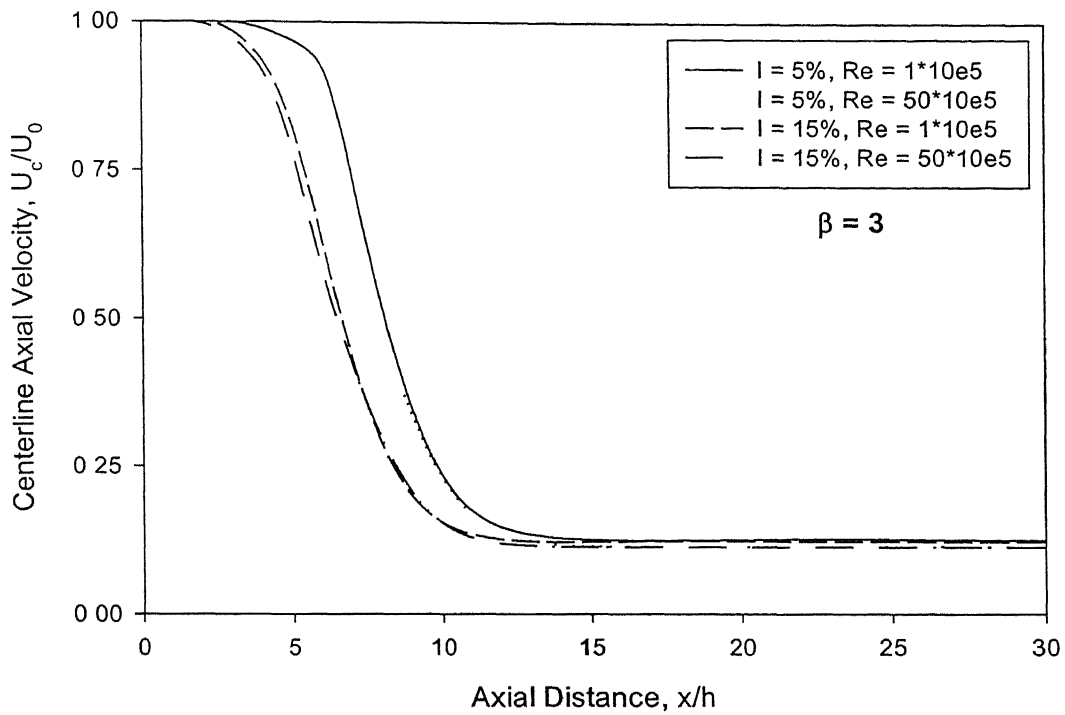
Fig. 4.7 Mean Centerline Axial Velocity distribution for Expansion Ratio = 3

Table.4.1 Variation in Uniform flow attaining length with Expansion ratio and Turbulence Intensity

Expansion Ratio	Turbulence Intensity, I (%)	Axial Distance at which Uniform flow is attained, x/h
1.5	5	50
	15	35
2	5	25
	15	21
3	5	16
	15	13

41

Fig.4.8 through Fig.4.10 show the distribution of mean centerline axial velocity for different expansion ratios for three turbulence intensities 5%, 10% and 15% respectively for inlet Reynolds number 1×10^5. It can be noted that, there is a considerable difference in centerline axial velocity profiles for different expansion ratios. Same trend can also be seen in the case of higher Reynolds number considered in this study, which is 50×10^5, from Fig.4.11, Fig.4.12 and Fig.4.13 drawn for turbulence intensities 5%, 10% and 15% respectively. Longer potential core is a feature of larger expansion ratios. But, it attains uniform flow at a shorter distance downstream from the dump plane. Therefore, from study of centerline axial velocity distribution, it can be concluded that Reynolds number is not a major factor governing the velocity profile, but inlet turbulence level and expansion ratio do affect the flowfield considerably.
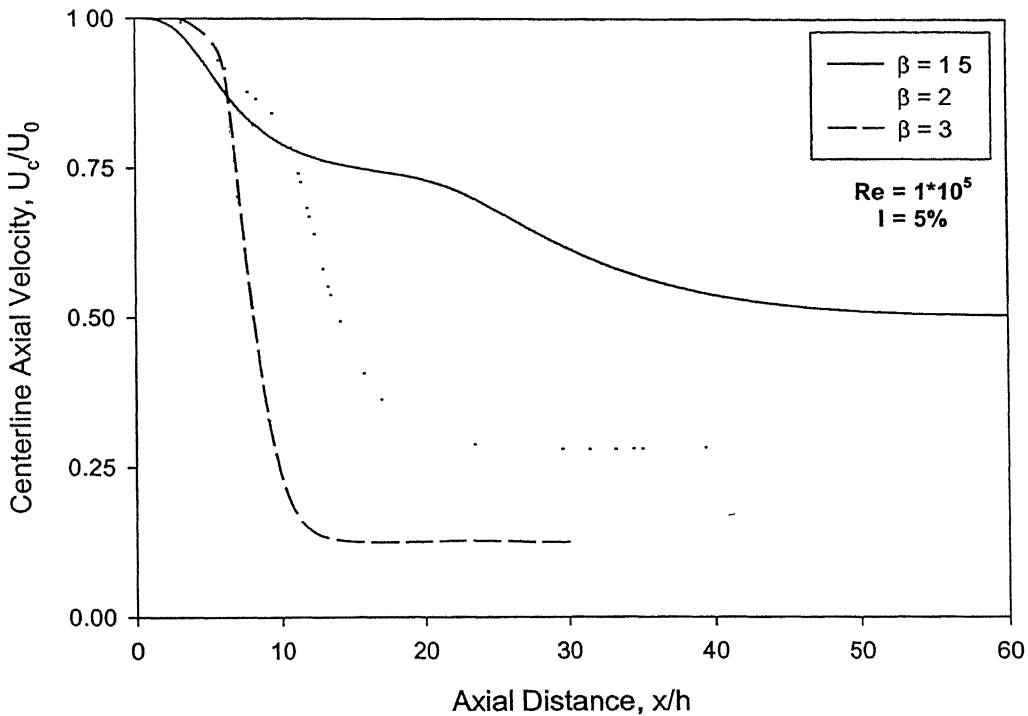

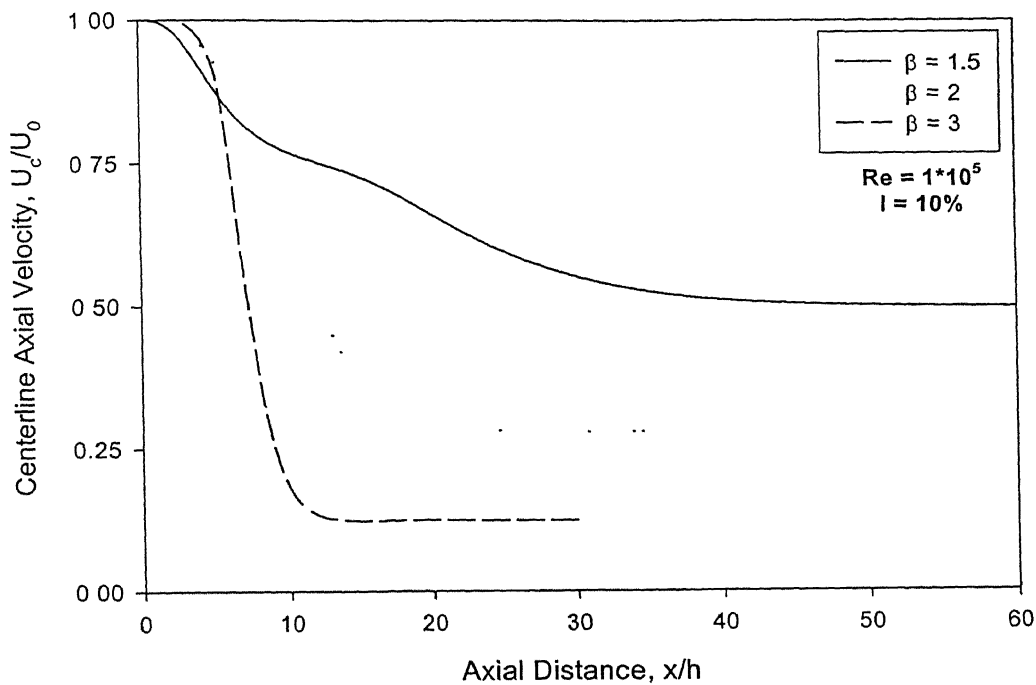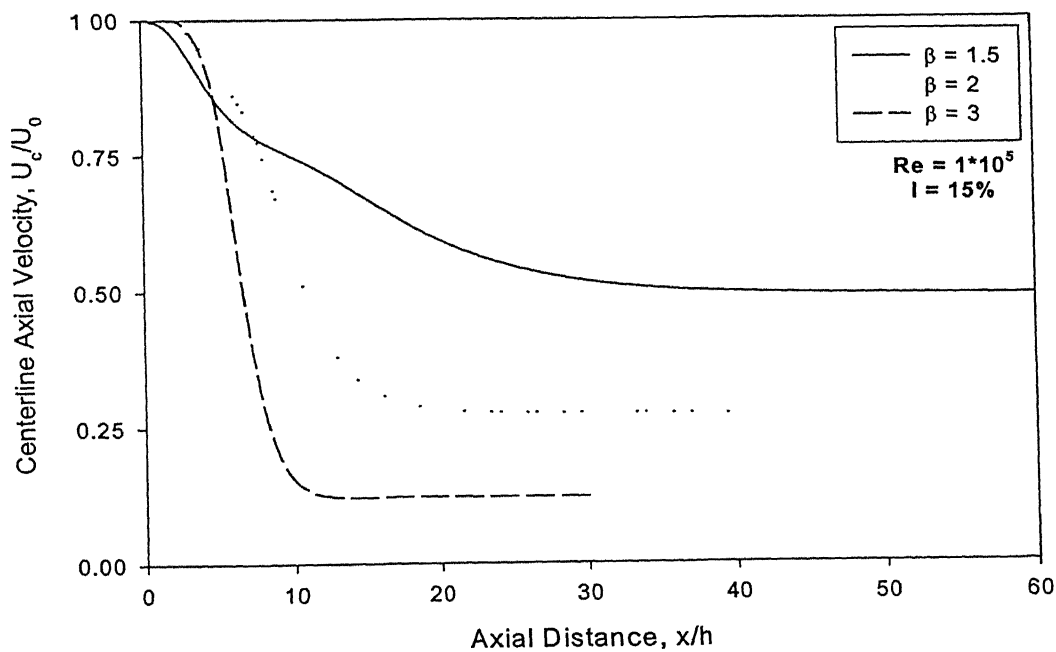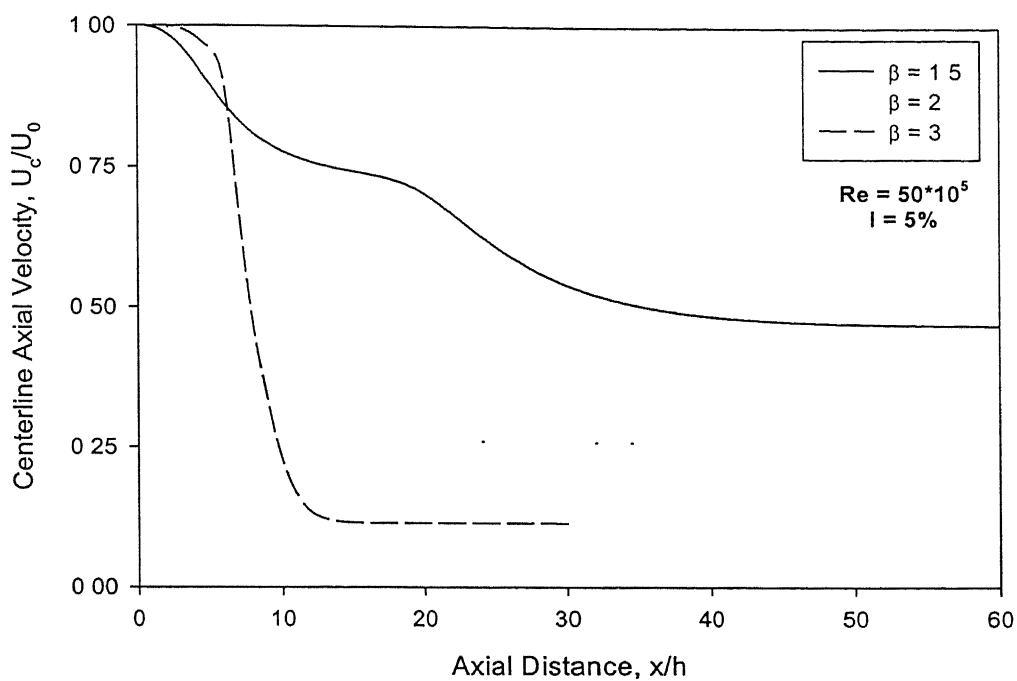**Fig. 4.8 Mean Centerline Axial Velocity distribution for Reynolds Number = 1×10^5; Turbulence Intensity = 5%**

Fig. 4.9 Mean Centerline Axial Velocity distribution for Reynolds Number $= 1 \times 10^5$, Turbulence Intensity $= 10\%$

Fig. 4.10 Mean Centerline Axial Velocity distribution for Reynolds Number $= 1 \times 10^5$, Turbulence Intensity $= 15\%$

43

Fig. 4.11 Mean Centerline Axial Velocity distribution for Reynolds Number = 50×10^5**, Turbulence Intensity = 5%**
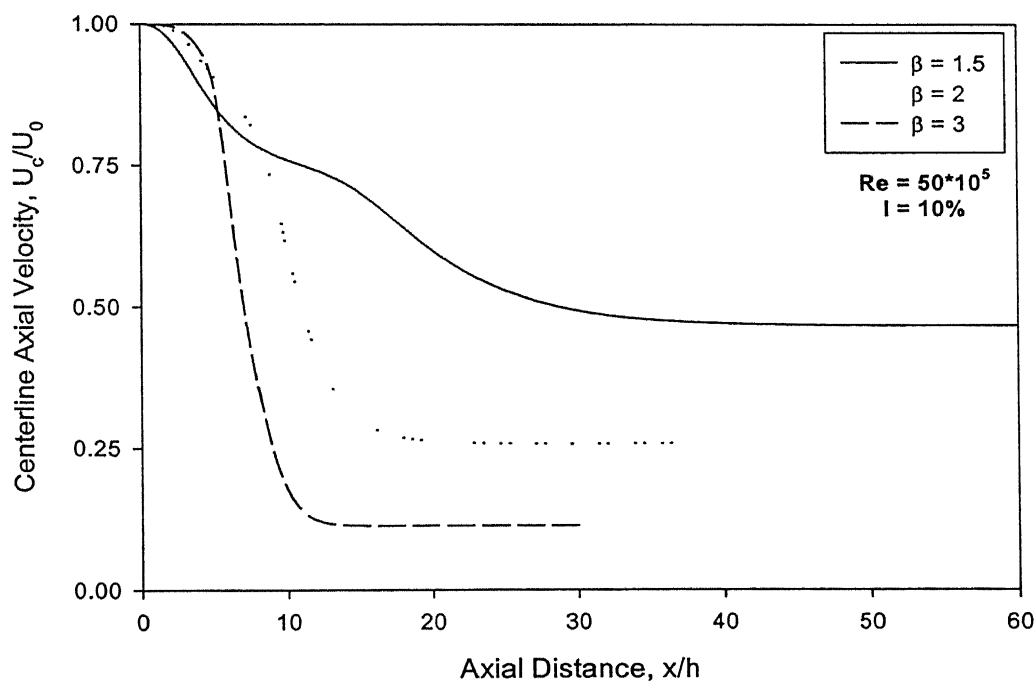

Fig. 4.12 Mean Centerline Axial Velocity distribution for Reynolds Number = 50×10^5**, Turbulence Intensity = 10%**
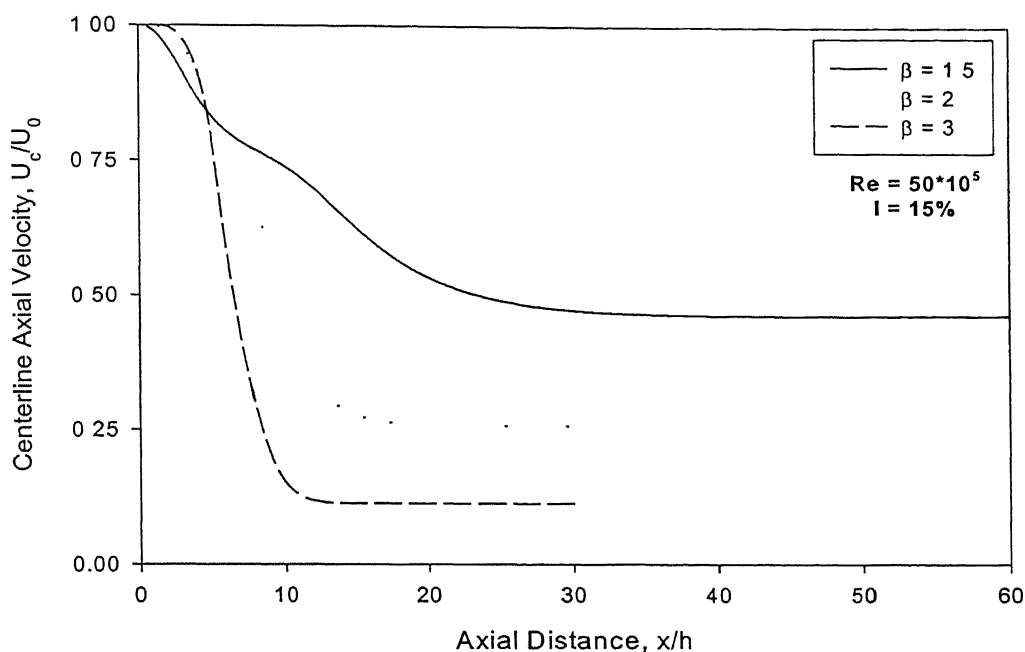
Fig. 4.13 Mean Centerline Axial Velocity distribution for Reynolds Number = 50×10^5, Turbulence Intensity = 15%

4.2.2 Mean Axial Velocity Profile

Fig.4.14, Fig.4.15 and Fig.4.16 show axial velocity profile at various axial locations from the dump plane for D/d=1.5 at Re=1×10^5. At x=0.5h, the effect of turbulence intensity is predominant in the recirculation region and in the shear layer region, but not in the central core region, where distribution is almost same. At x=5h and 10h, turbulence level does affect the flow at all radial locations. At x=5h with I=5%, recirculation is still present, as evident from the presence of negative axial velocity, whereas, for I=15%, reattachment of flow seems to be attained already. Also recirculation size is more at x=0.5h, and high velocity gradient can be seen in the shear layer. Various flow regimes downstream of the dump plane are marked in Fig. 4.14. At x=10h, start of the growth of secondary boundary layer after reattachment is clearly seen. At x=10h, profile is more developed for I=15% than for I=5%. So the turbulence intensity is a dominant factor in determining the overall flow field compared to any other parameters. Axial velocity profile at various axial locations, x=0.5h, x=5h and x=10h for expansion ratio 3 is drawn in Fig.4.17, Fig.4.18 and Fig.4.19 respectively. At x=0.5h, turbulence level has no effect on the flowfield.
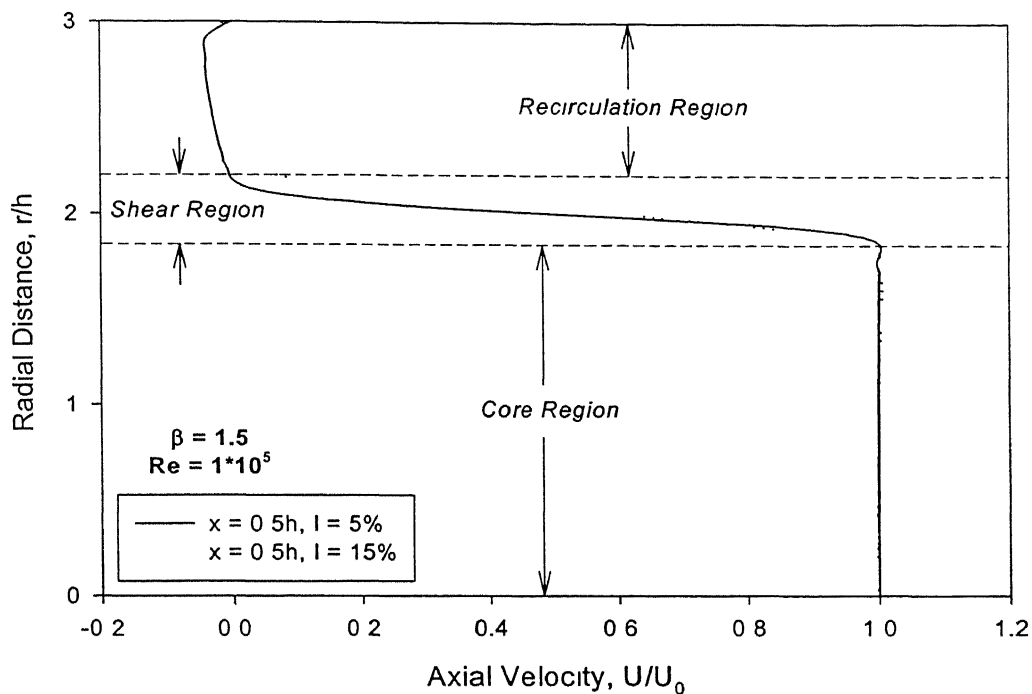
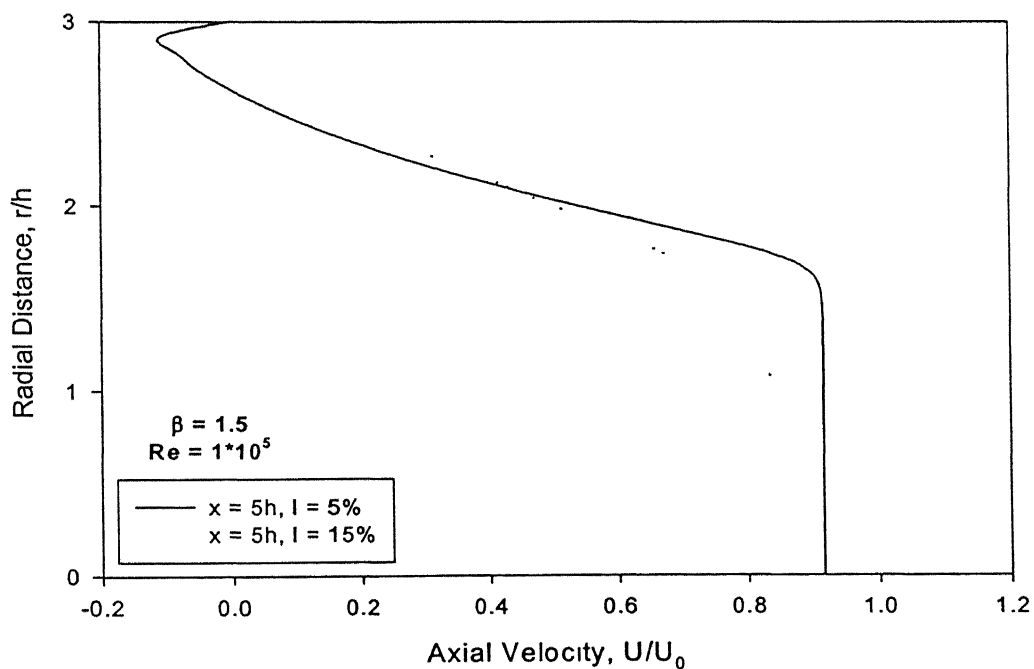**Fig. 4.14 Mean Axial Velocity profile at x = 0.5h for Expansion Ratio = 1.5, Reynolds Number = 1×10^5**

Fig. 4.15 Mean Axial Velocity profile at x = 5h for Expansion Ratio = 1.5, Reynolds Number = 1×10^5
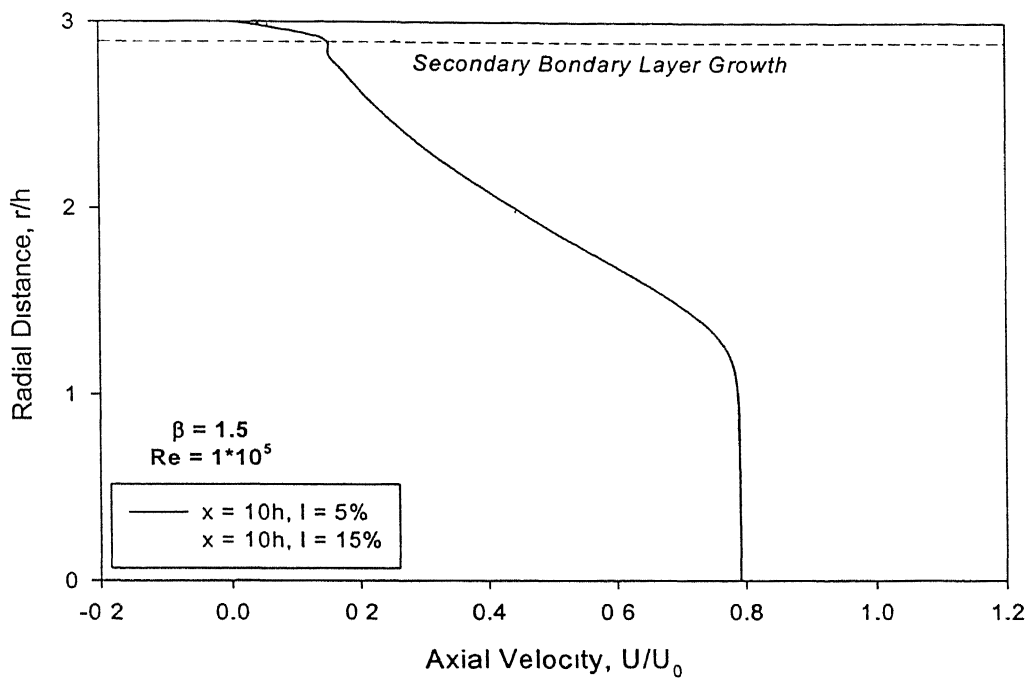
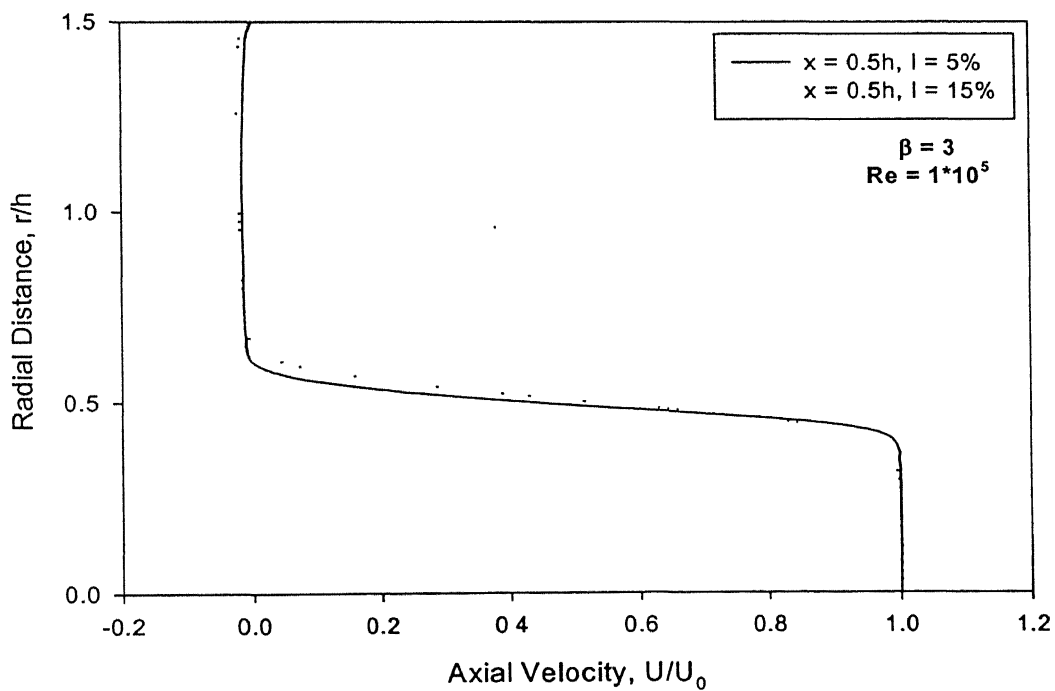**Fig. 4.16 Mean Axial Velocity profile at x = 10h for Expansion Ratio = 1.5, Reynolds Number = 1×10⁵**

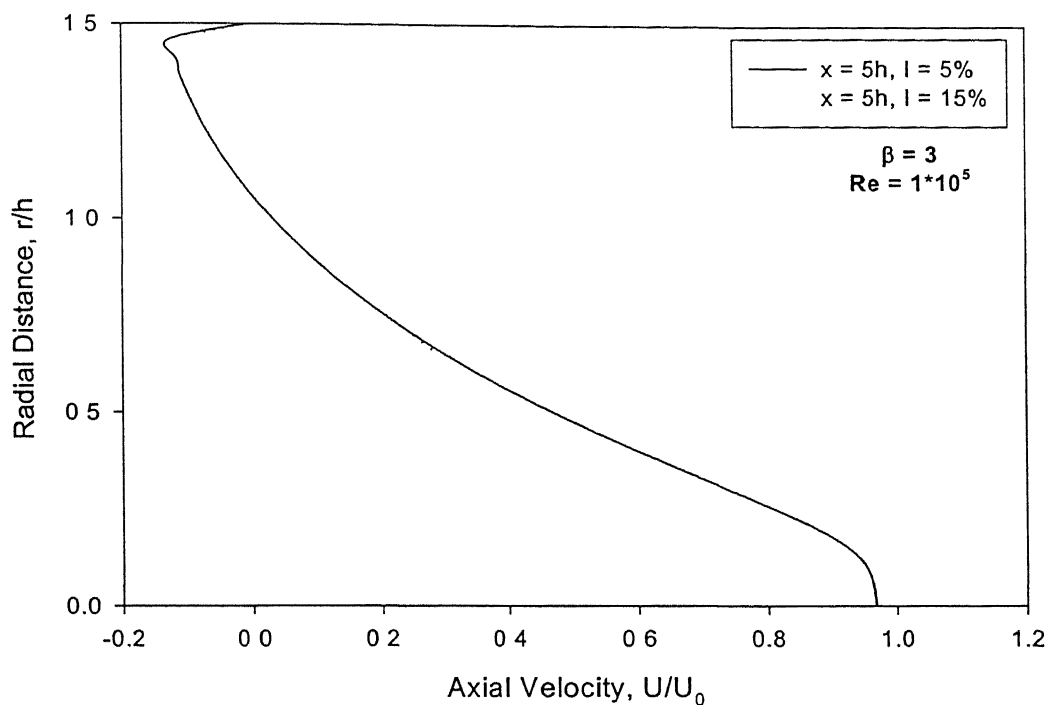**Fig. 4.17 Mean Axial Velocity profile at x = 0.5h for Expansion Ratio = 3, Reynolds Number = 1×10⁵**

Fig. 4.18 Mean Axial Velocity profile at x = 5h for Expansion Ratio = 3, Reynolds Number = 1×10^5
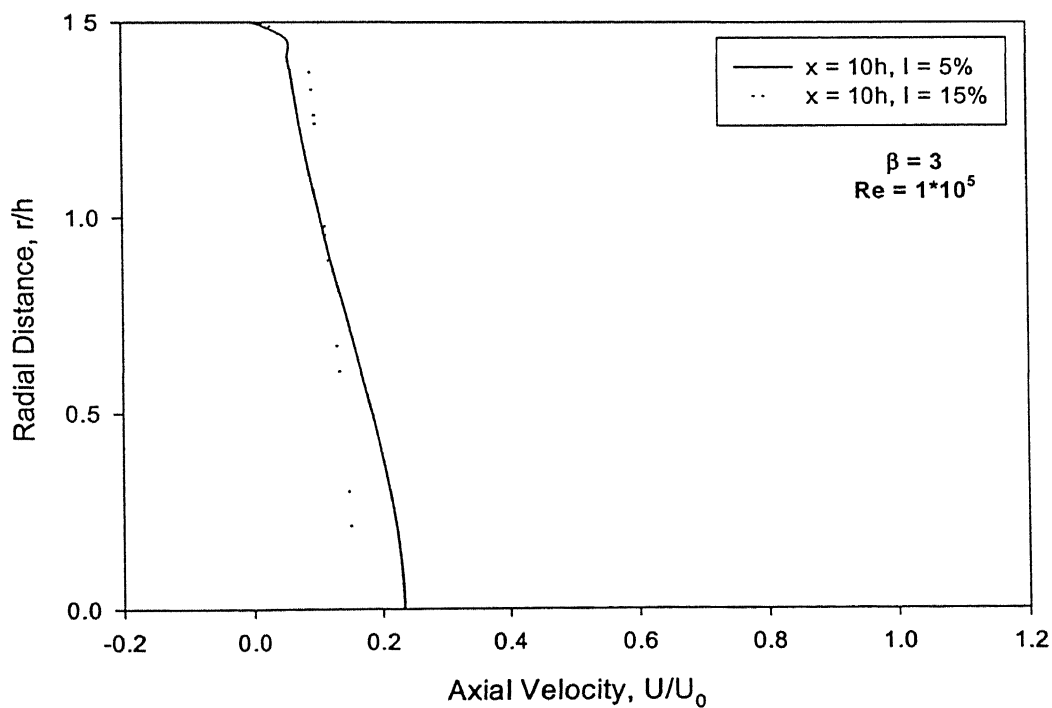

Fig. 4.19 Mean Axial Velocity profile at x = 10h for Expansion Ratio = 3, Reynolds Number = 1×10^5

The axial velocity contours for expansion ratio 1.5 at two different turbulence intensities, 5% and 15% at Reynolds number 1×10^5 is given in Fig.4.20 and Fig.4 21 respectively Maximum negative velocity comes out to be $-0.19U_0$ and $-0.22U_0$ in the recirculation region for intensity level 5% and 15% respectively. This result clearly shows, how the strength of recirculation varies as turbulence level changes. More turbulence intensity makes recirculation stronger. Next two figures, Fig.4.22 and Fig 4 23 show the axial velocity contours for expansion ratio 2 at intensity levels of 5% and 15% respectively. For turbulence level of 5%, the maximum negative velocity gives a value of $-0 167U_0$, whereas it is $-0.189U_0$ for turbulence intensity of 15%. Axial velocity contours for the same inlet flow conditions as above for expansion ratio 3 is made in Fig.4.24 and Fig.4.25 For turbulence level of 5% and 15%, the maximum negative velocity in the flowfield becomes $-0.142U_0$ and $-0.155U_0$ respectively. The maximum negative axial velocity encountered in the flowfield in each of the above cases is tabulated in Table.4.2. Hence, from the axial velocity contours it may be observed that with increase in turbulence intensity, and with decrease in expansion ratio, the strength of the recirculation zone is getting better and hence it pulls the reattachment point further upstream towards the dump plane. It can also be seen that with the increase in expansion ratio, the effect of turbulence intensity is decreasing.

Table.4.2 Variation in maximum negative Axial Velocity in the flowfield with the Expansion Ratio and Turbulence Intensity

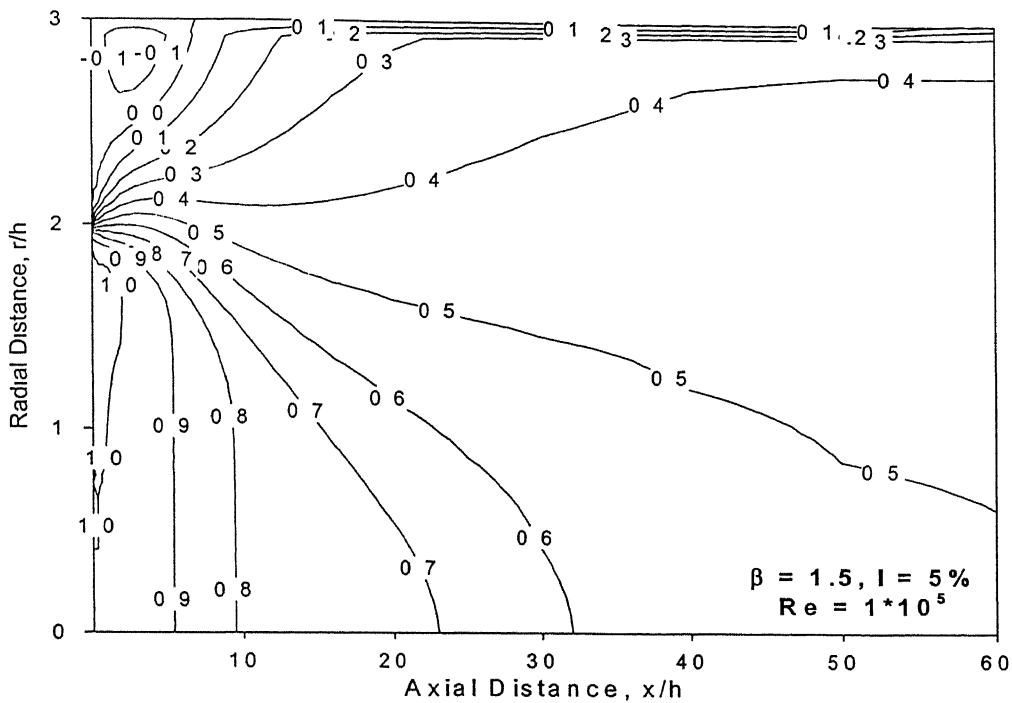| Expansion Ratio	Turbulence Intensity, I (%)	Maximum Negative Axial Velocity, U/U_0
1.5	5	-0.190
	15	-0.220
2	5	-0.167
	15	-0.189
3	5	-0.142
	15	-0.155

Fig. 4.20 Axial Velocity contours for Expansion Ratio = 1.5, Reynolds Number = 1×10^5, Turbulence Intensity = 5%
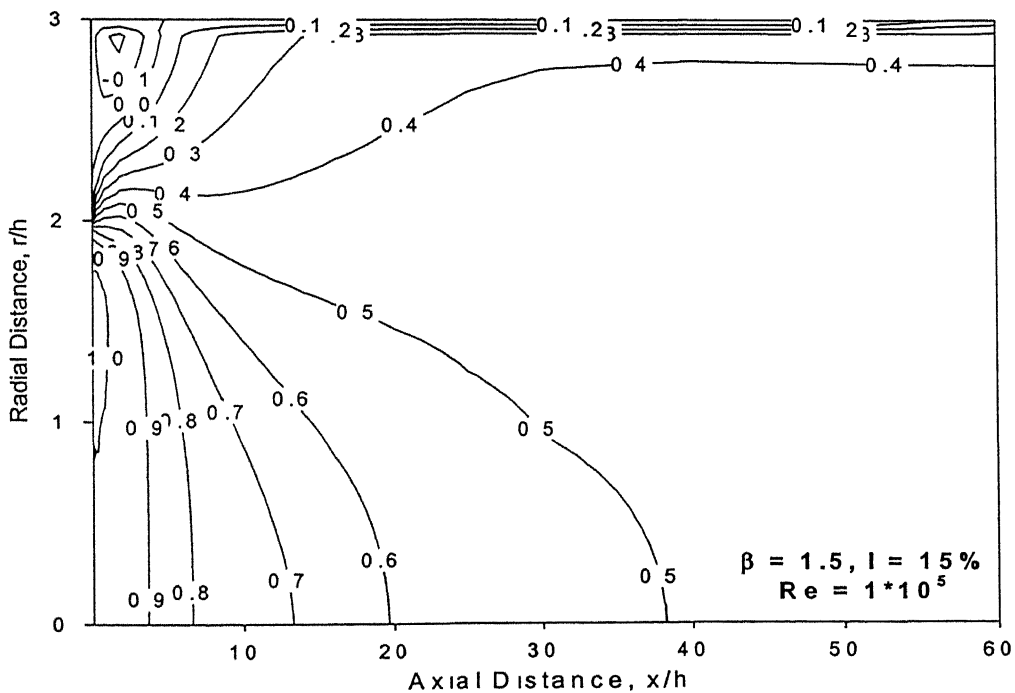

Fig. 4.21 Axial Velocity contours for Expansion Ratio = 1.5, Reynolds Number = 1×10^5, Turbulence Intensity = 15%
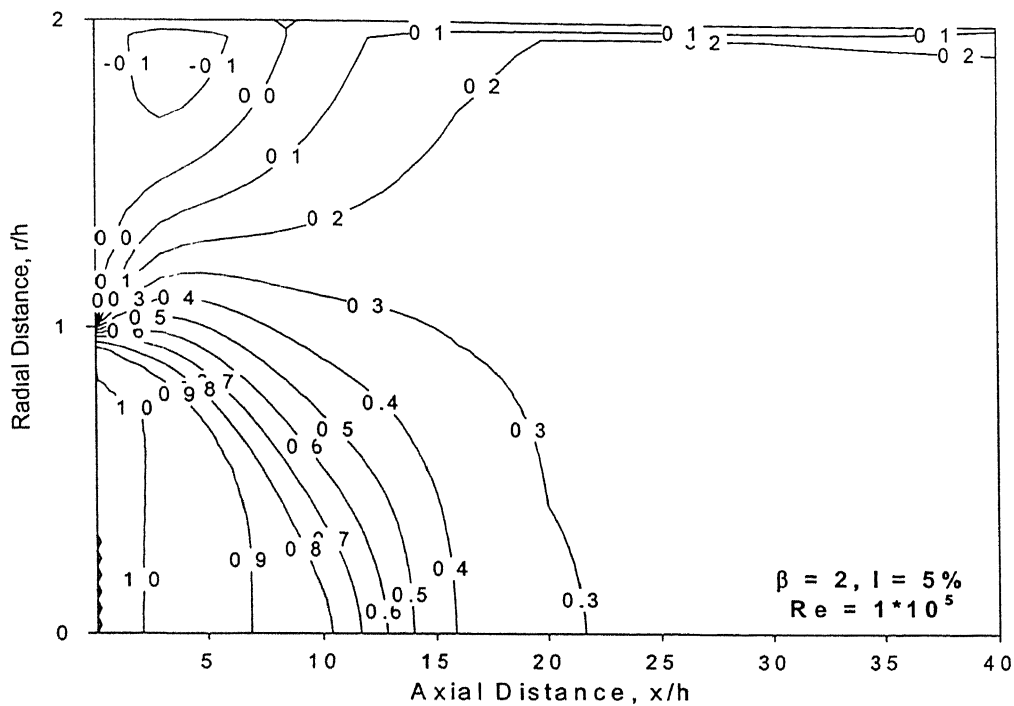
Fig. 4.22 Axial Velocity contours for Expansion Ratio = 2, Reynolds Number = 1×10^5, Turbulence Intensity = 5%
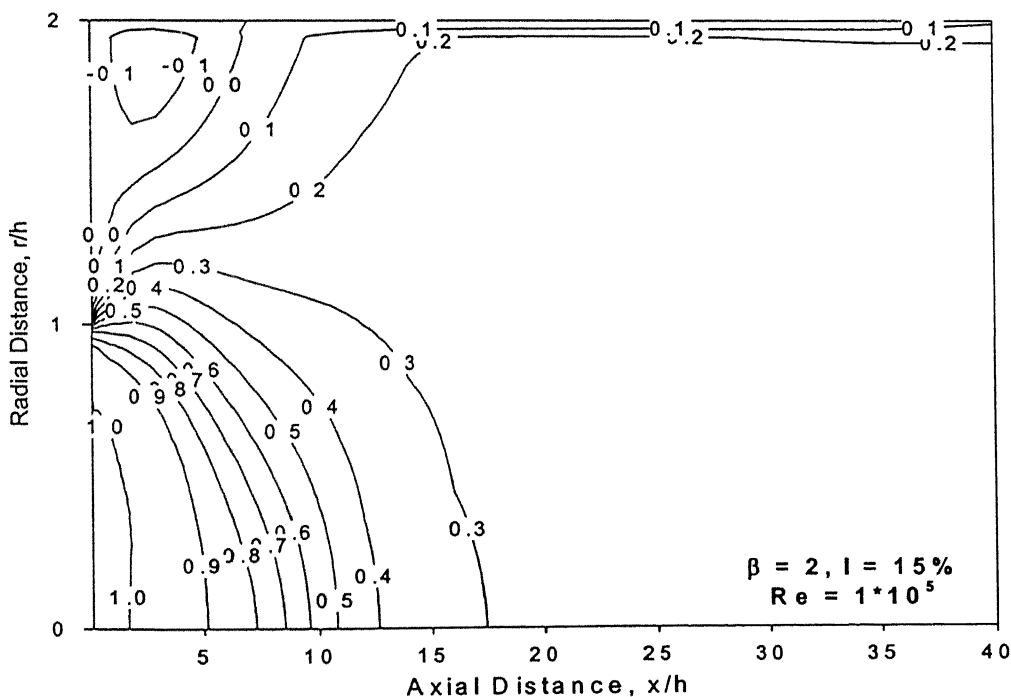

Fig. 4.23 Axial Velocity contours for Expansion Ratio = 2, Reynolds Number = 1×10^5, Turbulence Intensity = 15%

51

4.2.3 Reattachment Length

The recirculation size is a benchmark criterion in modelling studies of dump combustor (Gabruk and Roe, 1994). The *reattachment length*, RL, defined by intersection of zero axial velocity contours with the combustor wall is a measure of extends of recirculation size (Gabruk and Roe, 1994). The variation of reattachment length with Re, I and β are studied. The variation of reattachment length with turbulence intensity for expansion ratio 1.5 is shown in Fig.4.26 over a wide range of Reynolds numbers. It can be seen that reattachment length decreases with increase in inlet turbulence level for all Reynolds number considered in the present study. But the influence of turbulence intensity in the decrease of reattachment length is not so predominant in the case of the Reynolds number considered, 0.05×10^5, which is just above the transition (from laminar to turbulent) Reynolds number. But the decrease in reattachment length with the increase in turbulence intensity is quite clear in the case of other higher Reynolds numbers. However, in the Reynolds number range $0.5 \times 10^5 - 1 \times 10^5$, for same turbulence intensity, there is not much change in reattachment length. However, the reattachment length decreases for same turbulence intensity for Re = 50×10^5. The reason for this behaviour remains to be understood. From this result it is concluded that if Reynolds number goes above a limiting value, the reattachment length is more or less same for the same turbulence level irrespective of the inlet velocity. The increase of the turbulence level decreases the reattachment length due to the energy supply to the separating shear layer, which is a major factor determining the reattachment length.

Fig.4.27 and Fig.4.28 show the change in reattachment length with turbulence intensity for expansion ratios 2 and 3 respectively. In terms of variation of reattachment length with Reynolds number similar trend is observed as in Fig.4.26, even though there is a considerable change in magnitude of the reattachment length. For expansion ratios 2 and 3, the curves are getting closer, which means that the change in reattachment length with the change in Reynolds number is less sensitive at larger expansion ratios. It can be concluded that for the same expansion ratio, the reattachment length is minimum for low turbulence Reynolds number, increases with increase in Reynolds number, reaches a maximum limit and again decreases for higher turbulence Reynolds number.
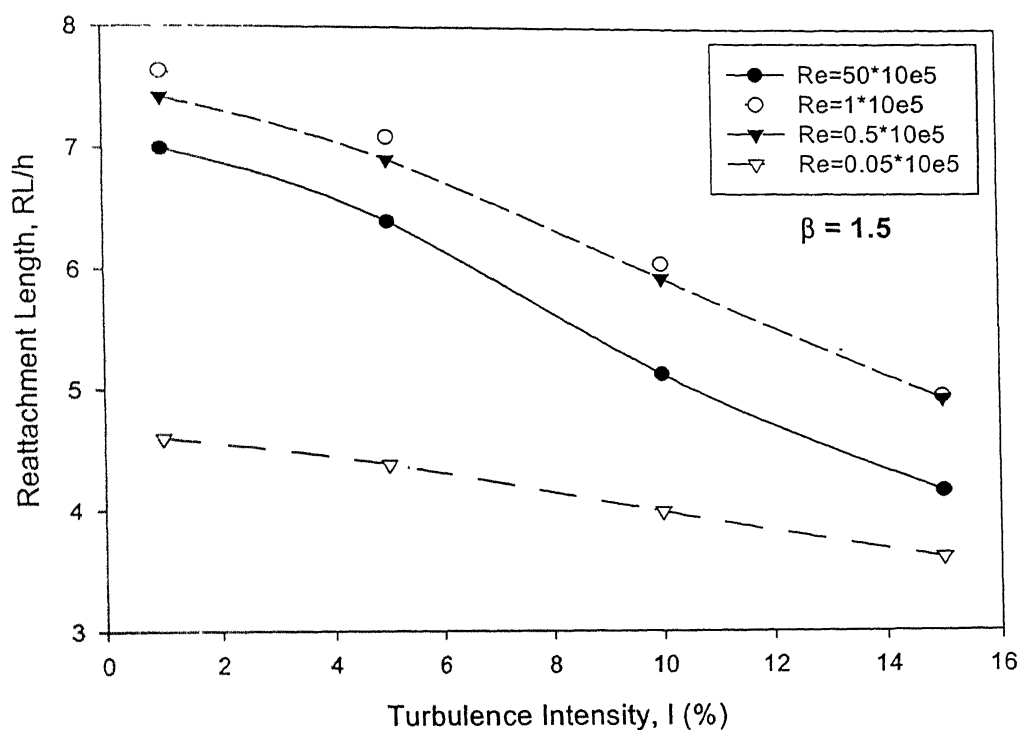
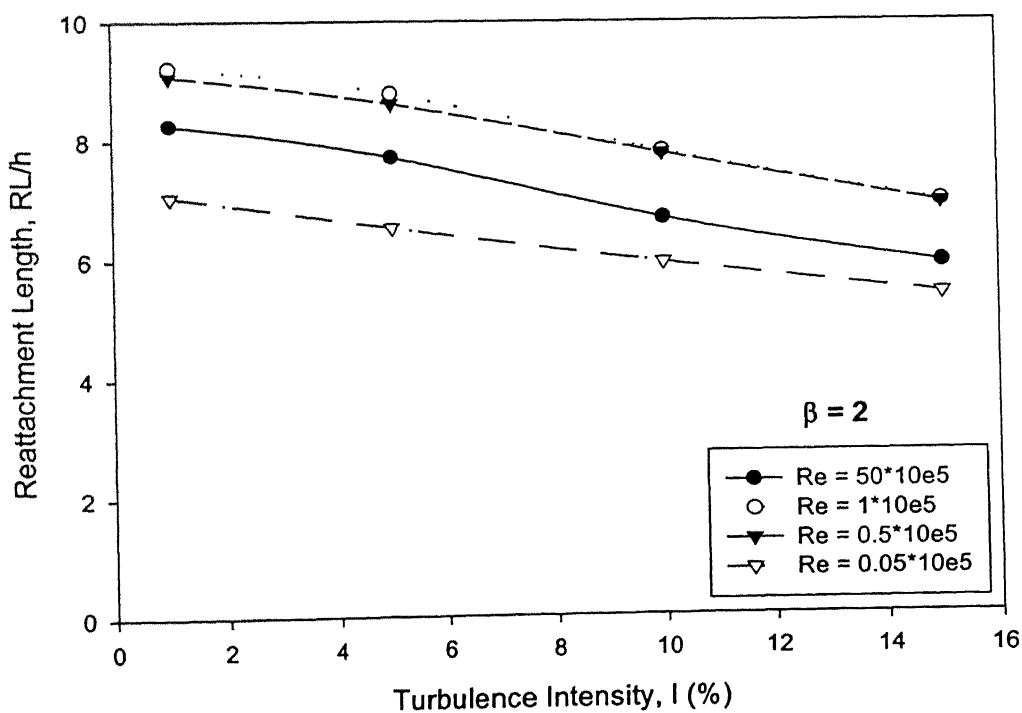**Fig. 4.26 Reattachment length variation for Expansion Ratio = 1.5**

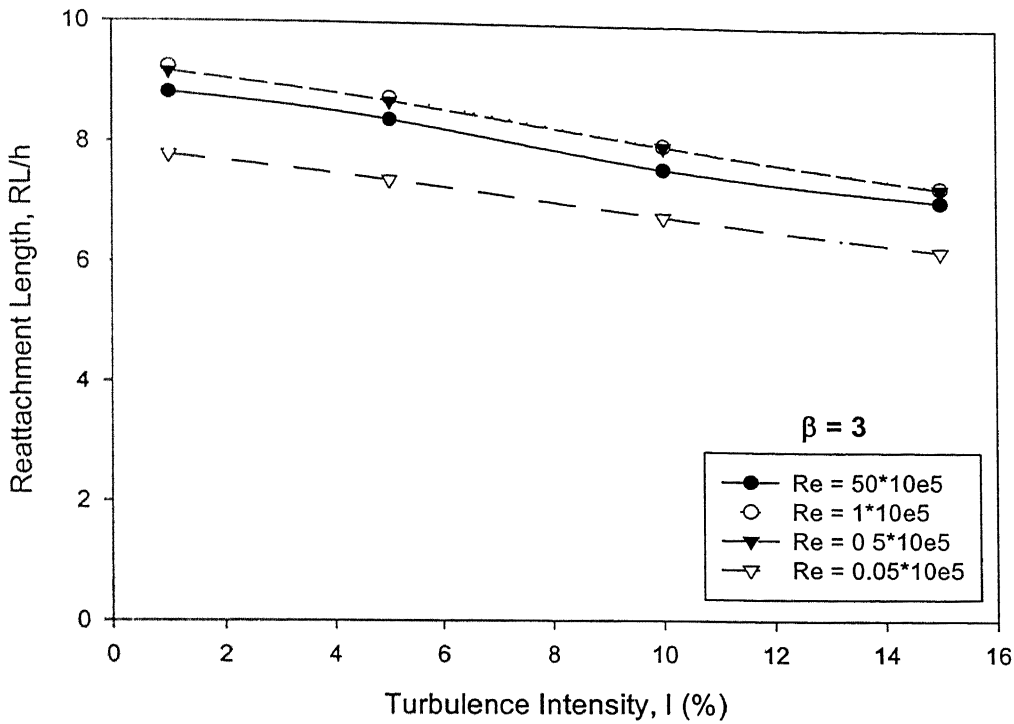**Fig. 4.27 Reattachment length variation for Expansion Ratio = 2**

Fig. 4.28 Reattachment length variation for Expansion Ratio = 3

The effect of expansion ratios on reattachment length for different Reynolds numbers is given in Fig.4.29, Fig.4.30, Fig.4.31 and Fig.4.32. It is noticeable from Fig.4.29 that there is not much change in reattachment length with change in turbulence intensity at very low Reynolds number. Also there is a huge decrease in reattachment length for expansion ratio 1.5 by 35% and 44% compared to expansion ratios 2 and 3 respectively for the same flow conditions. For Reynolds number 0.5×10^5 and 1×10^5 (Fig.4.30 and Fig.4.31) curves for expansion ratio 2 and 3 merges, but still, the reattachment length are comparatively lower for expansion ratio 1.5 for the same flow conditions. Also change in reattachment length with the increase in turbulence intensity becomes significant. For Reynolds number 50×10^5, as seen from Fig.4.32, the curves are showing a non-linear behaviour. From these data it can be concluded that the reattachment length decreases with decrease in expansion ratio for Re = 0.05×10^5 and 50×10^5. In contrast, the reattachment length for Re = 0.5×10^5 and 1×10^5 increases when β increases from 1.5 to 2, but does not change much with further increase in β. This behaviour remains to be explained.
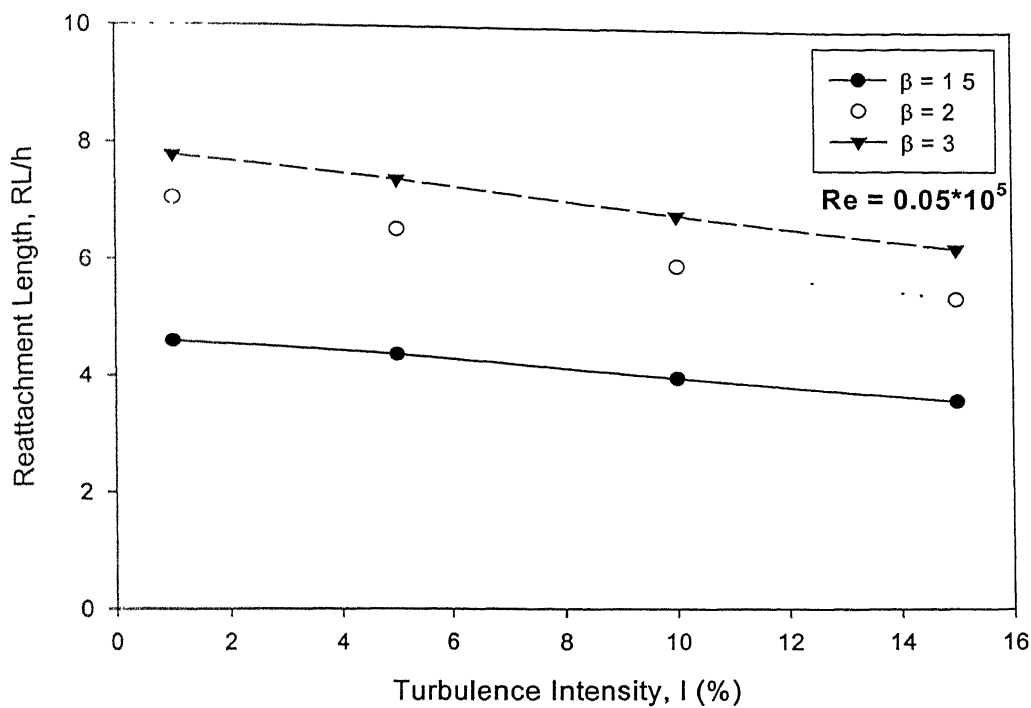
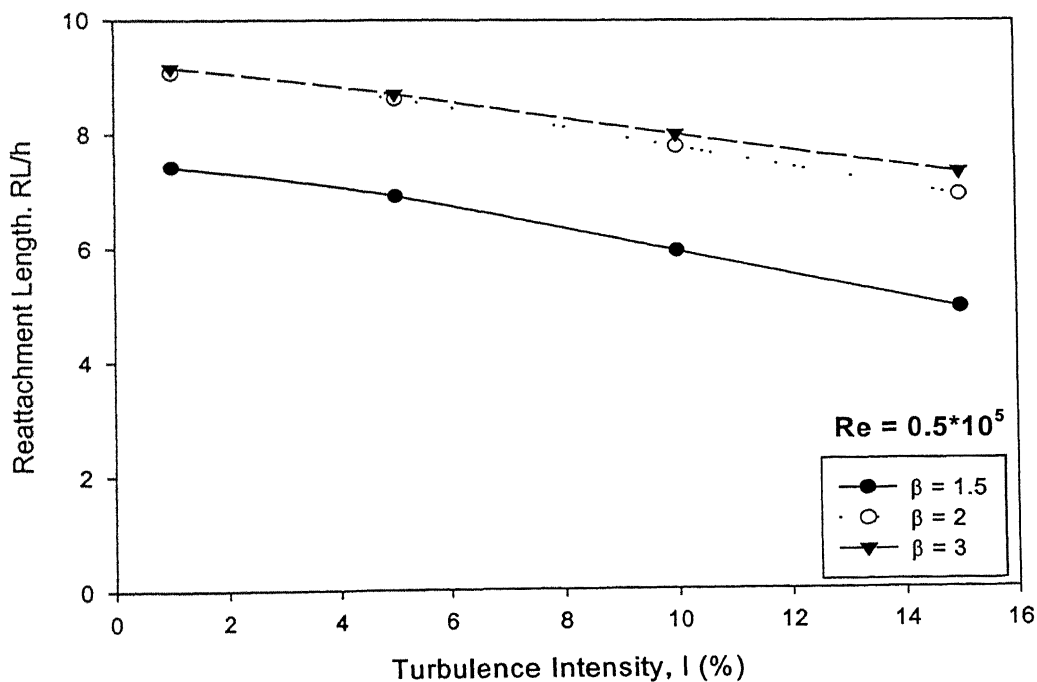**Fig. 4.29 Reattachment length variation for Reynolds Number = 0.05×10^5**

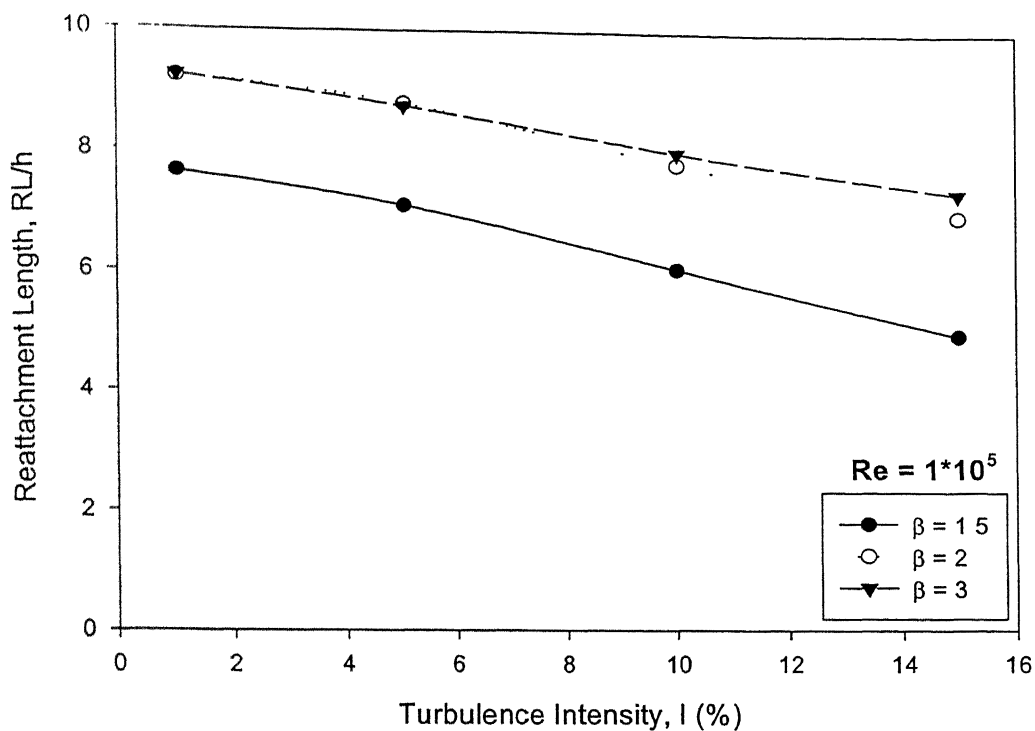**Fig. 4.30 Reattachment length variation for Reynolds Number = 0.5×10^5**

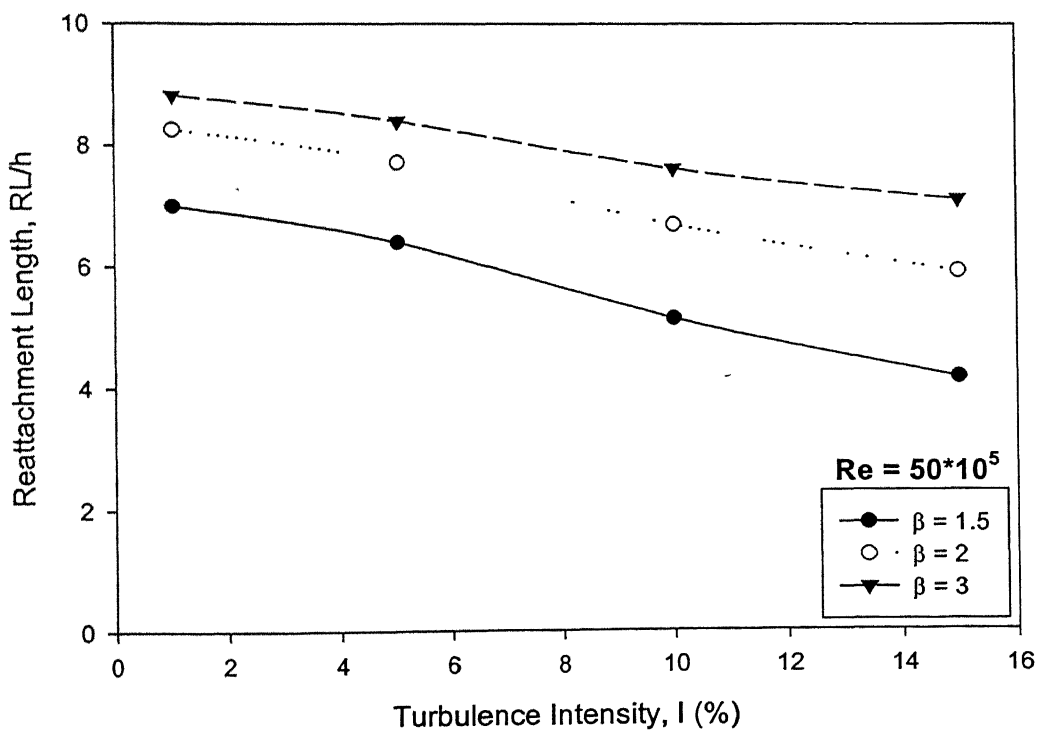**Fig. 4.31 Reattachment length variation for Reynolds Number = 1×10^5**

Fig. 4.32 Reattachment length variation for Reynolds Number = 50×10^5

From this study it is found that reattachment length decreases with the increase in inlet turbulence intensity for all parameters considered, i.e., for both the Reynolds number and expansion ratio, β, even though the magnitude may vary for each case. So inlet turbulence intensity is the single major factor governing the reattachment length and hence the recirculation size in a Dump combustor. This commensurate the findings of many previous researchers like Zemanick and Dougall (1970), Moon and Rudinger (1977) and So and Ahmed (1988, 1989). Higher turbulence intensity means, more turbulence, which, in turn enhances the mixing of fluid, and thereby provides stronger recirculation and hence decreases the reattachment length.

4.2.4 Radial Velocity

From axial velocity distribution within the flowfield it is quite clear that, inlet Reynolds number does not have much influence on the flow fields. Hence, from here onwards, only variations in expansion ratio and inlet turbulence intensity are considered as the main variable parameters in the study. Radial velocity contours for expansion ratio 1.5 at turbulence intensities 5% and 15% are given in Fig.4.33 and Fig.4.34 respectively. Radial velocity is maximum in the shear region and minimum in the recirculation region particularly very close to the wall. But the presence of a secondary recirculation zone as reported by two previous researchers [Durret et al (1988), Kangovi et al (1979)] is not detected here. The test conditions of these researchers were meant for higher Reynolds number and smaller expansion ratio than in the test conditions of the present study. This might be the reason for the formation of the secondary recirculation zone. Radial velocity contours for expansion ratio 2 at turbulence intensities 5% and 15% are shown in Fig.4.35 and Fig.4.36 respectively. It can be noted that as the expansion ratio increases the magnitude of both maximum and minimum radial velocities reduces considerably. This is also clear from Fig.4.37 and Fig.4.38, which are the radial velocity contours for expansion ratio 3 at 5% and 15% turbulent intensities respectively. It can be noted that as the shear layer reattachment occurs, the secondary boundary layer growth starts. The flow starts to become uniform, and thereafter the radial velocity magnitude becomes negligible. From the radial velocity contours the maximum and the minimum radial velocity encountered in the flowfield, normalized by inlet centerline velocity, are listed in Table.4.1.
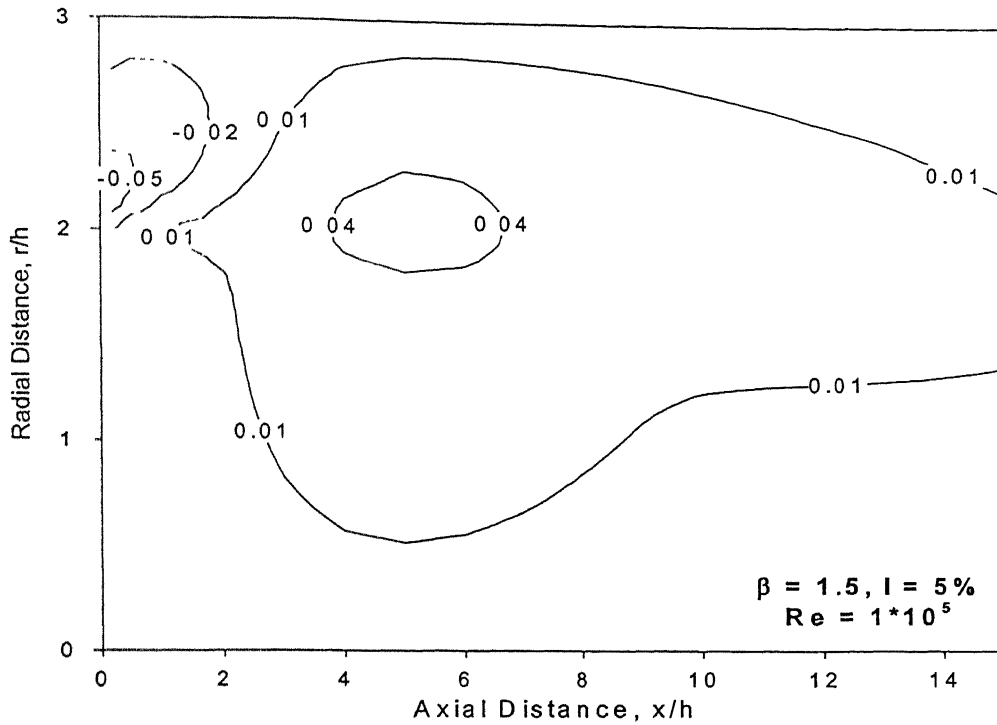
Fig. 4.33 Radial Velocity contours for Expansion Ratio = 1.5, Reynolds Number = 1×10^5, Turbulence Intensity = 5%
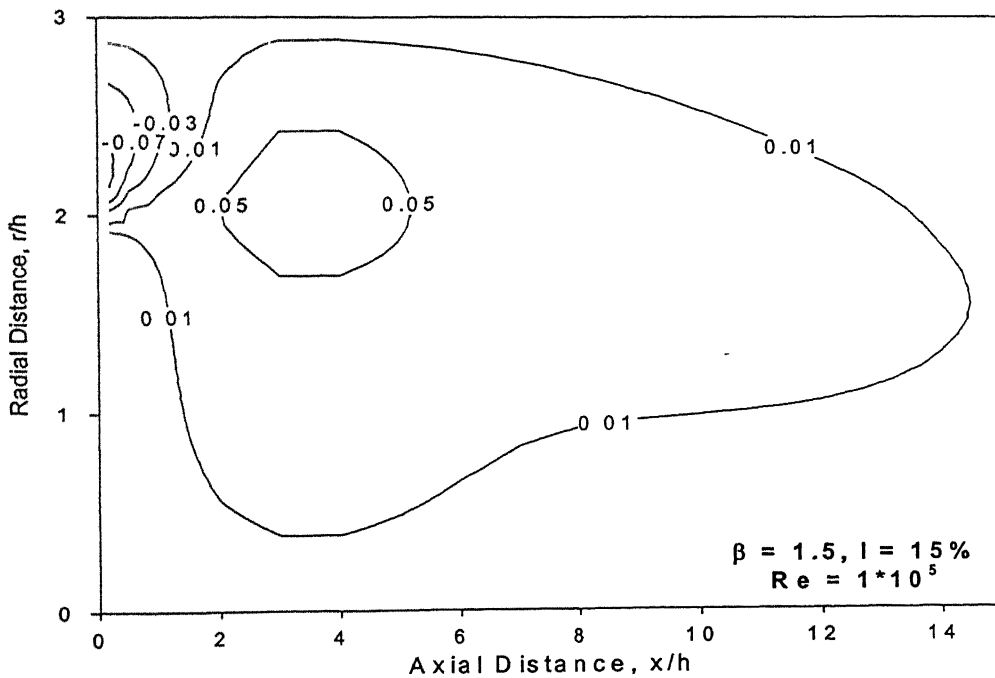

Fig. 4.34 Radial Velocity contours for Expansion Ratio = 1.5, Reynolds Number = 1×10^5, Turbulence Intensity = 15%
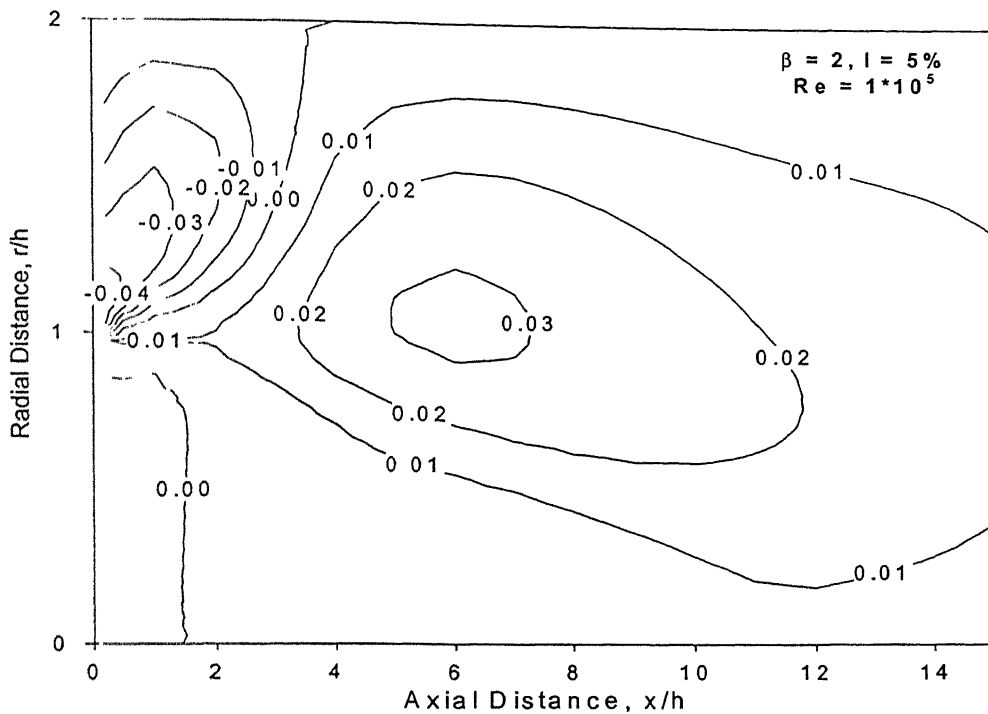
Fig. 4.35 Radial Velocity contours for Expansion Ratio = 2, Reynolds Number = 1×10^5, Turbulence Intensity = 5%
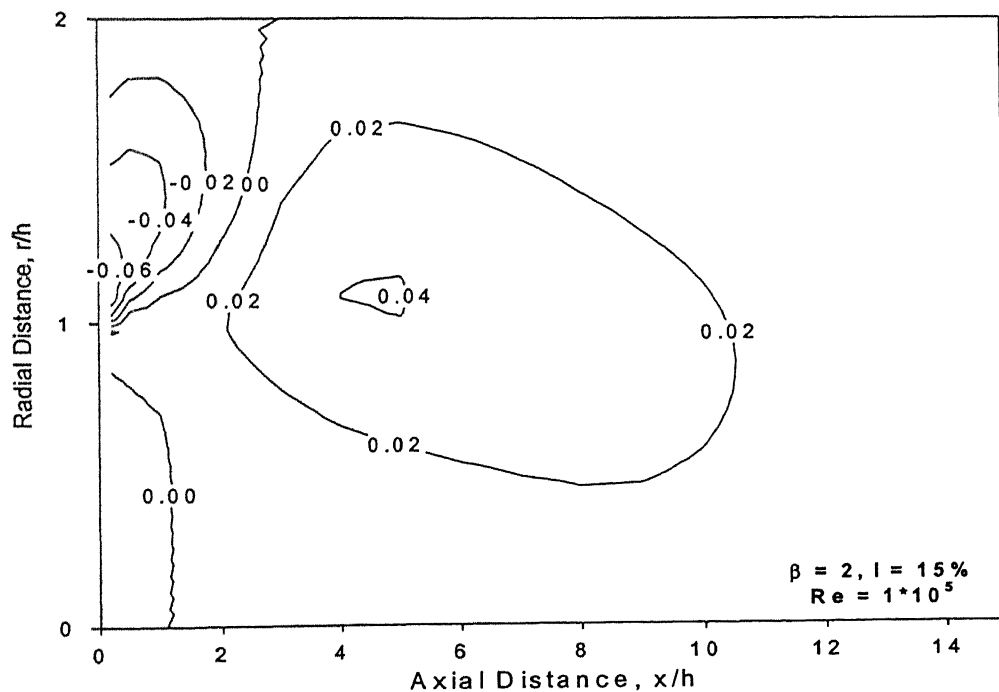

Fig. 4.36 Radial Velocity contours for Expansion Ratio = 2, Reynolds Number = 1×10^5, Turbulence Intensity = 15%
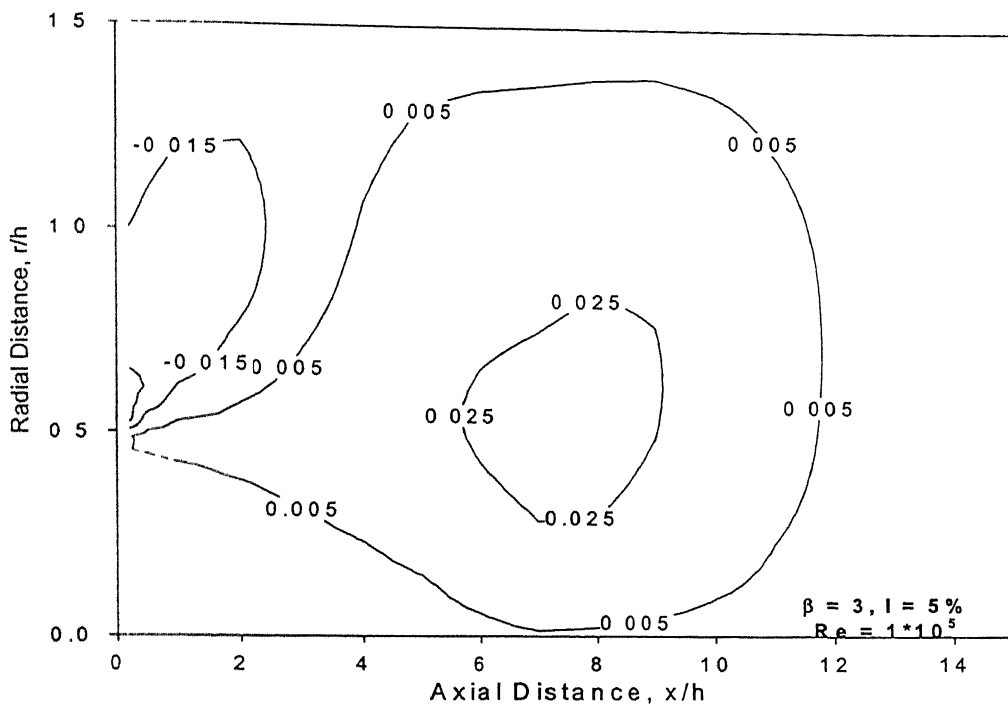
Fig. 4.37 Radial Velocity contours for Expansion Ratio = 3, Reynolds Number = 1×10^5, Turbulence Intensity = 5%
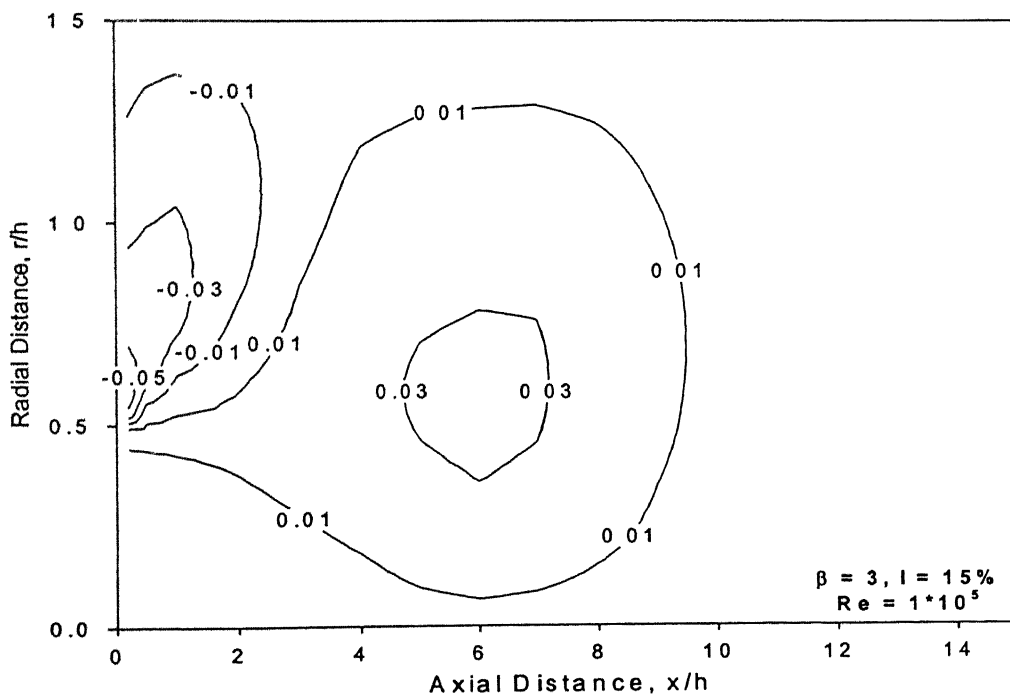

Fig. 4.38 Radial Velocity contours for Expansion Ratio = 3, Reynolds Number = 1×10^5, Turbulence Intensity = 15%

Table.4.3 Variation in Radial Velocity Magnitudes in the Flowfield with the Expansion Ratio and Turbulence Intensity

Expansion Ratio	Turbulence Intensity, I (%)	Radial Velocity, v/U_0	
		Maximum	Minimum
1.5	5	0.046	-0.059
	15	0 066	-0.119
2	5	0.032	-0.047
	15	0 040	-0.073
3	5	0 030	-0.041
	15	0.033	-0.061

It can be noted that with the increase in turbulence intensity the magnitude of both maximum and minimum radial velocities are increasing. However, for expansion ratio 3, there is not much significant difference between radial velocities at different intensities. It can be concluded that, with the increase in expansion ratio, the effect of increase in turbulence intensity on the flowfield reduces considerably. It can be noted that similar trend is observed in axial velocity profile study.

4.2.5 Static Pressure

A study on wall static pressure distribution is made in this section. Pressure has been normalised with inlet dynamic pressure, $(\rho U_0^2/2)$. Wall static pressure distribution along the axial direction is shown for expansion ratios 1.5, 2 and 3 in Fig.4.39, Fig.4.40 and Fig.4.41 respectively. On sudden expansion pressure reduces, keeps constant for some downstream distance and then a sudden increase occurs. This is in agreement with the findings of Kangovi and Page (1979). It can be noted that zero crossing occurs before the reattachment point. Also with the increase in turbulence intensity the zero crossing occurs well upstream than in the lower turbulence intensities. Minimum pressure is also high in the case of larger intensities, which means larger suction force and a stronger recirculation zone. For expansion ratio of 1.5 the zero crossing occurs at 2.8h and 2.1 h for I= 5% and I=15% respectively. For β=2, it occurs at 3.15h and 2.7h respectively. For β=3, it is 3.5 and 3.1h respectively. Even though zero crossing is delayed in the case of

larger expansion ratios, uniform static pressure is achieved in the case of larger expansion ratios at a much shorter distance than that in the smaller expansion ratios.
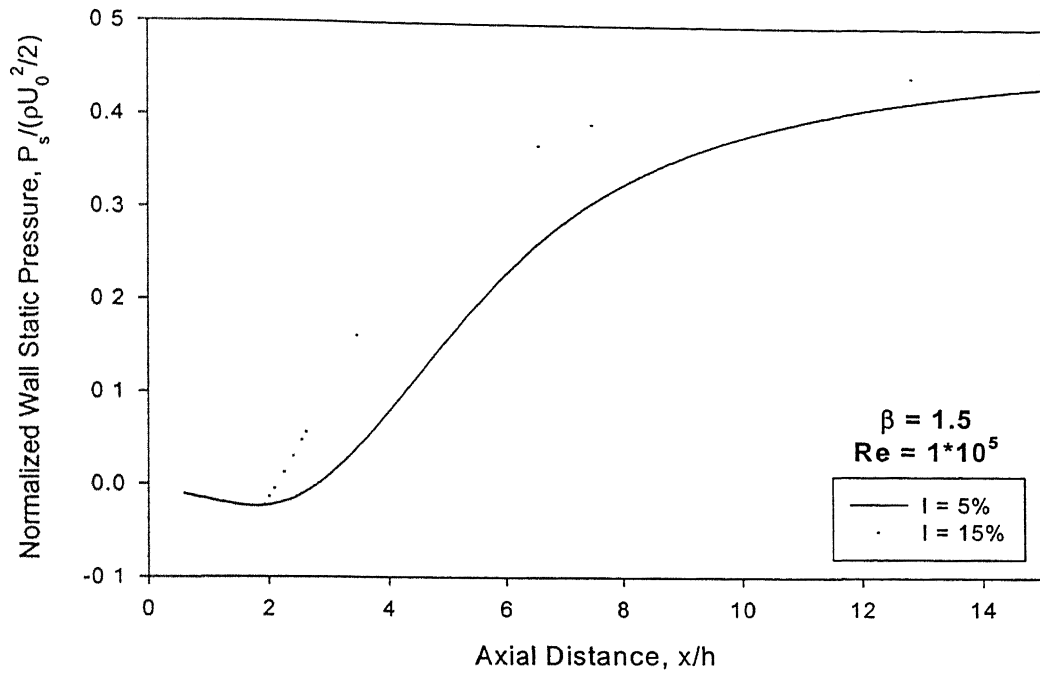

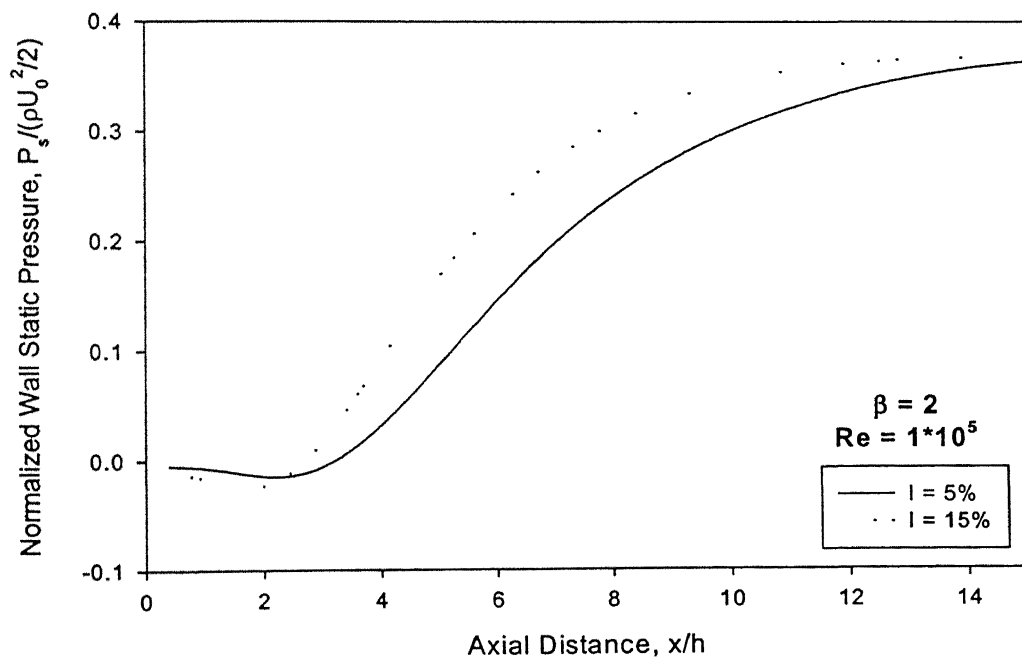Fig. 4.39 Wall Static Pressure for Expansion Ratio = 1.5, Reynolds Number = 1×10^5

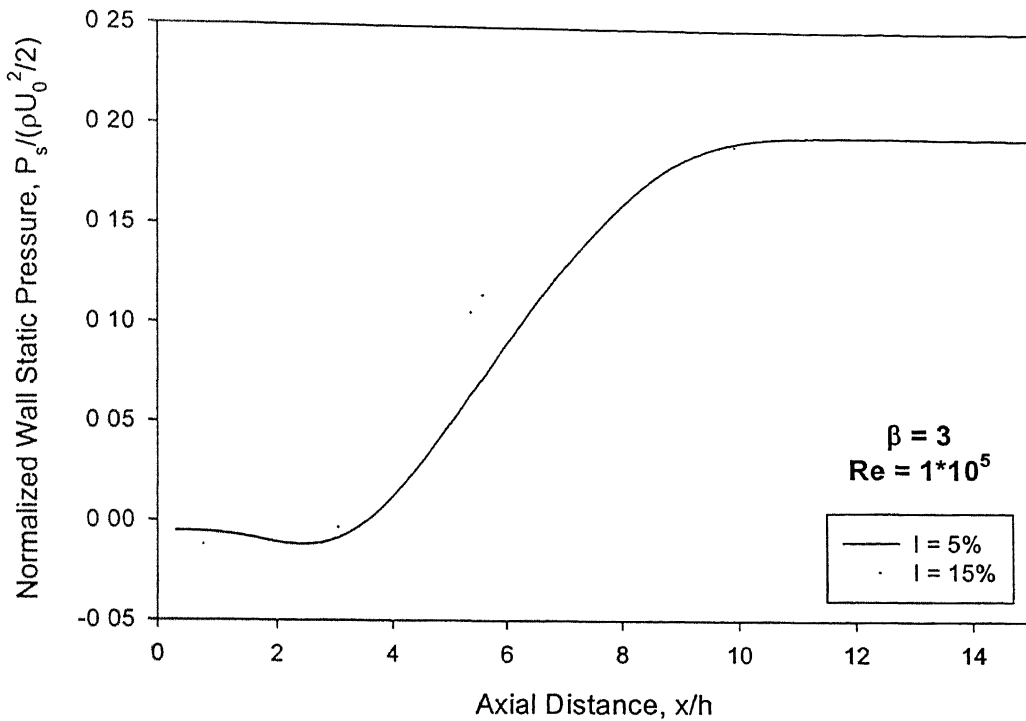Fig. 4.40 Wall Static Pressure for Expansion Ratio= 2, Reynolds Number= 1×10^5

Fig. 4.41 Wall Static Pressure for Expansion Ratio= 3, Reynolds Number= 1×10^5

4.2.6 Turbulent Kinetic Energy

Turbulent kinetic energy, which is an important quantity governing turbulent flowfield, is discussed in this section. Since velocity determines the magnitude of kinetic energy, two different Reynolds numbers have been considered for the analysis. Turbulent kinetic energy has been normalised by maximum kinetic energy encountered in the corresponding flow field. The maximum turbulent kinetic energy clearly followed the dividing streamline, where strong production of turbulence is expected. First, turbulent energy distribution at Reynolds number 1×10^5 is considered. Turbulent kinetic energy contours for an expansion ratio of 1.5 at turbulence intensities 5% and 15% are shown in Fig.4.42 and Fig.4.43 respectively. Turbulent kinetic energy contours for an expansion ratio of 2 at turbulence intensities 5% and 15% are shown in Fig.4.44 and Fig.4.45 respectively. Turbulent energy contours for an expansion ratio of 3 at turbulence intensities 5% and 15% are shown in Fig.4.46 and Fig.4.47 respectively. It is observed

that the maximum turbulent kinetic energy region moves upstream for higher turbulent intensities Also the maximum kinetic energy for higher turbulence intensities is lower than that of lower turbulence intensities. This may be due to the fact that at high turbulence intensities fluctuation velocities in axial and radial directions are higher; these velocity components diffuse the turbulent kinetic energy out of the shear layer towards the recirculation region and the central core region (Yang and Yu, 1983). This will in turn increases the velocity components in the axial and radial directions within the recirculation region. This might be the reason why the shorter and stronger reattachment lengths and shorter potential core at higher intensities have been observed. Turbulent kinetic energy distribution at Reynolds number, 50×10^5 is also studied. Turbulent energy contours for an expansion ratio of 1.5 at turbulence intensities 5% and 15% are shown in Fig.4.48 and Fig.4.49 respectively. Turbulent energy contours for an expansion ratio of 2 at turbulence intensities 5% and 15% are shown in Fig.4.50 and Fig.4.51 respectively. Turbulent energy contours for an expansion ratio of 3 at turbulence intensities 5% and 15% are shown in Fig.4.52 and Fig.4.53 respectively. It can be noted that, at higher Reynolds numbers the maximum kinetic energy region in the shear layer is more developed or expanded than that in the case of lower Reynolds numbers. This region extends even within the recirculation zone in the radial direction. This might be the reason for getting slightly shorter recirculation size for the Reynolds number 50×10^5. It is also more distributed in the axial direction compared to the lower Reynolds number value considered which is 1×10^5. For both the Reynolds number considered, the high kinetic energy region occurred in the shear layer, where the velocity gradients are very large. However the peak kinetic energy calculated was very near to the inlet where the separation of the shear layer starts. But this kinetic energy diminishes in magnitude within one-step height from the dump plane.
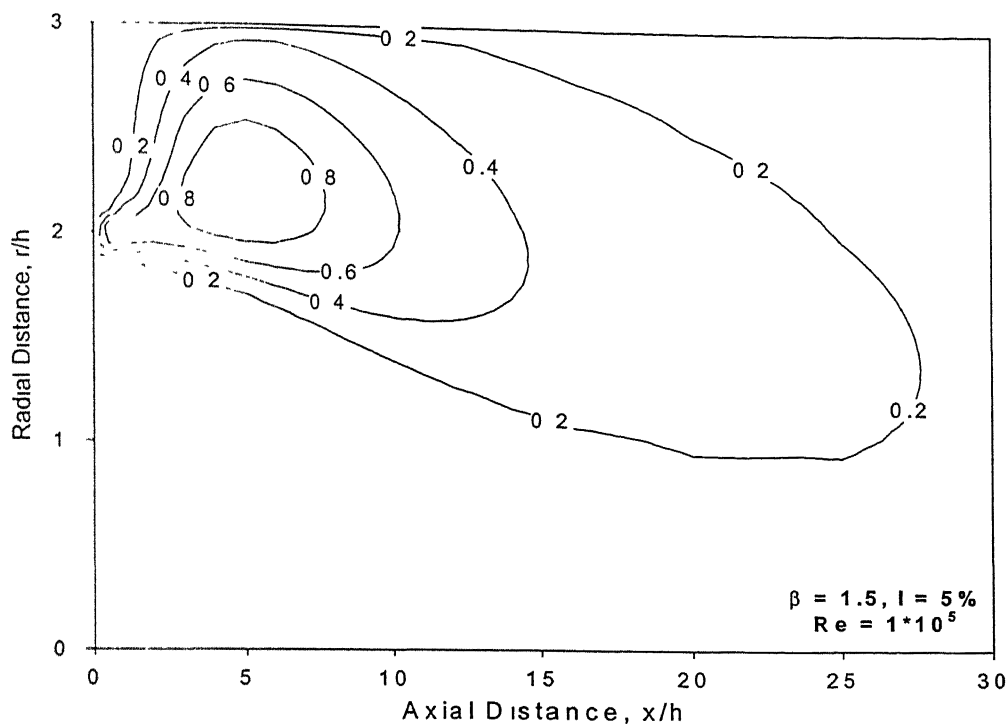
Fig. 4.42 Normalised Turbulent Kinetic Energy contours for Expansion Ratio = 1.5, Reynolds Number = 1×10^5, Turbulence Intensity = 5%

Fig. 4.43 Normalised Turbulent Kinetic Energy contours for Expansion Ratio = 1.5, Reynolds Number = 1×10^5, Turbulence Intensity = 15%
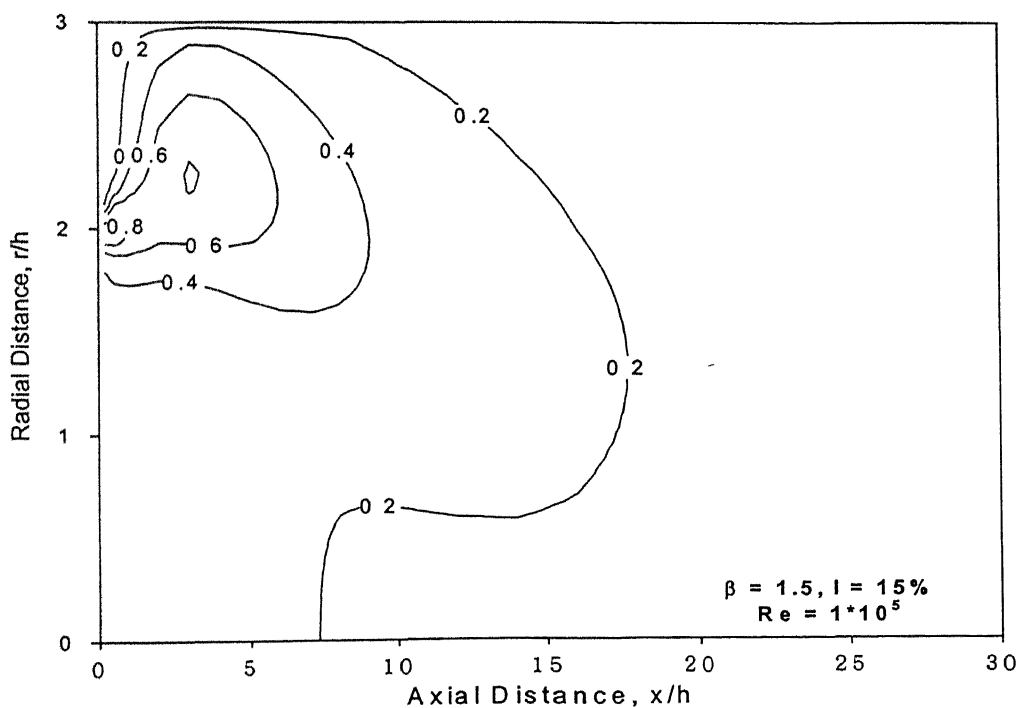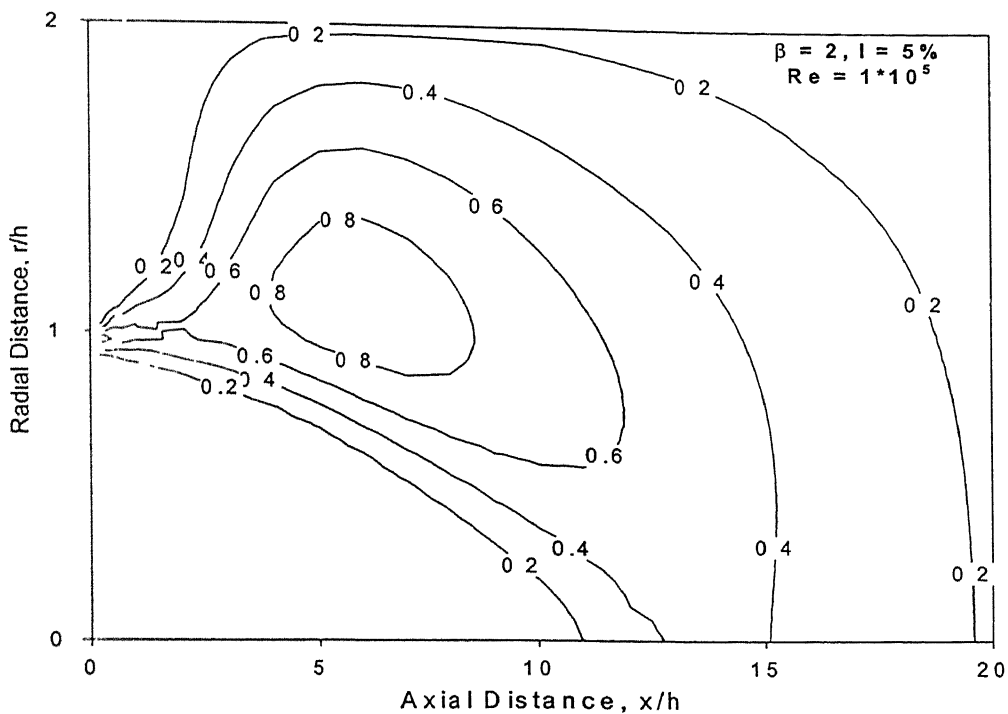
Fig. 4.44 Normalised Turbulent Kinetic Energy contours for Expansion Ratio = 2, Reynolds Number = 1×10⁵, Turbulence Intensity = 5%
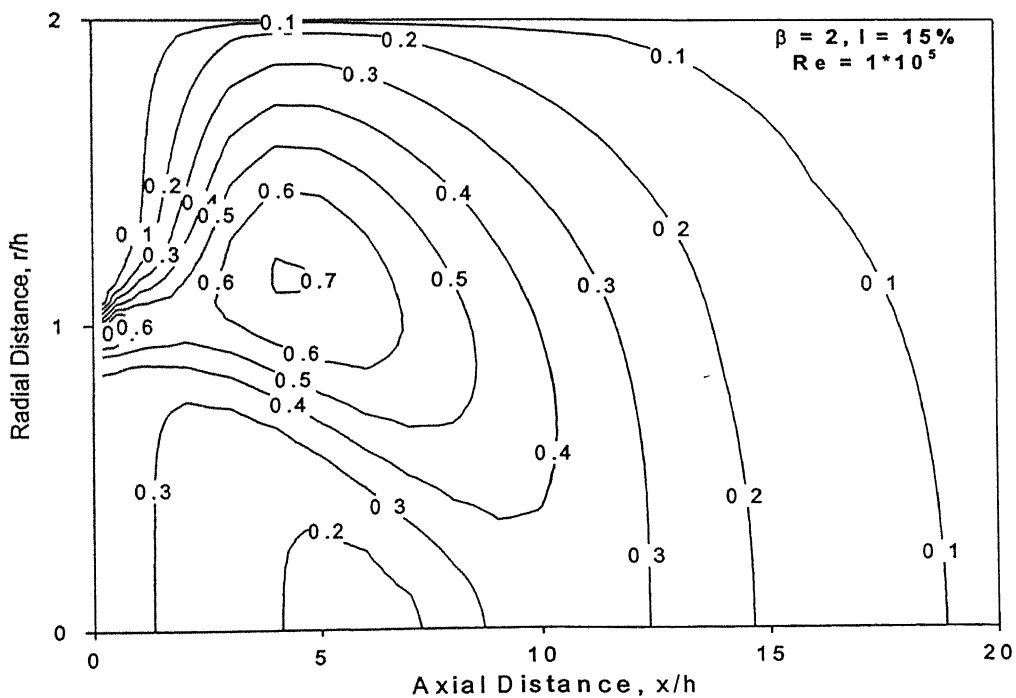

Fig. 4.45 Normalised Turbulent Kinetic Energy contours for Expansion Ratio = 2, Reynolds Number = 1×10⁵, Turbulence Intensity = 15%
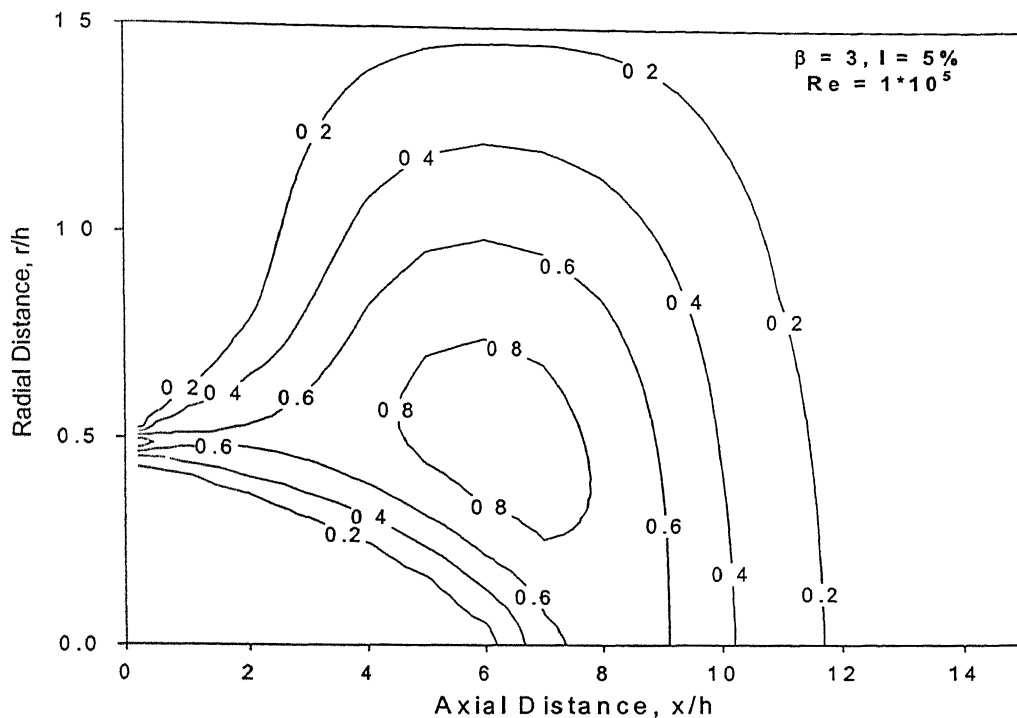
67

Fig. 4.46 Normalised Turbulent Kinetic Energy contours for Expansion Ratio = 3, Reynolds Number = 1×10⁵, Turbulence Intensity = 5%
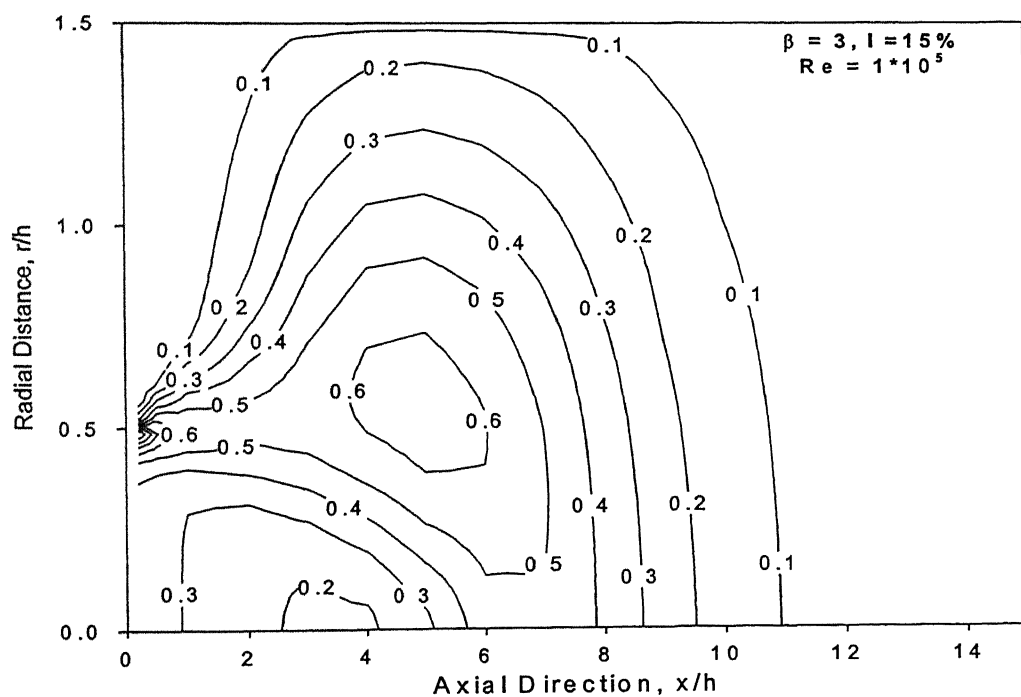

Fig. 4.47 Normalised Turbulent Kinetic Energy contours for Expansion Ratio = 3, Reynolds Number = 1×10⁵, Turbulence Intensity = 15%
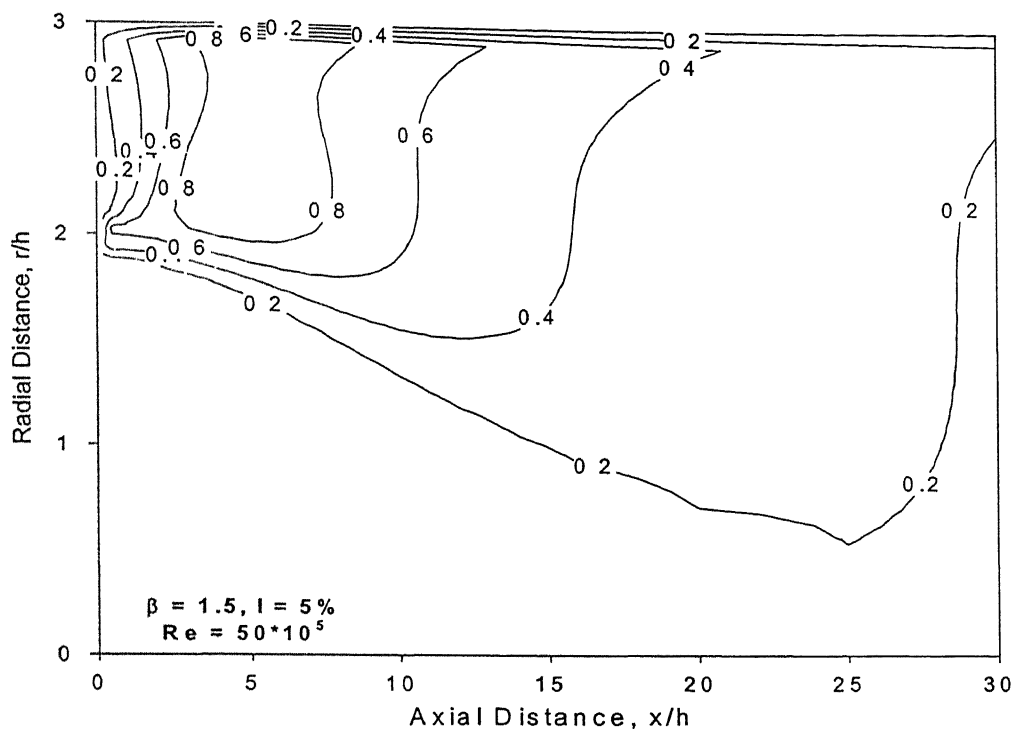
Fig. 4.48 Normalised Turbulent Kinetic Energy contours for Expansion Ratio = 1.5, Reynolds Number = 50×10^5, Turbulence Intensity = 5%

Fig. 4.49 Normalised Turbulent Kinetic Energy contours for Expansion Ratio = 1.5, Reynolds Number = 50×10^5, Turbulence Intensity = 15%

Fig. 4.50 Normalised Turbulent Kinetic Energy contours for Expansion ratio = 2, Reynolds Number = 50×10^5, Turbulence Intensity = 5%
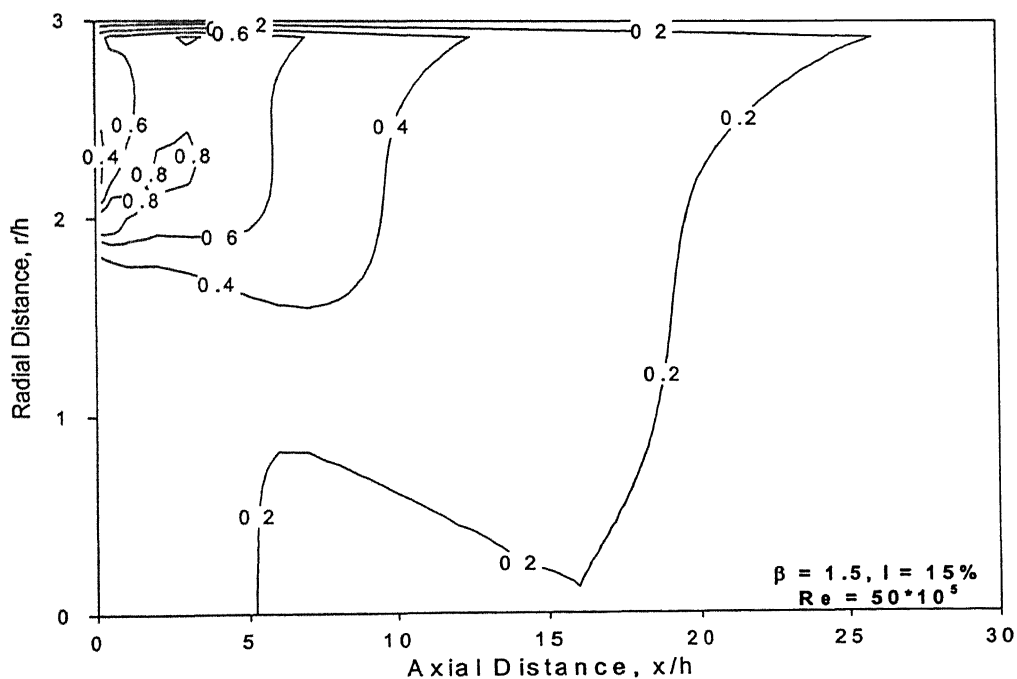

Fig. 4.51 Normalised Turbulent Kinetic Energy contours for Expansion Ratio = 2, Reynolds Number = 50×10^5, Turbulence Intensity = 15%
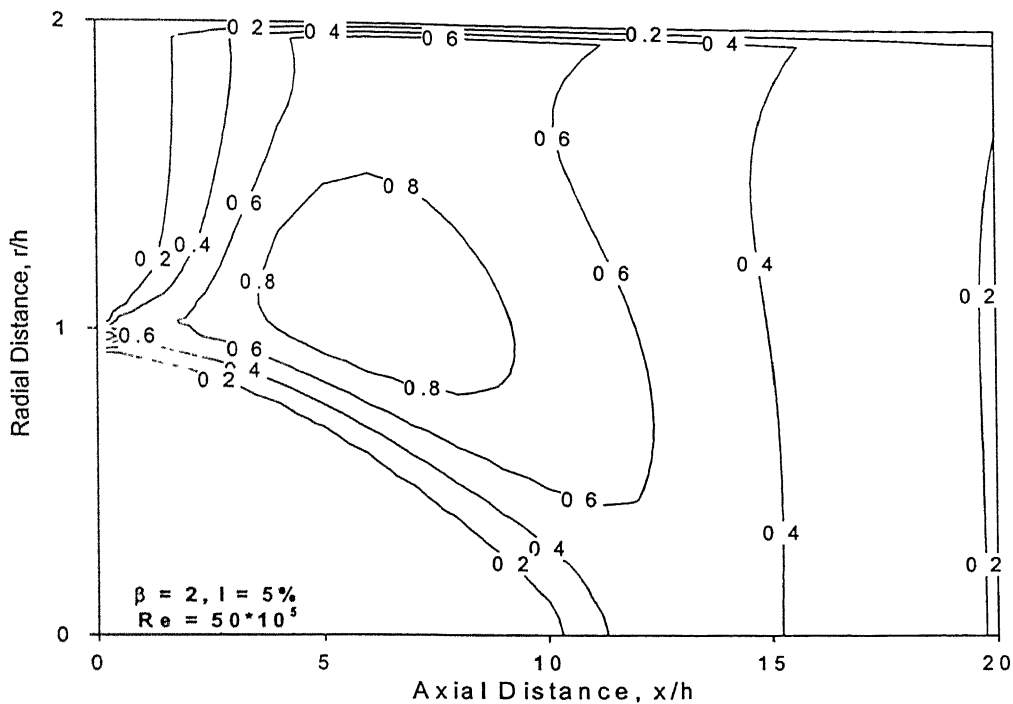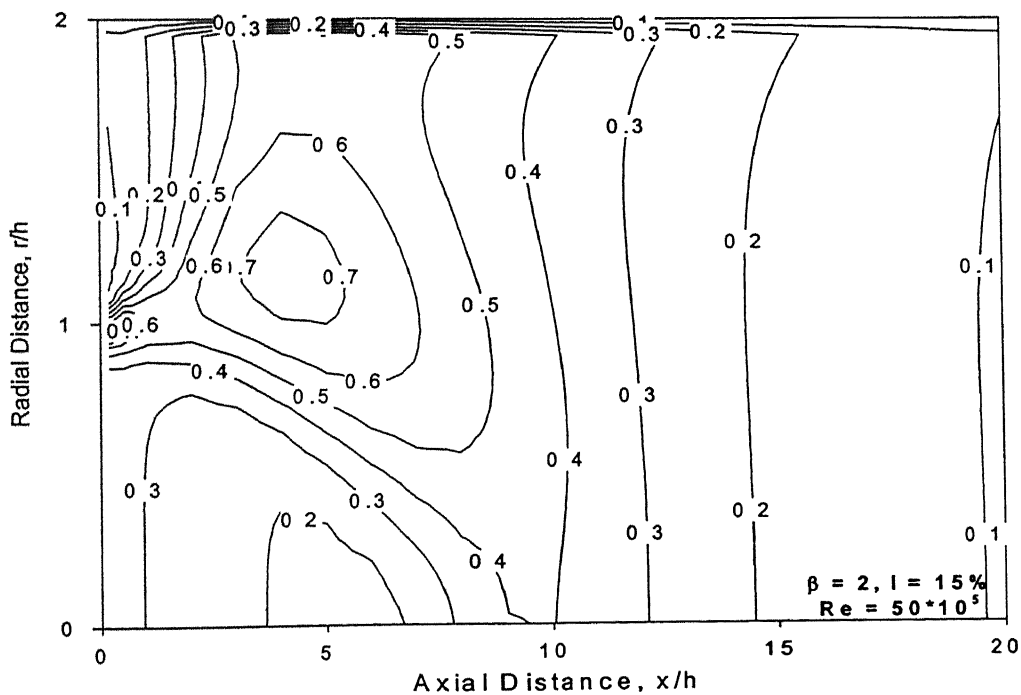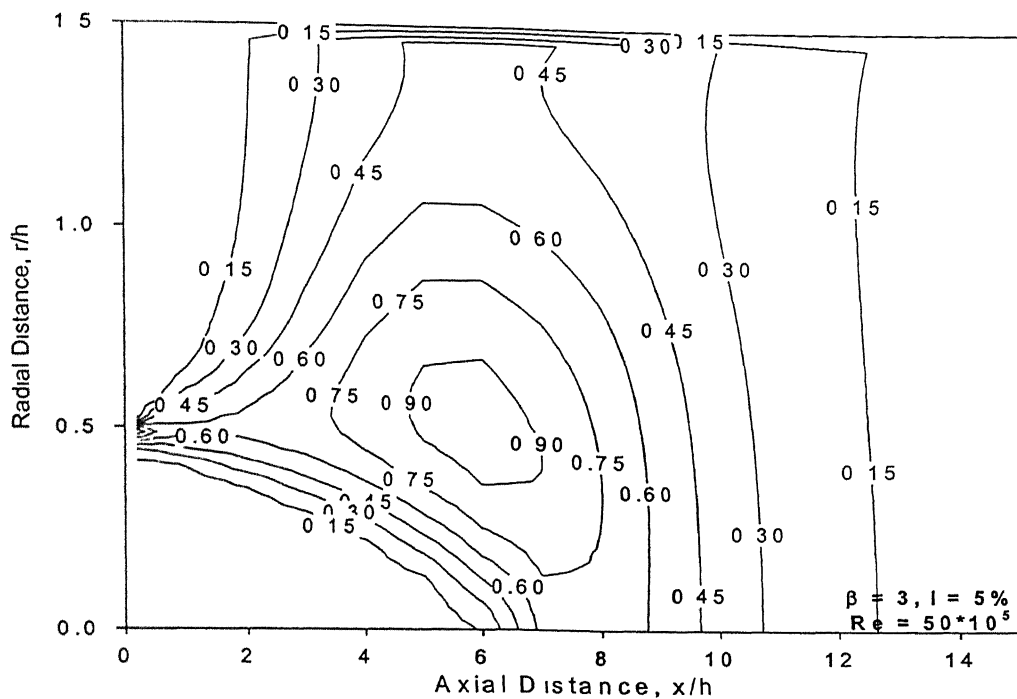
70

Fig. 4.52 Normalised Turbulent Kinetic Energy contours for Expansion Ratio = 3, Reynolds Number = 50×10^5, Turbulence Intensity = 5%

Fig. 4.53 Normalised Turbulent Kinetic Energy contours for Expansion Ratio = 3, Reynolds Number = 50×10^5, Turbulence Intensity = 15%
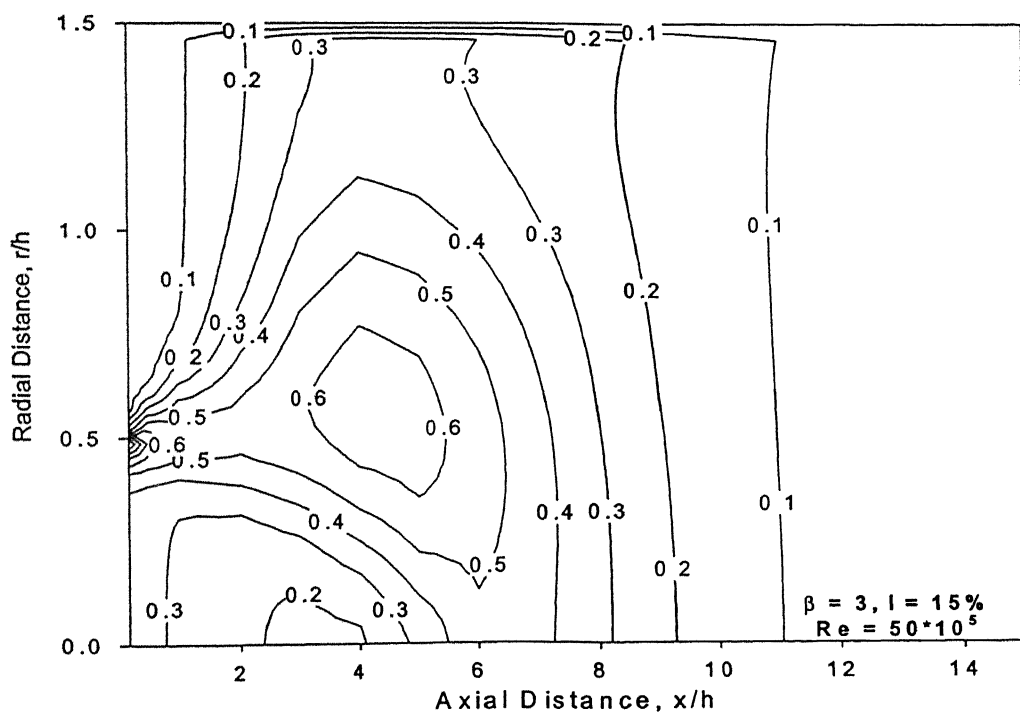
4.2.7 Turbulent Dissipation Rate

Turbulent dissipation rate, which is a measure of dissipation of turbulent quantities, is predominant in the shear layer, where high turbulent intensity is expected Turbulent dissipation has been normalised by maximum turbulent dissipation rate encountered in the corresponding flow field. Turbulent dissipation rate for expansion ratio 1 5 at turbulence intensities of 5% and 15% is given in Fig.4 54 and Fig.4.55 respectively. Fig.4.56 and Fig.4.57 show contours of the same for an expansion ratio 2 at turbulence intensities 5% and 15% respectively. Dissipation rate is also significant very close to the wall for expansion ratios 1.5 and 2, whereas it is not so in the case of expansion ratio 3. This is evident from Fig.4.58 and Fig.4.59, which are drawn for expansion ratio 3, at turbulence intensities of 5% and 15% respectively. Peak value is obtained at a distance within one-step height of the dump plane. For higher turbulence intensities the very high values of turbulent dissipation rate are obtained close to the dump plane, where as it is shifted little bit in the downstream direction for smaller turbulence intensities.

4.2.8 Concluding Remarks

An extensive study on cold flow inside a dump combustor is made. Highly turbulent flow field inside the combustor is solved using k-ε turbulence model. Results were compared with experimental results for the validation of the code. Among various flow and geometrical parameters considered for finding the influence of each of these on flowfield, the inlet turbulence intensity is found to be the most dominant parameter determining the flowfield. This in turn affects the axial velocities, radial velocities, static pressure, turbulent kinetic energy and turbulent dissipation rate. However this effect is found to be decreasing with the increase in the expansion ratio. Increase in turbulence intensity increases the level of turbulence and in turn increases the magnitude of axial and radial velocities inside the recirculation region. This helps in reducing the reattachment length. It also helps in attaining uniform flow at a shorter axial distance. It is also found from axial velocity studies that inlet Reynolds number is not an important parameter governing the flowfield. From static pressure studies it is clear that maximum pressure recovery occurs only well downstream of the reattachment point. Both the turbulent kinetic energy and the turbulent dissipation rate are found to be maximum in the shear layer and this also keep increasing with the increase in turbulence intensity.
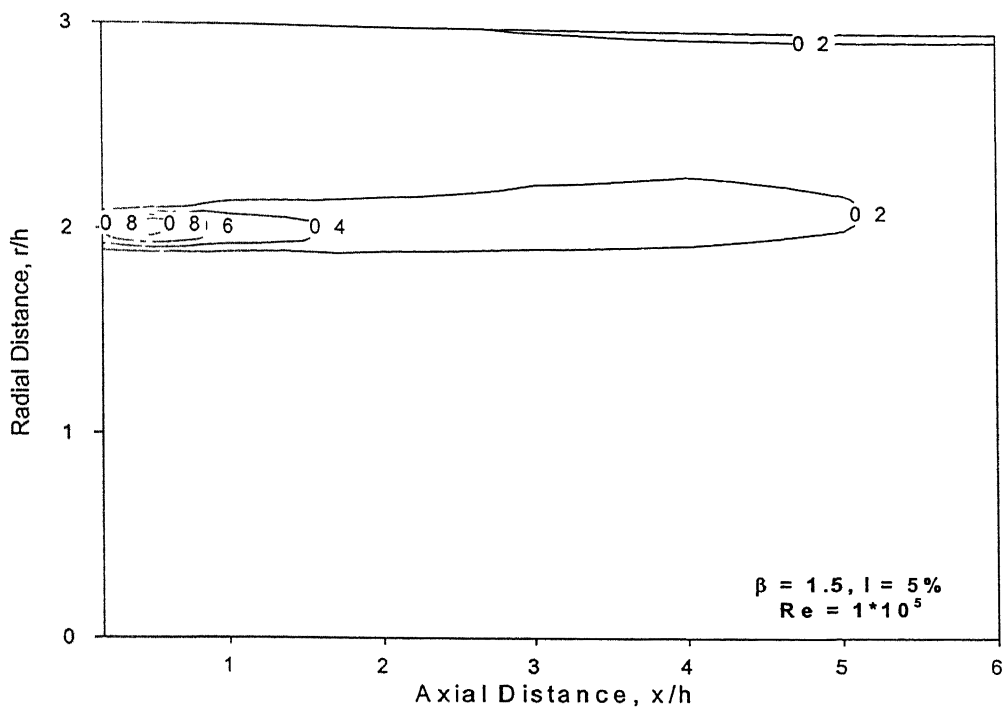
Fig. 4.54 Normalised Turbulent Dissipation Rate contours for Expansion Ratio = 1.5, Reynolds Number = 1×10^5, Turbulence Intensity = 5%

Fig. 4.55 Normalised Turbulent Dissipation Rate contours for Expansion Ratio = 1.5, Reynolds Number = 1×10^5, Turbulence Intensity = 15%
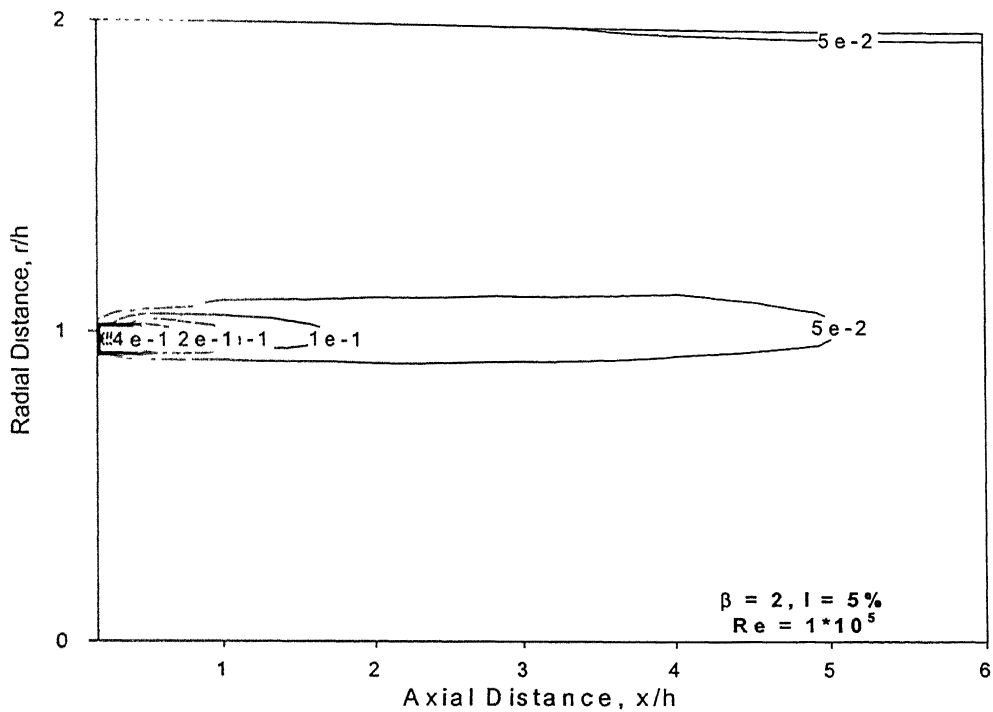
Fig. 4.56 Normalised Turbulent Dissipation Rate contours for Expansion Ratio = 2, Reynolds Number = 1×10^5, Turbulence Intensity = 5%

Fig. 4.57 Normalised Turbulent Dissipation Rate contours for Expansion Ratio = 2, Reynolds Number = 1×10^5, Turbulence Intensity = 15%
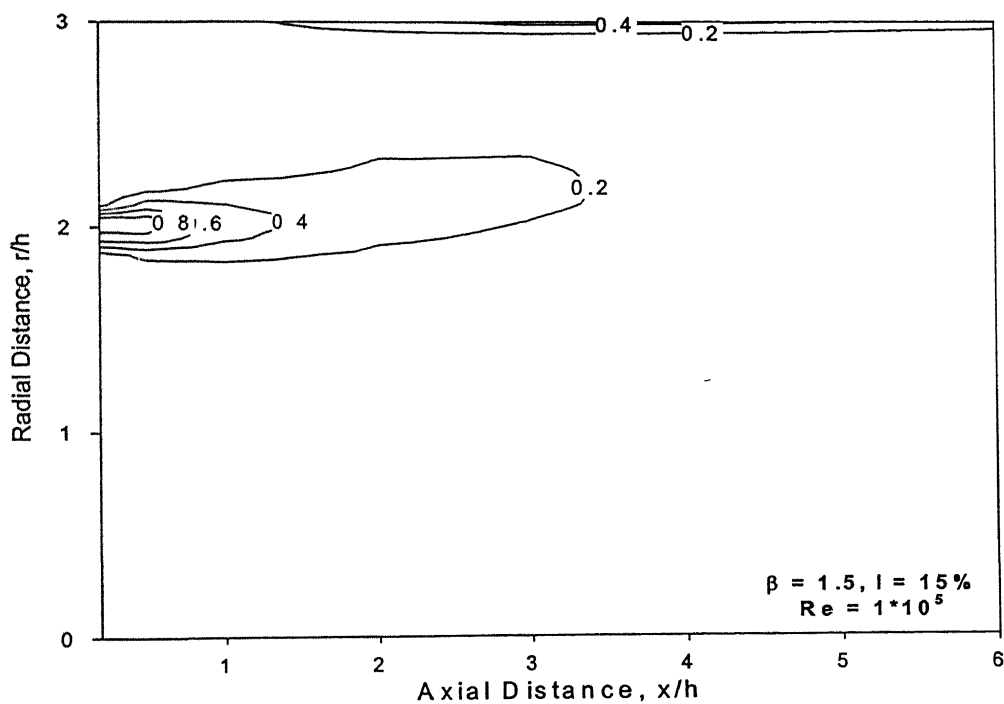
Fig. 4.58 Normalised Turbulent Dissipation Rate contours for Expansion Ratio = 3, Reynolds Number = 1×10⁵, Turbulence Intensity = 5%

Fig. 4.59 Normalised Turbulent Dissipation Rate contours for Expansion Ratio = 3, Reynolds Number = 1×10⁵, Turbulence Intensity = 15%
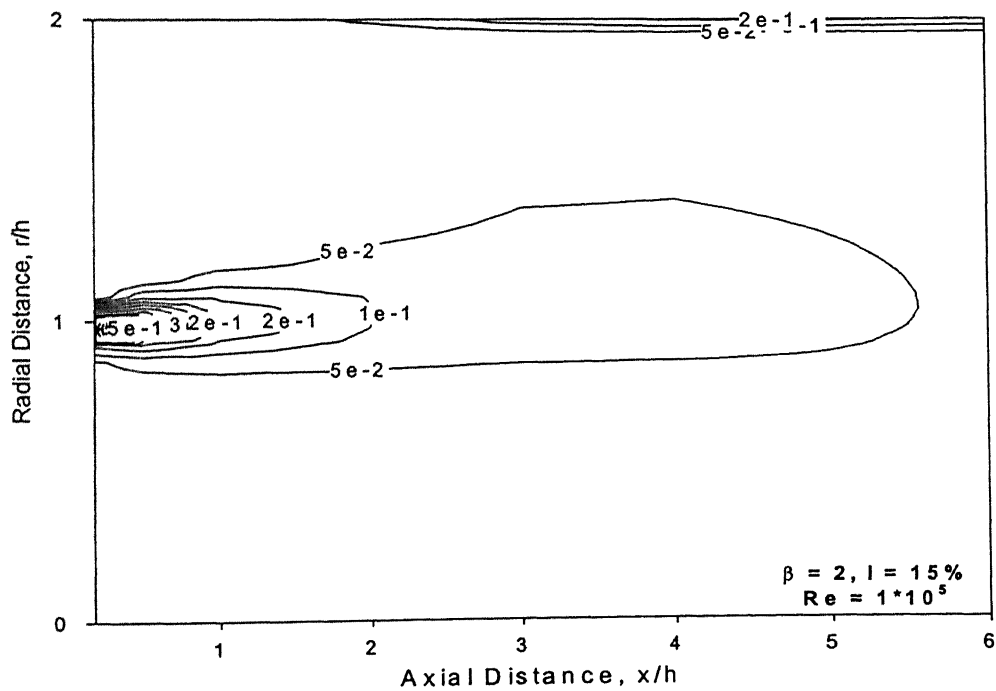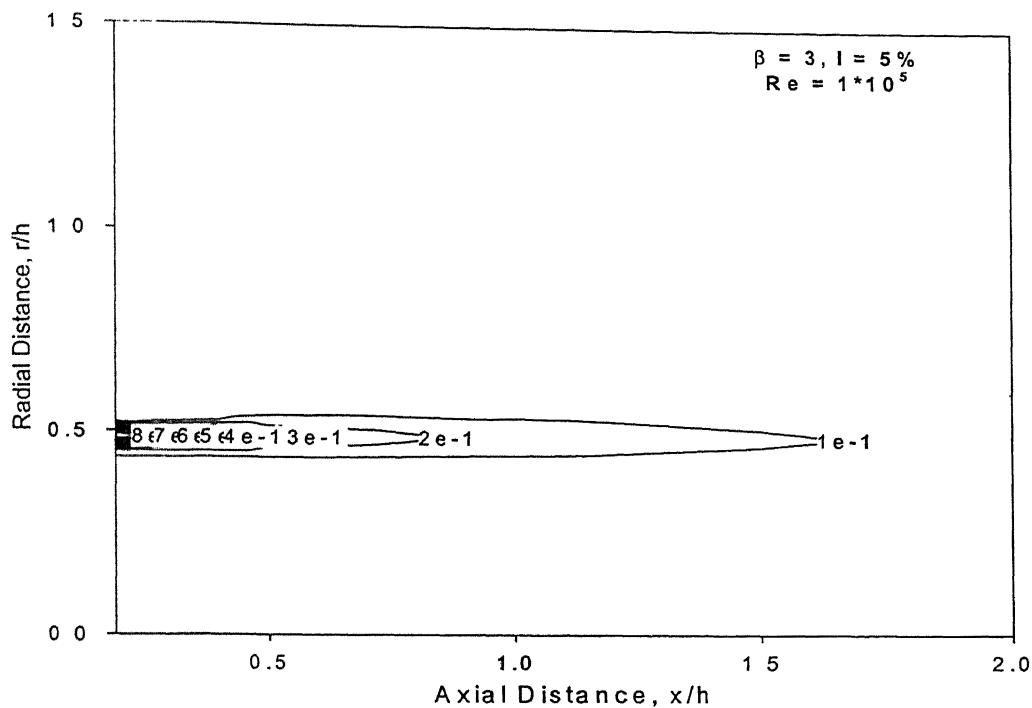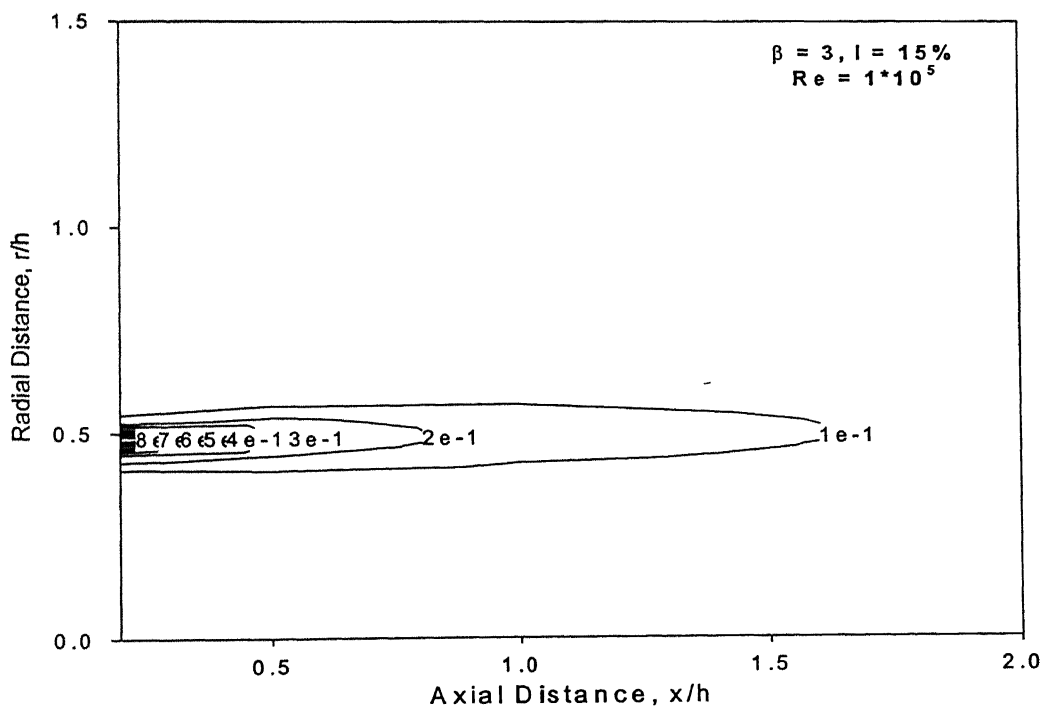
CHAPTER 5

REACTING FLOW

A study on turbulent reacting flow inside the dump combustor is presented in this chapter. A range of turbulence intensities, and geometries were tested with propane-air mixture at different equivalence ratios. The reacting flow has been modelled using fast chemistry Eddy Dissipation Concept (EDC). This study has been divided into three parts. The first part, comparing numerical predictions with the measured values from an experimental test case, which is exactly simulated, makes validation of the results. In the second part the effect of various flow and geometrical parameters that affect the reacting flowfield is studied. In the last part a comparison between the cold and reacting flow cases is made.

5.1 Comparison With Experimental Data

Numerical simulation of reacting flow is compared with the experimental work of Gould et al (1994). The geometrical and flow conditions exactly as in their work has been simulated for propane-air mixture with an overall equivalence ratio of 0.5 for β = 2. The axial velocity and the static temperature measured are compared with the present numerical results obtained. The axial velocity profiles at x=1h and 5h are shown in Fig.5.1 and Fig.5.2 respectively. The axial velocity is normalised with the inlet centerline velocity, U_0 for Reynolds number, Re = 1.15×10^5. It can be noted that the central core region at all axial locations virtually unchanged from that of the experimental case because the temperature in this region was near the inlet temperature. As the flow proceeds towards the wall, there is a considerable change in the profiles. The same trend persist for the static temperature profiles also, which in given in Fig.5.3 for x=1h and in Fig.5.4 for x=5h. Static temperatures have been normalised with inlet temperature, T_0, which, is 298 K. The shift in this trend may be attributed to the effect of heat transfer through the wall and the effect of turbulence intensity, which is a predominant force affecting the flow regime within the recirculation zone. It can be noted that, the comparison is only on the basis of quality, since, in the simulation, adiabatic wall conditions has been selected through out, and the inability of the

numerical predictions to account various dissipation losses associated with the actual combustion process.
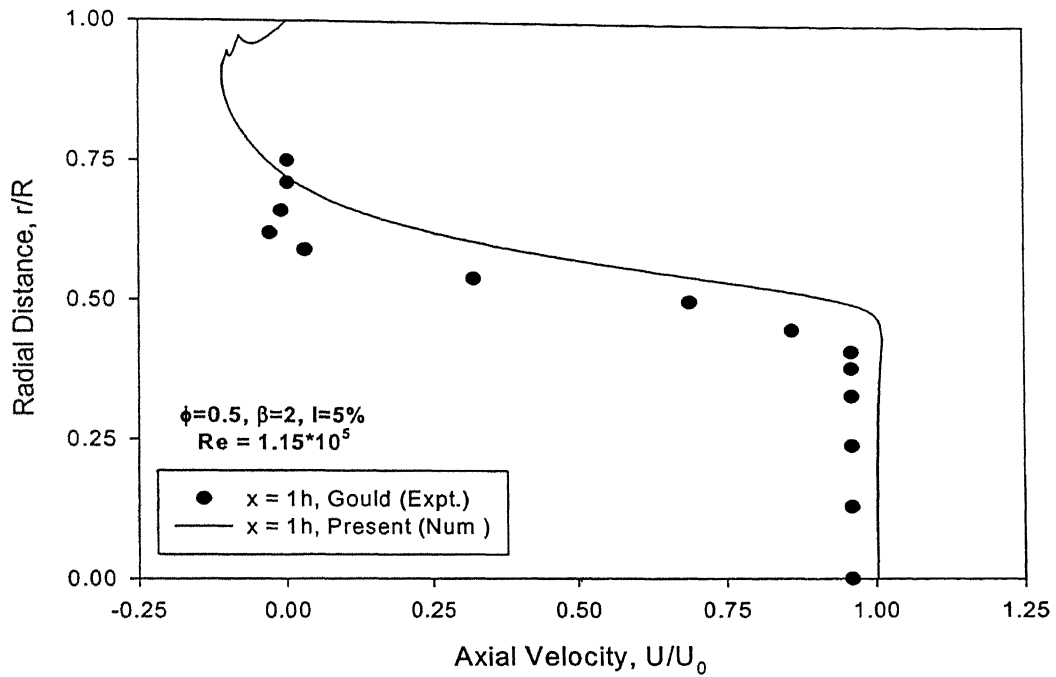

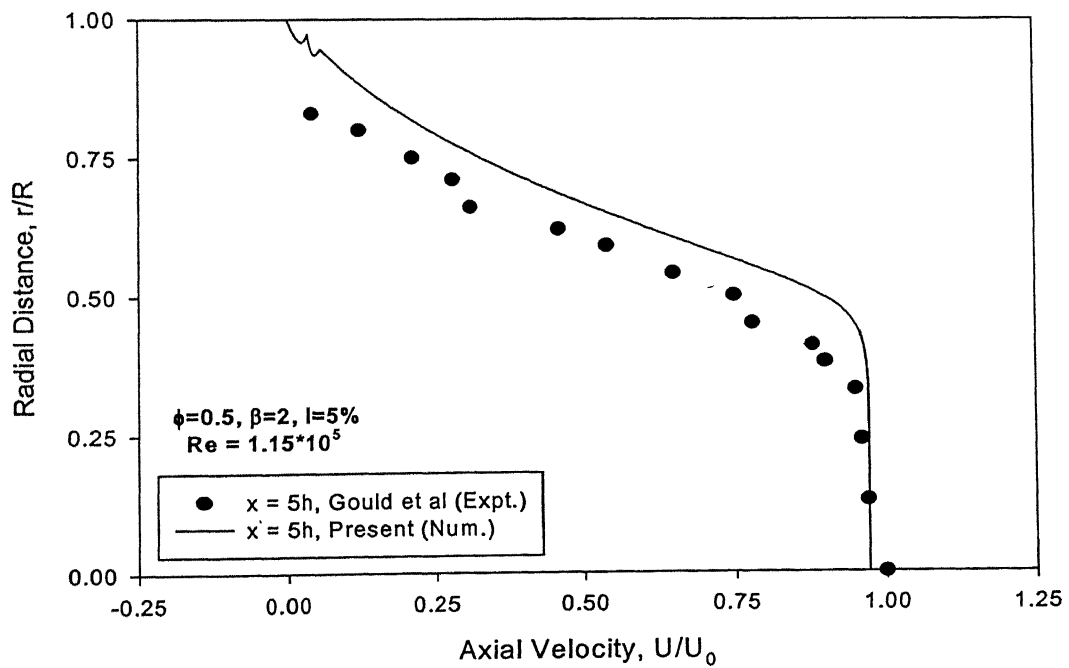**Fig.5.1 Axial velocity profiles at x = 1h**
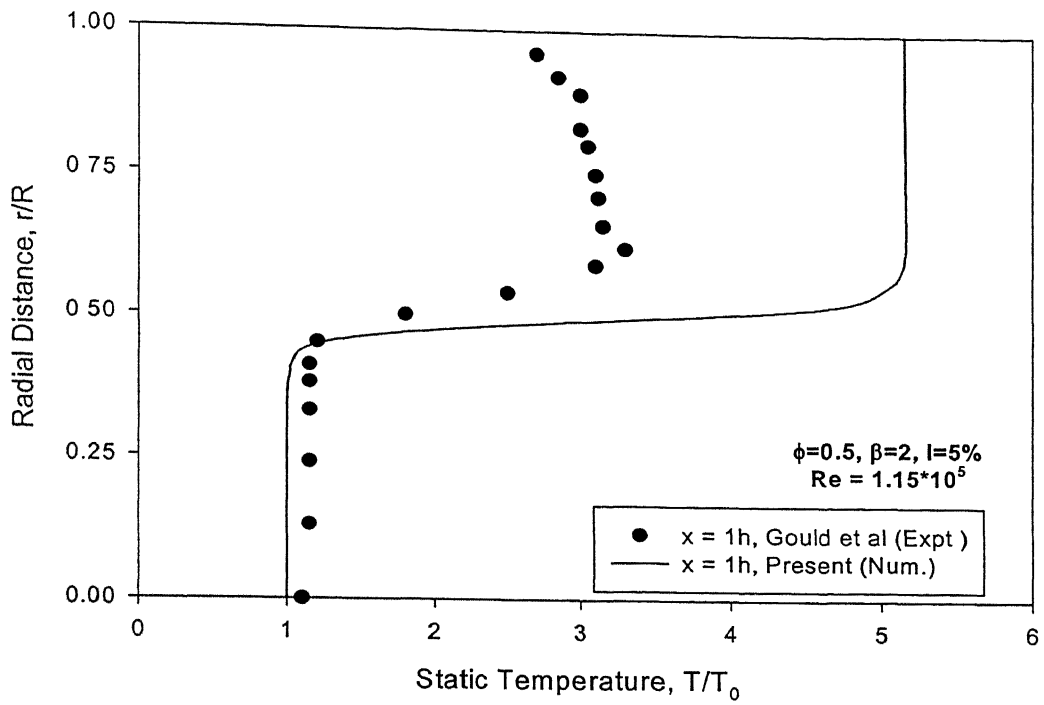

Fig.5.2 Axial velocity profiles at x = 5h

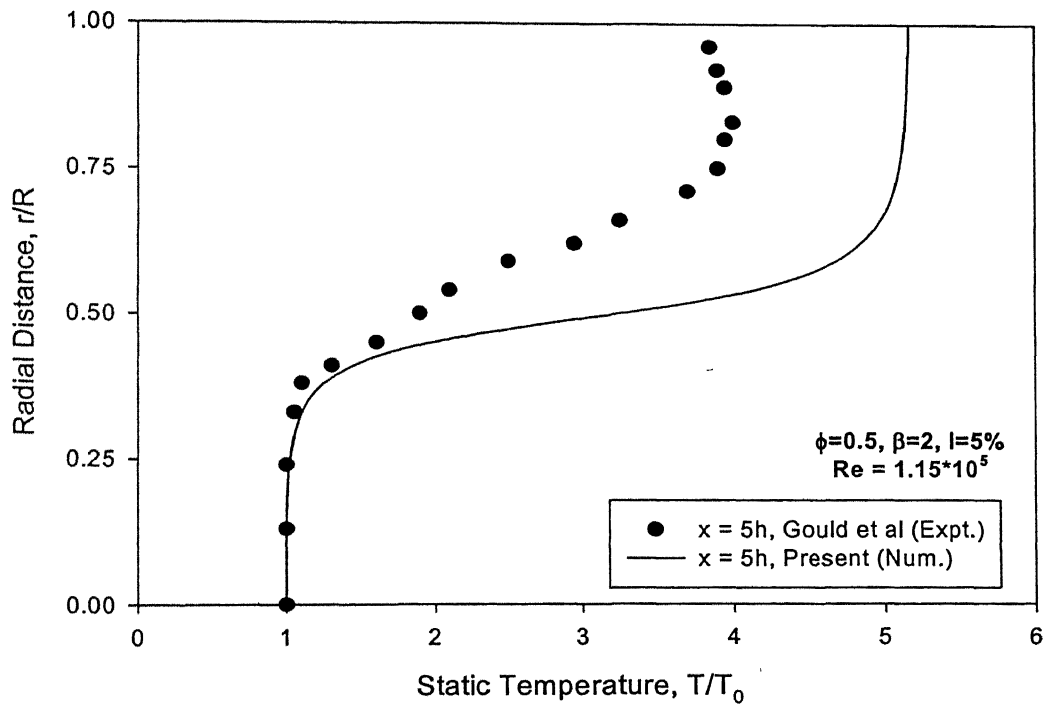**Fig.5.3 Static Temperature profiles at x = 1h**

Fig.5.4 Static Temperature profiles at x = 5h

5.2 Parametric Study

An extensive study on reacting flow quantities with more emphasis on static temperature, flame size and mass fraction is presented in this chapter. As in cold flow study other flow quantities such as axial velocity, radial velocity, turbulent kinetic energy and turbulent diffusion rate have also been investigated extensively. Since the cold flow study indicates that inlet flow Reynolds number is not an important parameter governing the flowfield. Hence in the reacting flow study only a representative Reynolds number, 1×10^5 has been used throughout, but varying other parameters such as inlet turbulence intensity, expansion ratio, and most importantly *overall equivalence ratio*, ϕ.

5.2.1 Mean Axial Velocity

The effect of various parameters such as overall equivalence ratio, turbulence intensity and expansion ratio on axial velocity profile in the flowfield is studied in this section. Fig.5.5, Fig.5.6 and Fig.5.7 show the distribution of centerline axial velocity, U_c, normalised with U_0, for different equivalence ratios 1.00, 0.75 and 0.50 respectively. All lengths have been normalized with step height, h of the combustor. On analysing the Fig.5.8, it is clear that after a short distance from the dump plane (after the high-speed potential core region), where the inlet temperature is maintained due to lack of combustion, there is a sudden increase in the centerline axial velocity due to the energy supply from the combustion products. Densities of the combustion products are less that that at the inlet, hence to obey the mass conservation principles, the velocity should increase. However this trend is not true for expansion ratio of 3 at lean mixture combustion, where the temperatures of the combustion products are not high enough to produce a significant change in density so to cause the velocity increase. In the case of expansion ratio 2, a maximum velocity of $2.1U_0$ is observed at equivalence ratio of 1.00 with an inlet intensity of 10%. The increase in centerline velocity is more for higher turbulent flow. The increased velocity in the radially growing shear layer, which is due to heat release, tends to preserve the central core region.
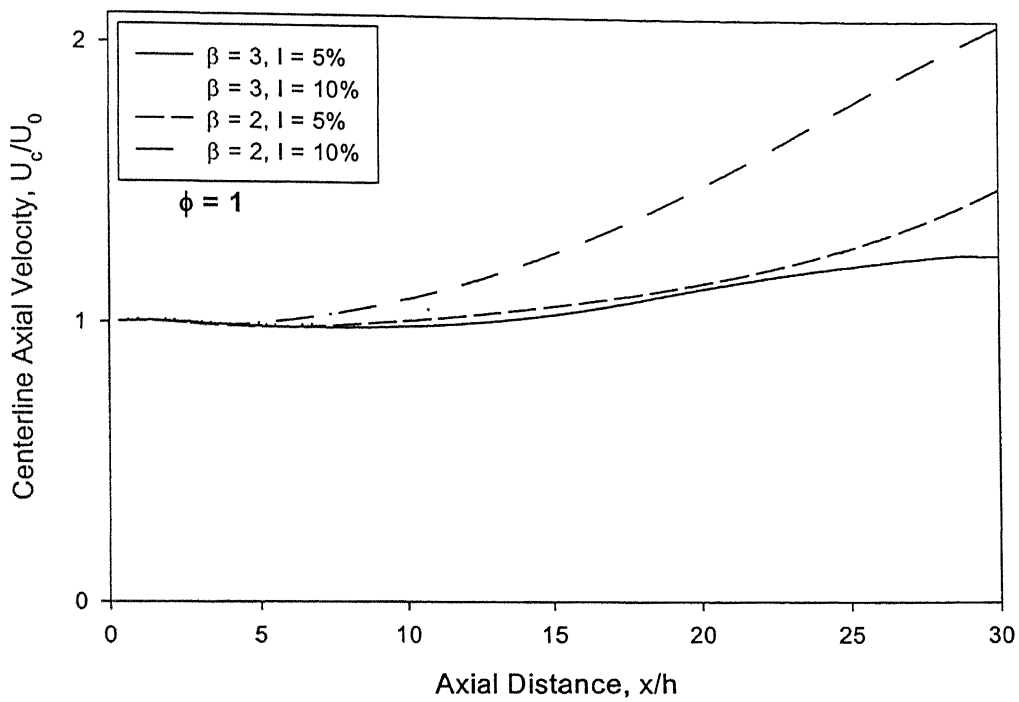
Fig. 5.5 Centerline Axial Velocity distribution for Equivalence Ratio = 1.00
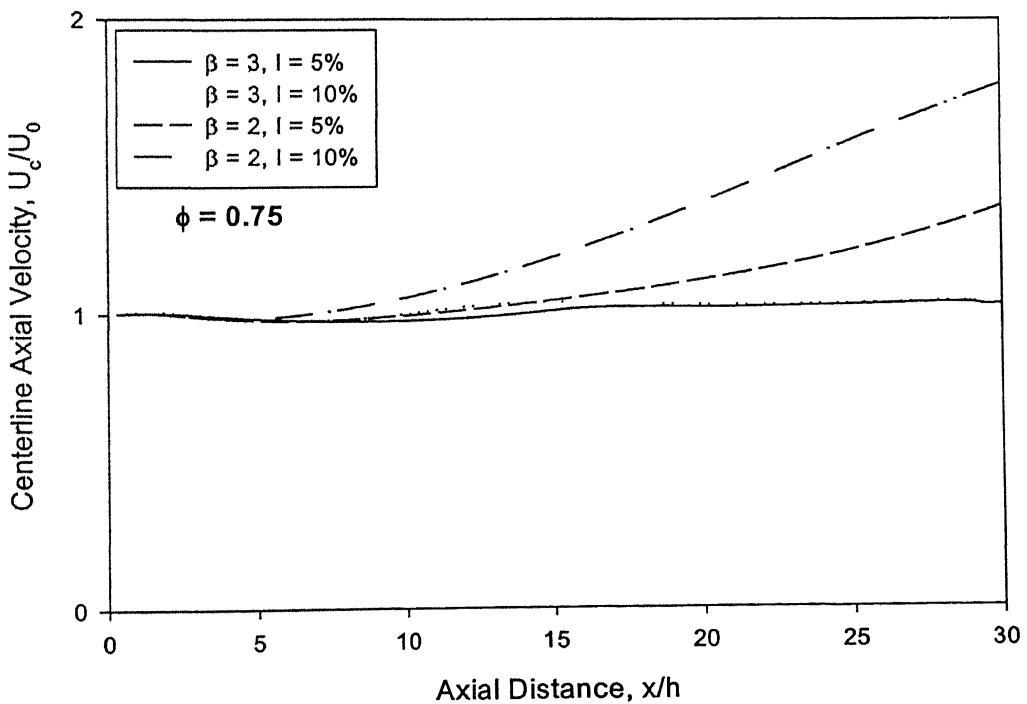

Fig. 5.6 Centerline Axial Velocity distribution for Equivalence Ratio = 0.75
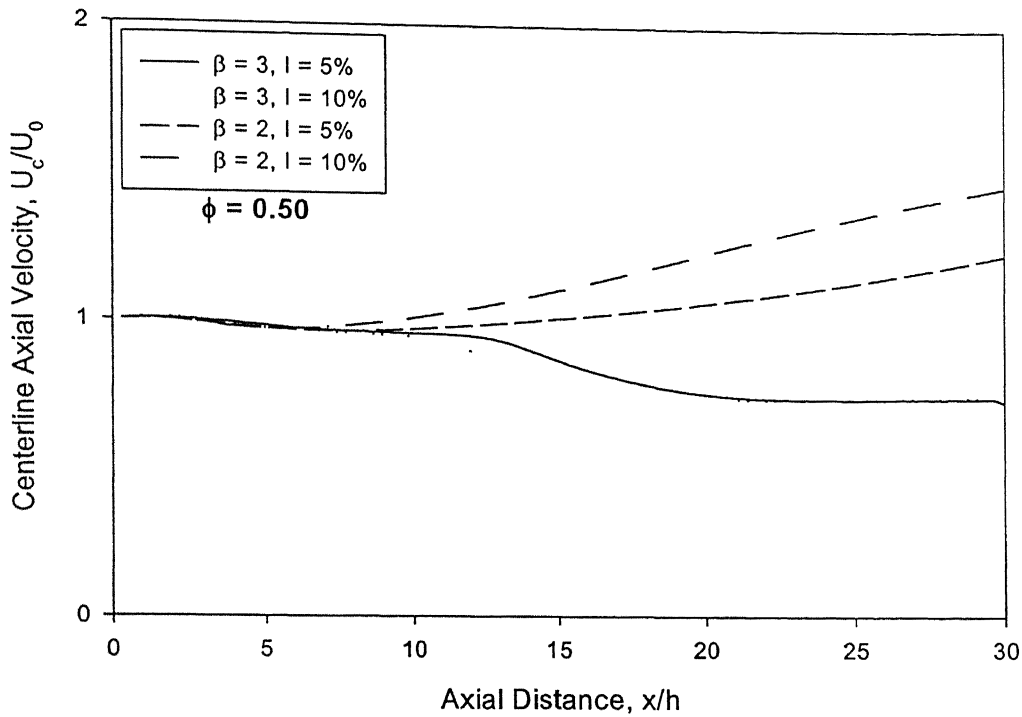
80

Fig. 5.7 Centerline Axial Velocity distribution for Equivalence Ratio = 0.50

Axial velocity contours for equivalence ratio of 0.5 at two different turbulence intensities 5% and 10% is given in Fig.5.8 and Fig.5.9 respectively. A stronger recirculation with higher negative axial velocities is obtained in the case of higher turbulence intensity as expected. However for larger equivalence ratio of 0.75 as given in Fig.5.10 and Fig.5.11 for turbulence intensities 5% and 10% respectively, a higher axial velocity distribution compared to the cold flow is obtained. This is even stronger for stoichiometric fuel air ratio as it is clear from Fig.5.12 and 5.13 for intensities 5% and 10% respectively. For all the cases, only one expansion ratio has been selected, which is 2. It can be noted that, for equivalence ratios of 0.75 and 1.00, at turbulence intensity of 5%, maximum velocity occurs not in the axis but slightly away from the axis in the radial direction. Also in all cases maximum velocity occurs near the combustor exit. Higher mean axial velocities in the shear layer found in the reacting flow case can attribute partly due to volumetric expansion. Similar observations have been made in the work of Gould et al (1994).

Fig. 5.8 Axial Velocity contours for Expansion Ratio = 2, Equivalence Ratio = 0.50, Reynolds Number = 1×10^5, Turbulence Intensity = 5%

Fig. 5.9 Axial Velocity contours for Expansion Ratio = 2, Equivalence Ratio = 0.50, Reynolds Number = 1×10^5, Turbulence Intensity = 10%
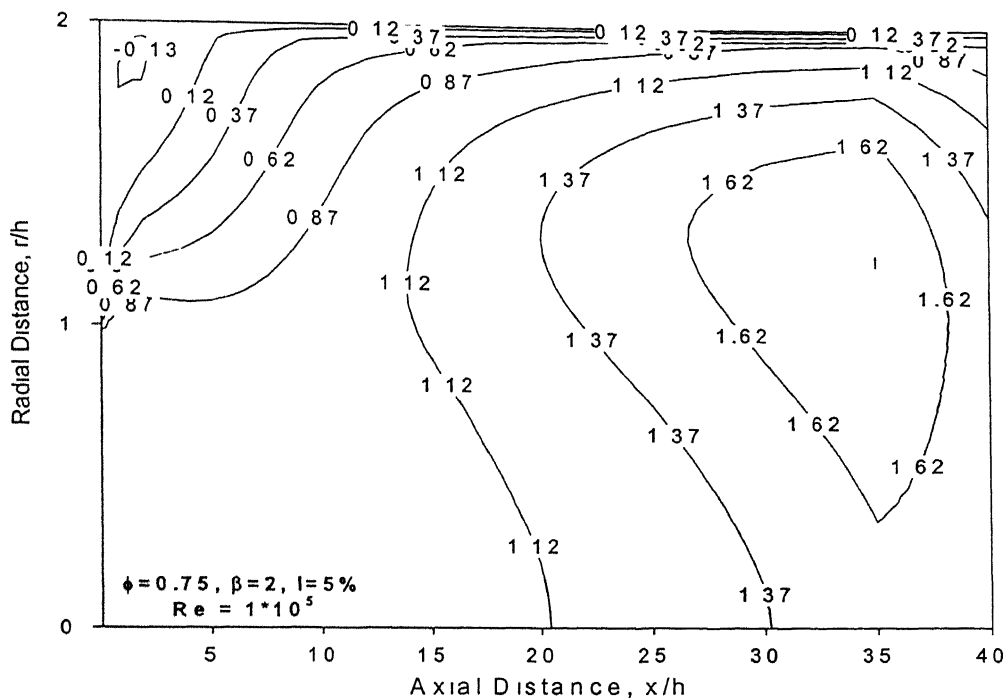
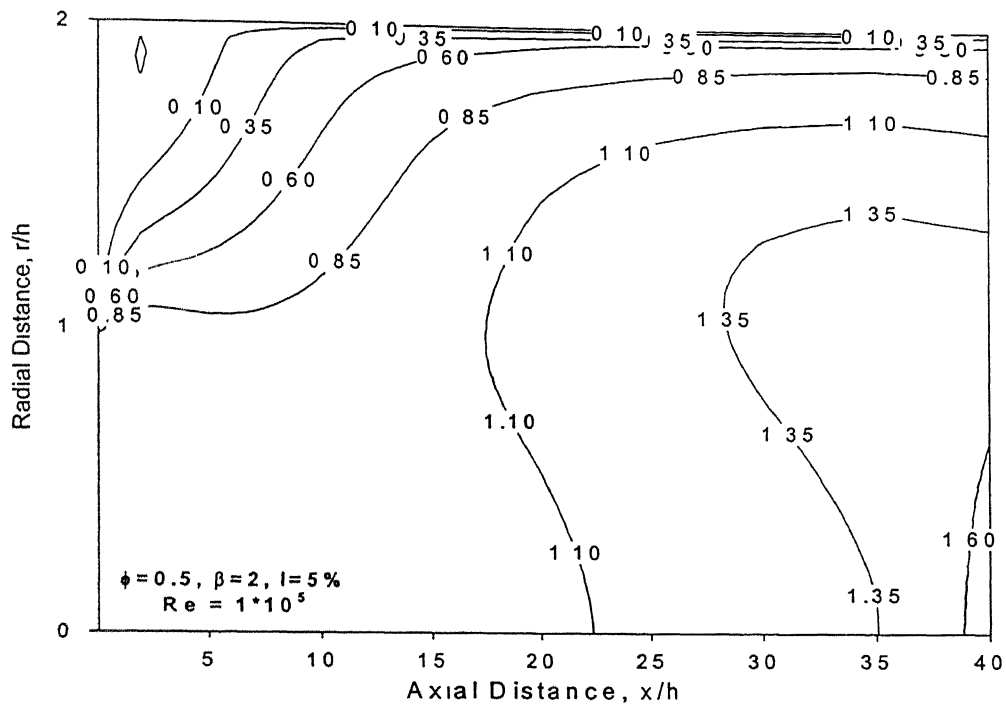**Fig. 5.10 Axial Velocity contours for Expansion Ratio = 2, Equivalence Ratio = 0.75, Reynolds Number = 1×10⁵, Turbulence Intensity = 5%**

Fig. 5.11 Axial Velocity contours for Expansion Ratio = 2, Equivalence Ratio = 0.75, Reynolds Number = 1×10⁵, Turbulence Intensity = 10%

$\phi = 1$, $\beta = 2$, $I = 5\%$
$Re = 1*10^5$

Fig. 5.12 Axial Velocity contours for Expansion Ratio = 2, Equivalence Ratio = 1.00, Reynolds Number = 1×10^5, Turbulence Intensity = 5%

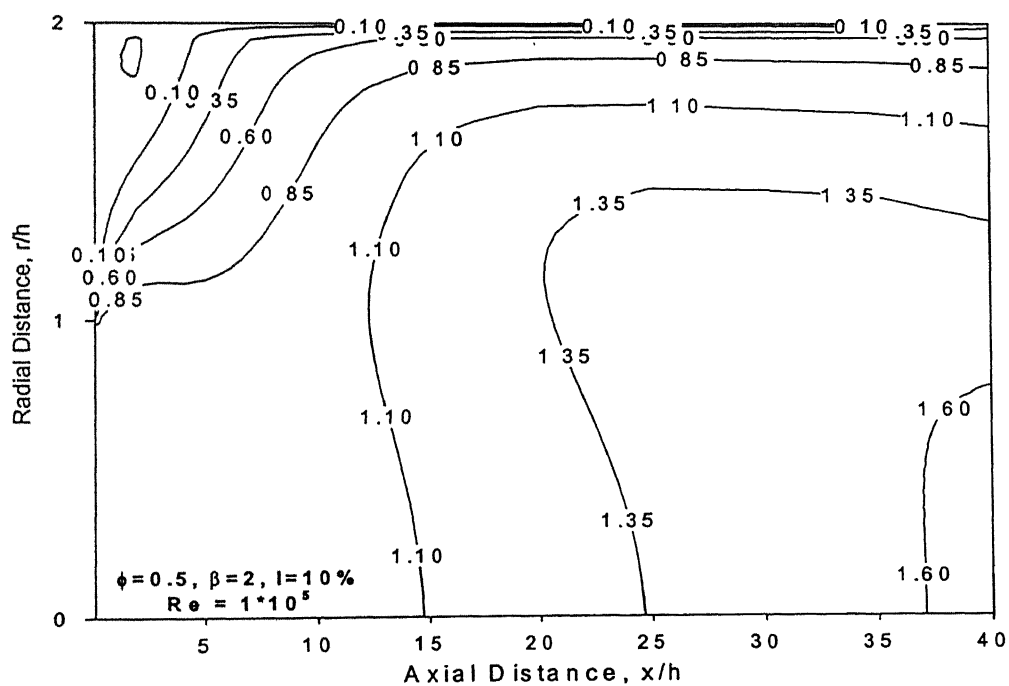$\phi = 1$, $\beta = 2$, $I = 10\%$
$Re = 1*10^5$

Fig. 5.13 Axial Velocity contours for Expansion Ratio = 2, Equivalence Ratio = 1.00, Reynolds Number = 1×10^5, Turbulence Intensity = 10%
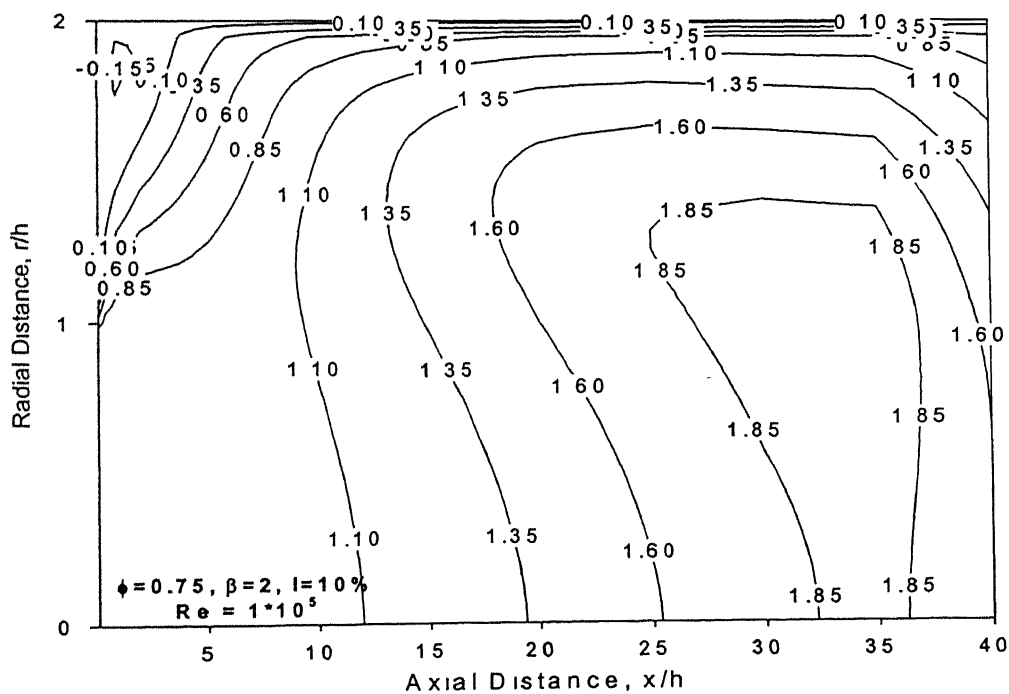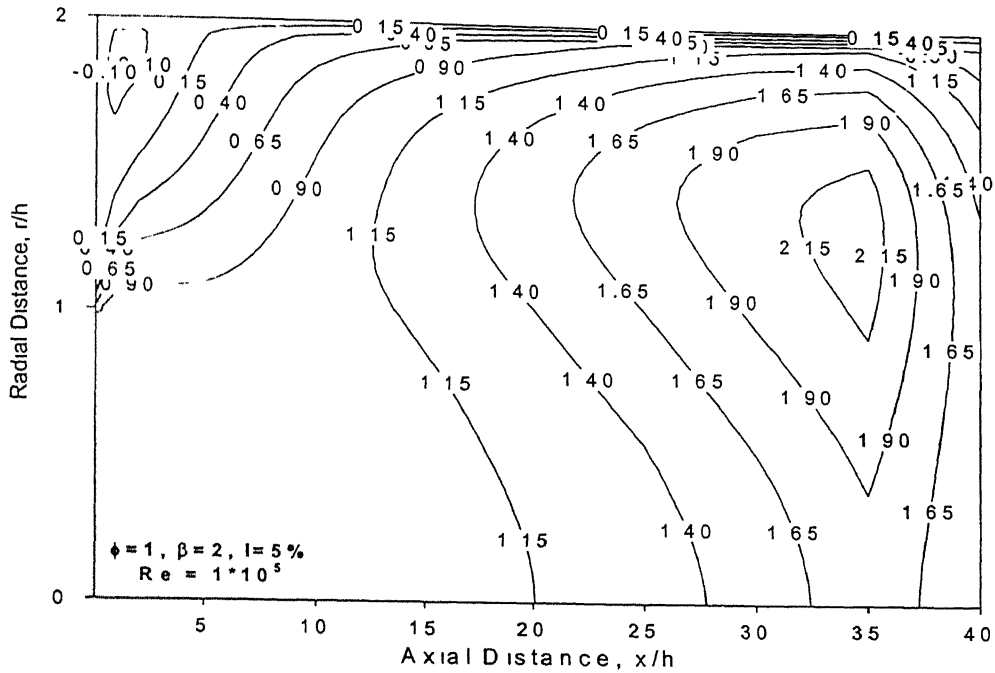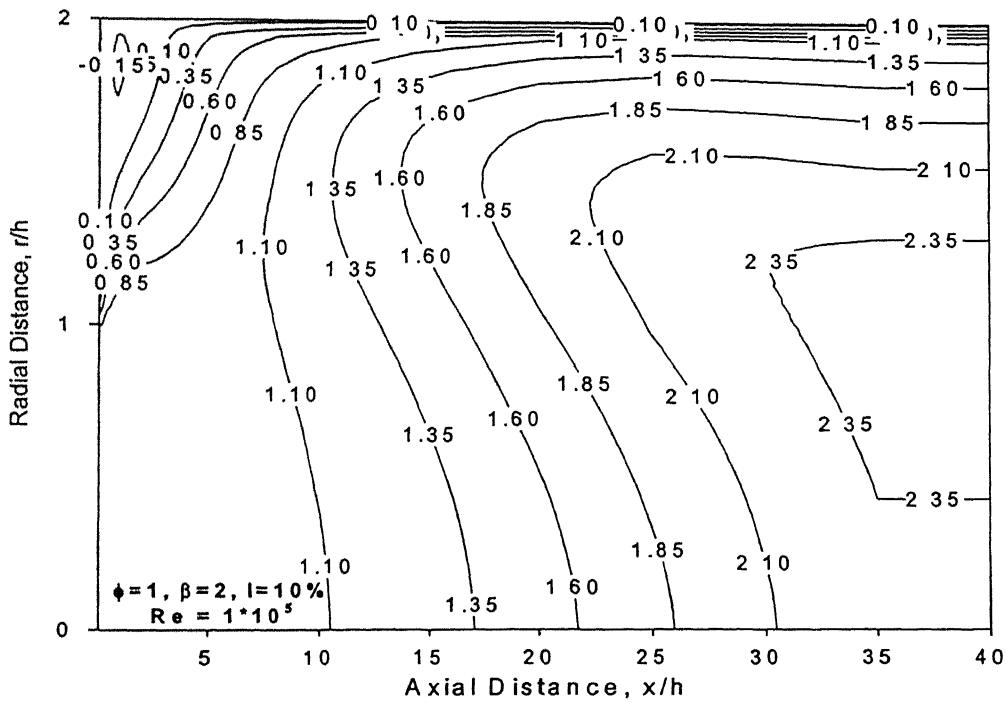
84

The maximum negative axial velocity encountered in the flowfield, which is in the recirculation region, in each of the above cases is tabulated in Table.5.1. It is noticeable that the equivalence ratio has not much influence on the negative axial velocities within the recirculation region, even though there is a slight increase in negative axial velocity with the increase in turbulence intensity.

Table.5.1 Variation in maximum negative Axial Velocity in the flowfield with the Equivalence Ratio and Turbulence Intensity for Expansion Ratio 2

Equivalence Ratio	Turbulence Intensity, I (%)	Maximum Negative Axial Velocity, U/U_0
0.50	5	-0.161
	10	-0.174
0.75	5	-0.154
	10	-0.172
1.00	5	-0.149
	10	-0.185

5.2.2 Reattachment Length

As stated in the cold flow case, the recirculation size is recommended as a benchmark criterion in modelling studies [9]. The influence of overall equivalence ratio and expansion ratio on reattachment length, RL is studied. The variation in reattachment length for different equivalence ratios ($\phi = 0.5$, 0.75 and 1.0) for expansion ratios of 2 and 3 is shown in Fig.5.14 and Fig.5.15 respectively. It can be seen that size of the recirculation zone, and hence the reattachment length is considerably increased for a lean mixture i.e., for lower equivalence ratios compared to stoichiometric mixture. The variation in reattachment length with variation in expansion ratio and equivalence ratio is given in Fig.5.16, where same trend can be observed as in the cold flow case. There is a reduction in reattachment length with reduction in expansion ratio, even though magnitude is considerably reduced as compared to the cold flow. The combustion-generated turbulence might have contributed in addition to the inlet turbulence to the

reduction in reattachment length. It can be summarised as the reacting flow mean axial velocities were higher due to heat release, and the recirculation zone was shorter than observed in the cold flow case.
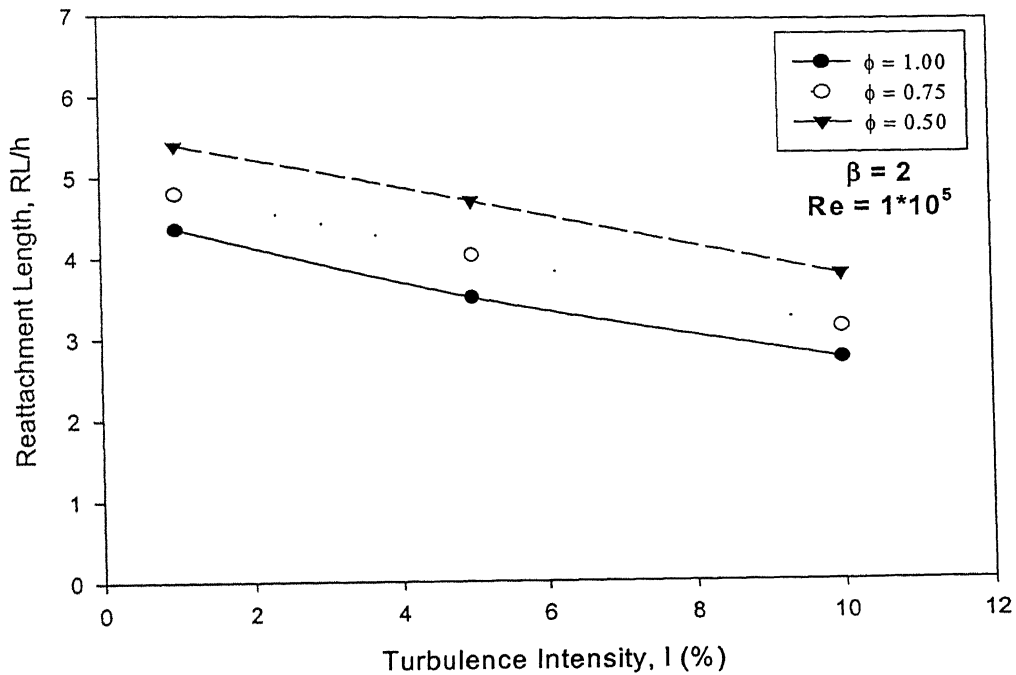

Fig. 5.14 Reattachment length variation for Expansion Ratio = 2, Reynolds Number = 1×10^5
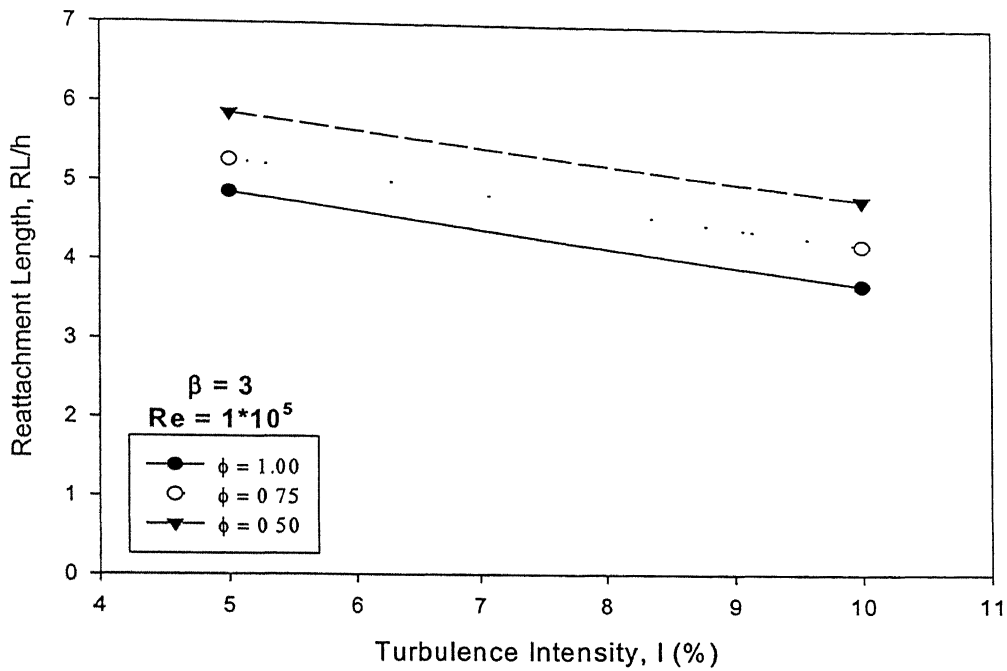
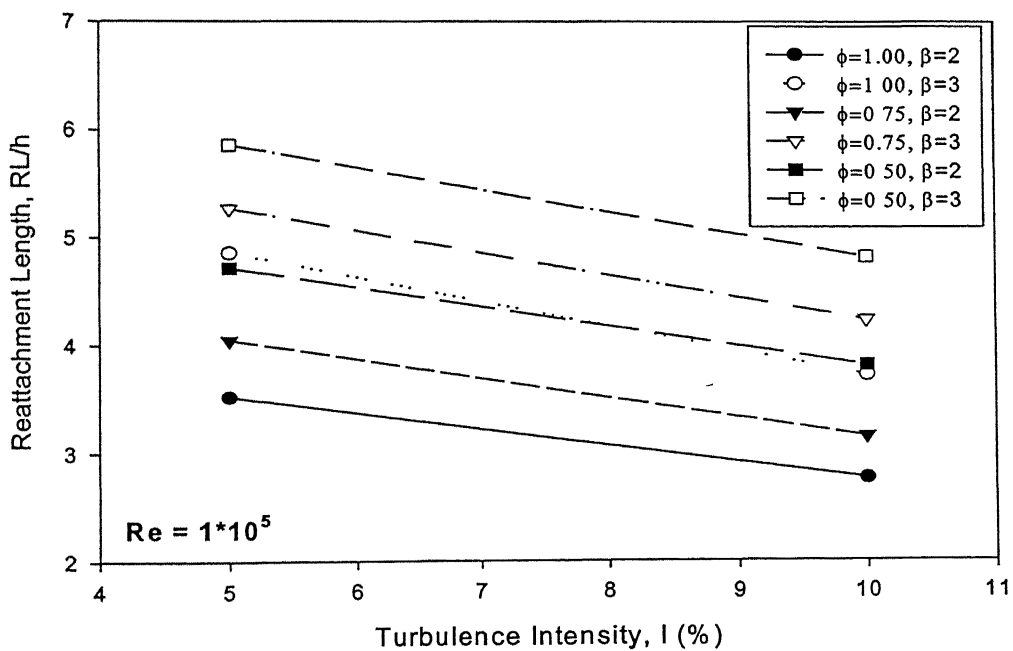Fig. 5.15 Reattachment length variation for Expansion Ratio = 3, Reynolds Number = 1×10^5

Fig. 5.16 Comparison of Reattachment length variation with Equivalence Ratio and Expansion Ratio for Reynolds Number 1×10^5

5.2.3 Radial Velocity

Fig 5.17 through Fig.5.22 shows the radial velocity contours for various equivalence ratios at two turbulence intensities 5% and 10%. In all figures it is clearly seen that maximum positive radial velocity occurs in the shear region and maximum negative radial velocity occurs in the recirculation region. Table.5.1 lists maximum and the minimum radial velocity encountered in the flowfield, normalized by inlet centerline velocity. All results are for expansion ratio of 2. It is found that the reacting case has a considerably shortened region of recirculation, associated with higher recirculation velocities.

Table.5.2 Variation in Radial Velocity Magnitudes in the Flowfield with the Equivalence Ratio and Turbulence Intensity for Expansion Ratio 2

Equivalence Ratio	Turbulence Intensity, I (%)	Radial Velocity, v/U_0	
		Maximum	Minimum
0.50	5	0.109	-0.091
	10	0.129	-0.113
0.75	5	0.136	-0.106
	10	0.154	-0.135
1.00	5	0.149	-0.118
	10	0.180	-0.146

Fig. 5.17 Radial Velocity contours for Expansion Ratio = 2, Equivalence Ratio = 0.50, Reynolds Number = 1×10^5, Turbulence Intensity = 5%

Fig. 5.18 Radial Velocity contours for Expansion Ratio = 2, Equivalence Ratio = 0.50, Reynolds Number = 1×10^5, Turbulence Intensity = 10%
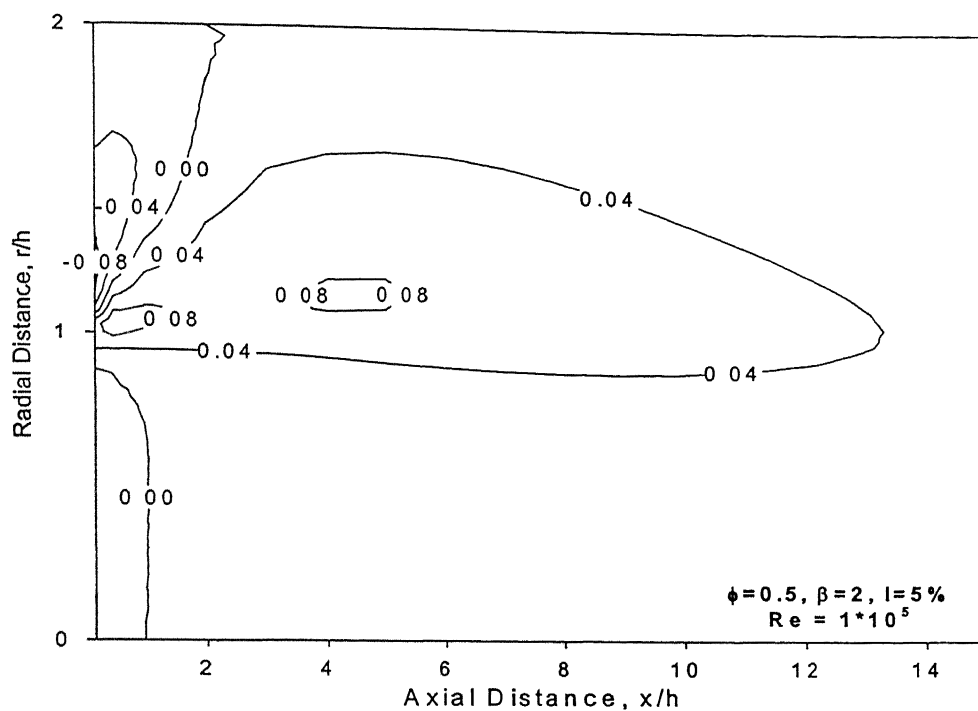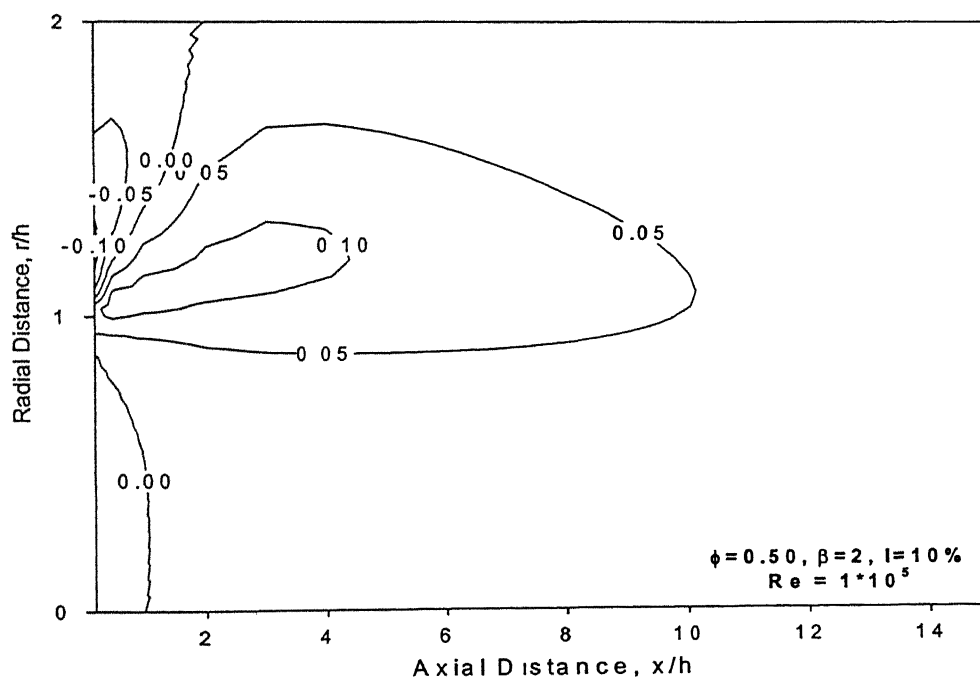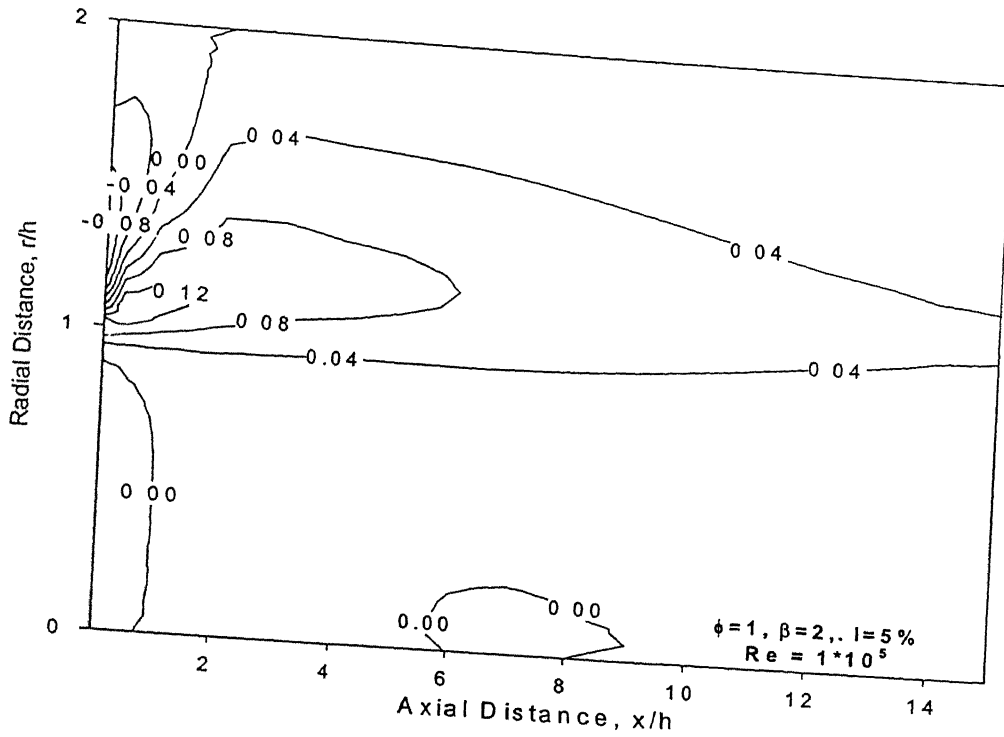
Fig. 5.21 Radial Velocity contours for Expansion Ratio = 2, Equivalence Ratio = 1.00, Reynolds Number = 1×10⁵, Turbulence Intensity = 5%
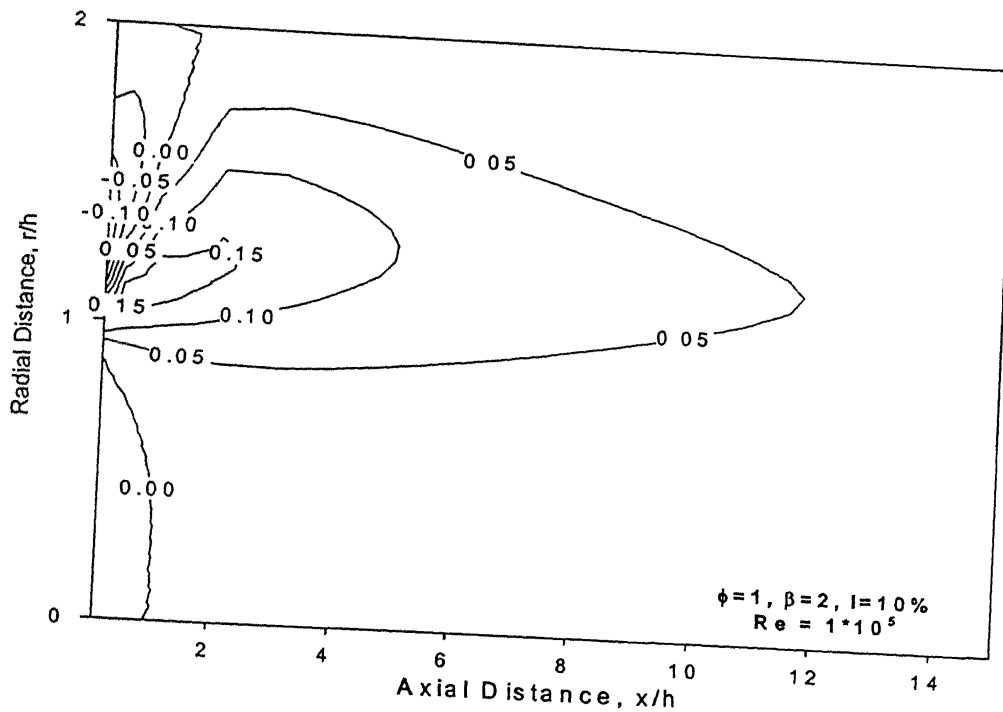

Fig. 5.22 Radial Velocity contours for Expansion Ratio = 2, Equivalence Ratio = 1.00, Reynolds Number = 1×10⁵, Turbulence Intensity = 10%

91

5.2.4 Static Temperature

Static temperature is one of the most important quantities to be considered in the reacting flow study. Static temperature is normalised using inlet air-fuel mixture temperature, which is ambient temperature, 300 K in this study. It can be kept in mind that propane–air mixture is used for reacting flow study. Two expansion ratios, 2 and 3, have been considered for temperature study. The adiabatic wall conditions have been assumed in the present model. As a result the adiabatic flame temperature will be the maximum temperature encountered in the flowfield. But the present numerical predictions have slightly over estimated the values of adiabatic temperatures. The difference in temperature was found to be more at higher turbulence intensities than that in lower turbulence intensities, which means that the combustion product temperature is influenced by the turbulence intensities. This difference in temperature was found to be maximum in the lower equivalence ratio than in the higher one. A comparison of adiabatic temperature with the temperatures predicted is given in Table.5.3.

Table.5.3 Comparison of Adiabatic Temperature with the Predicted Temperature

Equivalence Ratio, ϕ	Temperature (K)				
	Adiabatic	I = 5%		I = 10%	
		Predicted	% Difference	Predicted	% Difference
0.50	1495	1550	3.60	1570	5.00
0.75	1995	2030	1.75	2070	3.75
1.00	2395	2450	2.30	2490	3.97

Static temperature contours for equivalence ratio of 0.50 at expansion ratios 2 and 3 is given in Fig.5.23 to Fig.5.26. Fig.5.23 and Fig.5.25 represent temperature distribution for intensity 5%. Fig.5.24 and Fig.5.26 represent temperature distribution for intensity of 10%. However, for expansion ratio 3, the maximum temperature is attained along the axis at a shorter distance as compared to an expansion ratio of 2. However for the same

expansion ratio with the increase in the intensity, the maximum temperature is attained at a shorter distance. The turbulence intensity is found to be making the recirculation stronger, and this in turn will help in stabilising the flame. This means that in the case of expansion ratio 2, even after 25h downstream distance along the axis, combustion is not complete, leading to a mixture, which contains lot of unburned fuel. Such kind of trend is also observed for higher equivalence ratios 0.75 and 1.00 also. Fig.5.27 and Fig.5.28 represents temperature contours for equivalence ratio 0.75 at an expansion ratio 2 for intensities 5% and 10% respectively. Fig.5.29 and Fig.5.30 shows temperature contours for equivalence ratio 0.75 at an expansion ratio 3 for intensities 5% and 10% respectively.

Fig.5.31 and Fig.5.32 represents temperature contours for equivalence ratio 1.00 at an expansion ratio 2 for intensities 5% and 10% respectively. Fig.5.33 and Fig.5.34 gives temperature contours for equivalence ratio 1.00 at an expansion ratio 3 for intensities 5% and 10% respectively. All these figures reveal that, the maximum temperature is attained in the radial directions at all axial locations. The central core region remains relatively cool for some distance, due to lack of combustion in the potential core. Mean temperature observations show that the potential core stays relatively cool and that the maximum temperatures are achieved in the recirculation zone and the developing boundary layer downstream of the reattachment point.
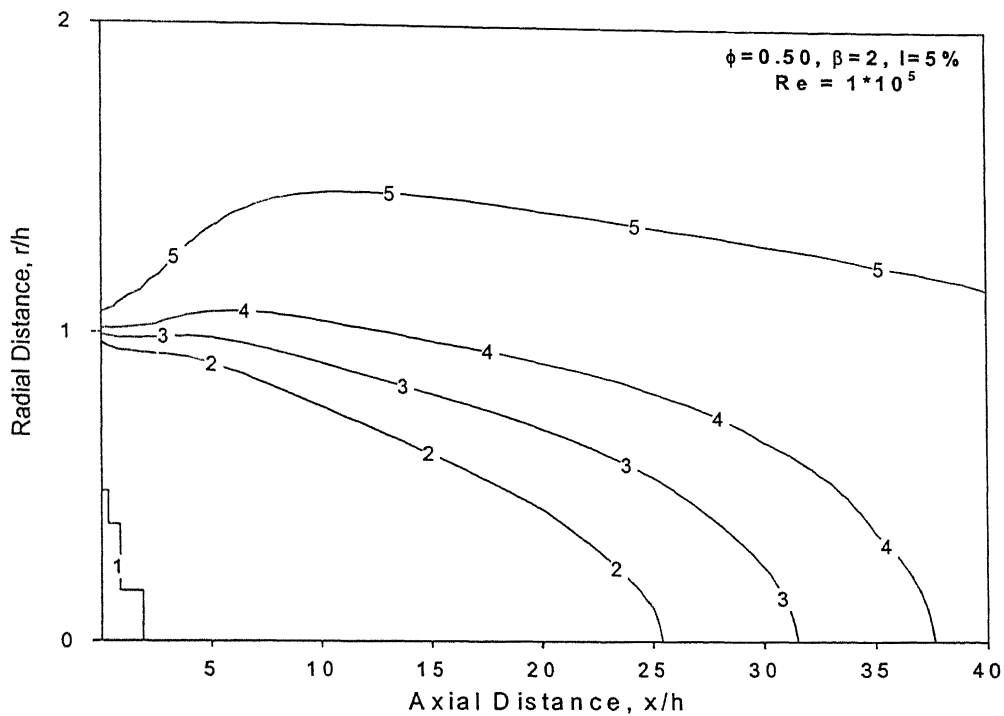
Fig. 5.23 Static Temperature contours for Expansion Ratio = 2, Equivalence Ratio = 0.50, Reynolds Number = 1×10^5, Turbulence Intensity = 5%

Fig. 5.24 Static Temperature contours for Expansion Ratio = 2, Equivalence Ratio = 0.50, Reynolds Number = 1×10^5, Turbulence Intensity = 10%

Fig. 5.25 Static Temperature contours for Expansion Ratio = 3, Equivalence Ratio = 0.50, Reynolds Number = 1×10^5, Turbulence Intensity = 5%

Fig. 5.26 Static Temperature contours for Expansion Ratio = 3, Equivalence Ratio = 0.50, Reynolds Number = 1×10^5, Turbulence Intensity = 10%
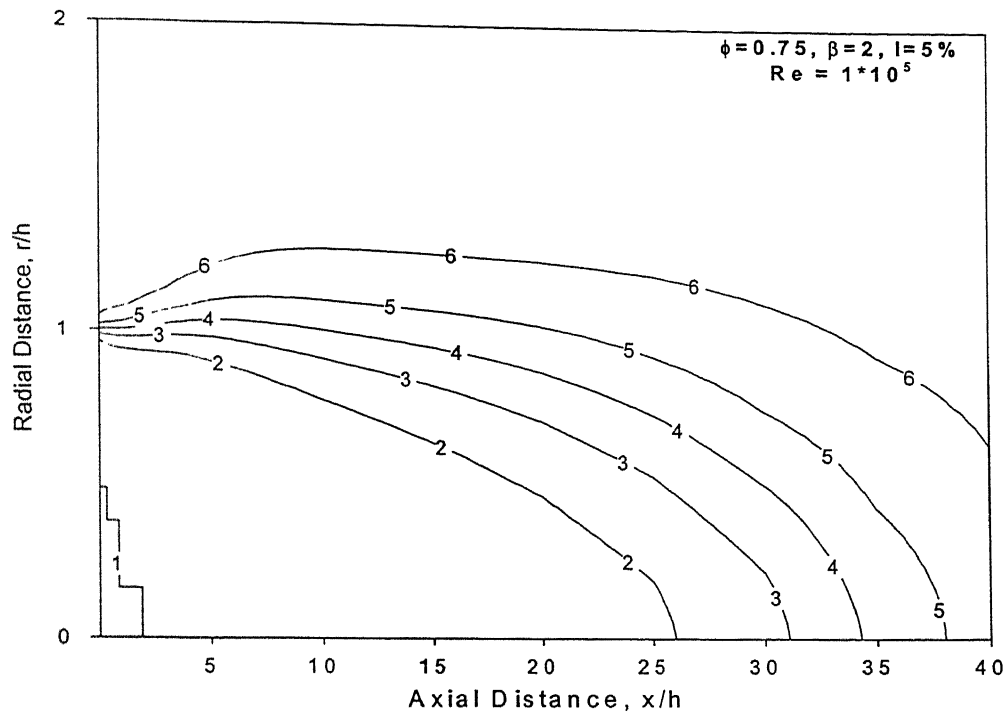
Fig. 5.27 Static Temperature contours for Expansion Ratio = 2, Equivalence Ratio = 0.75, Reynolds Number = 1×10^5, Turbulence Intensity = 5%
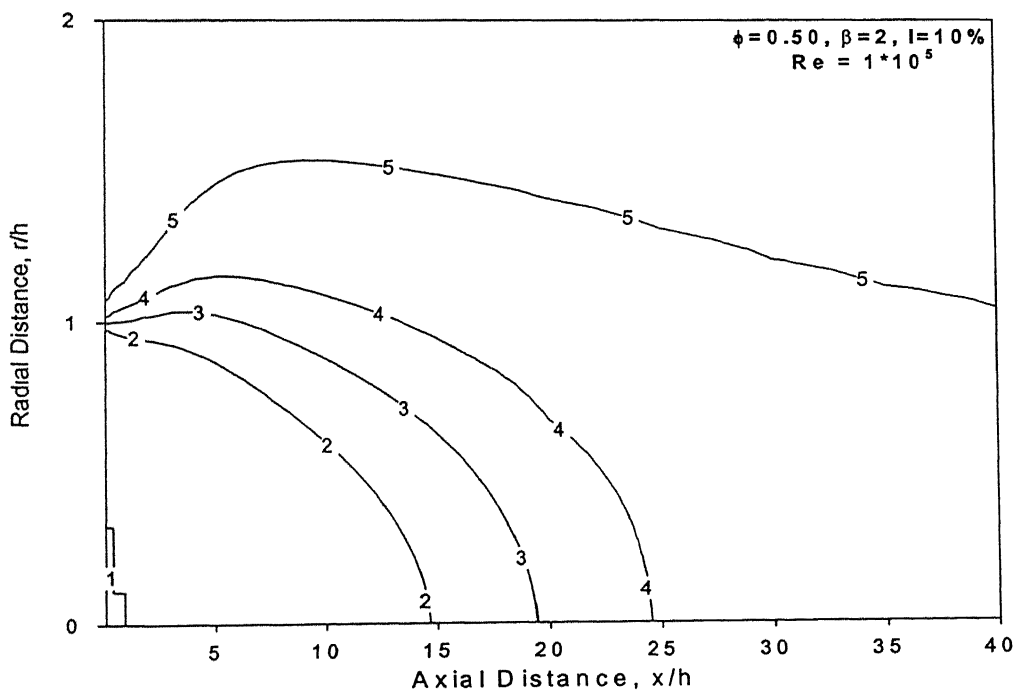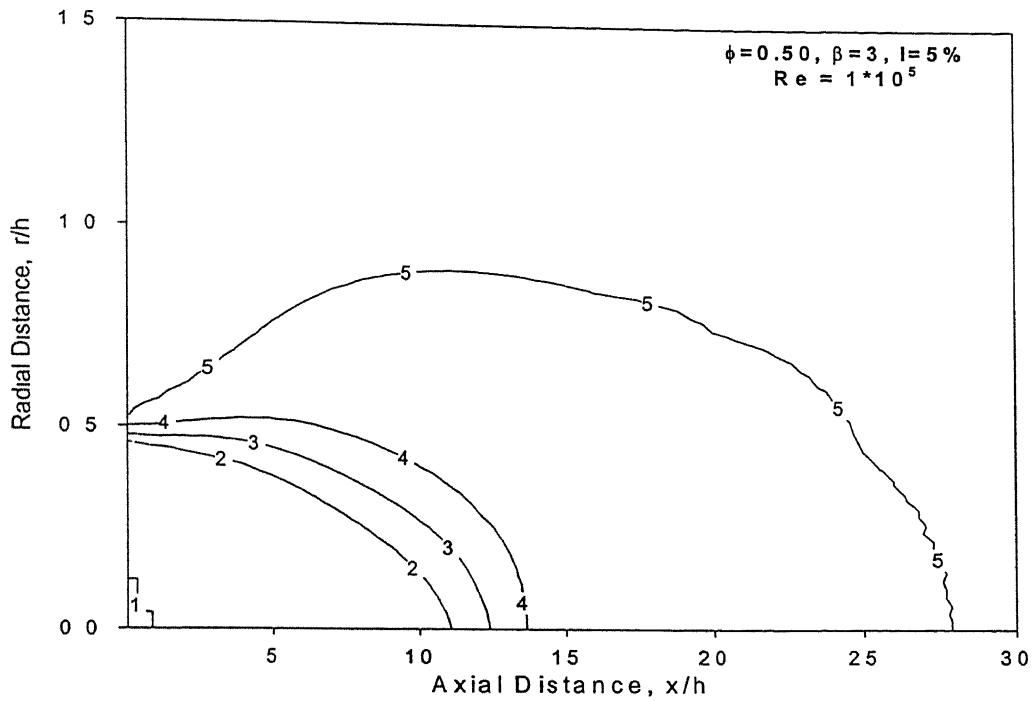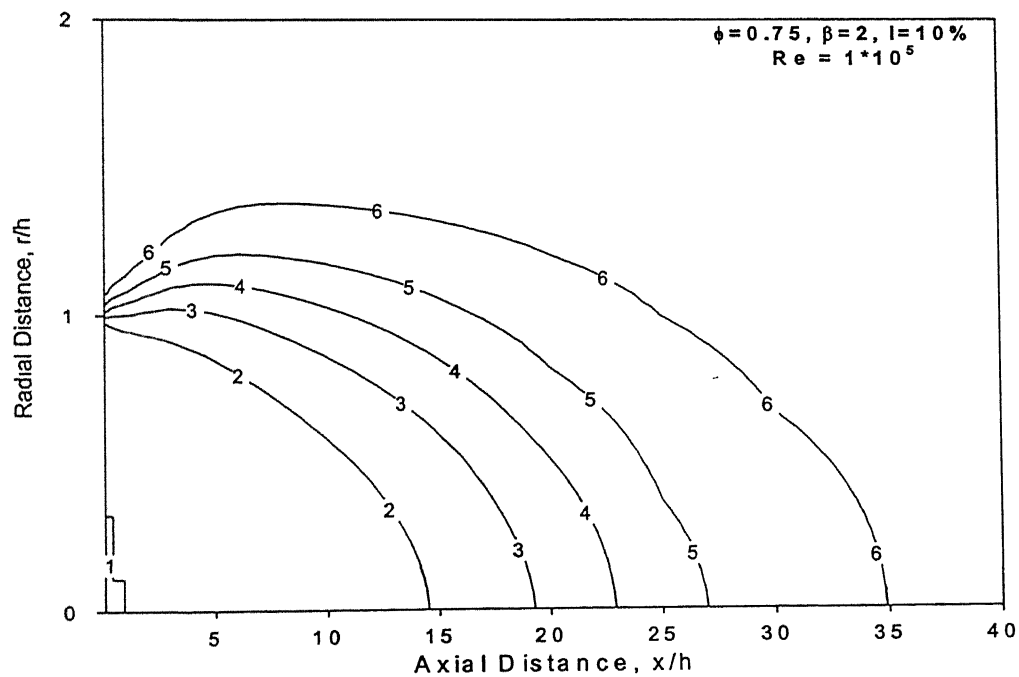

Fig. 5.28 Static Temperature contours for Expansion ratio = 2, Equivalence Ratio = 0.75, Reynolds Number = 1×10^5, Turbulence Intensity = 10%
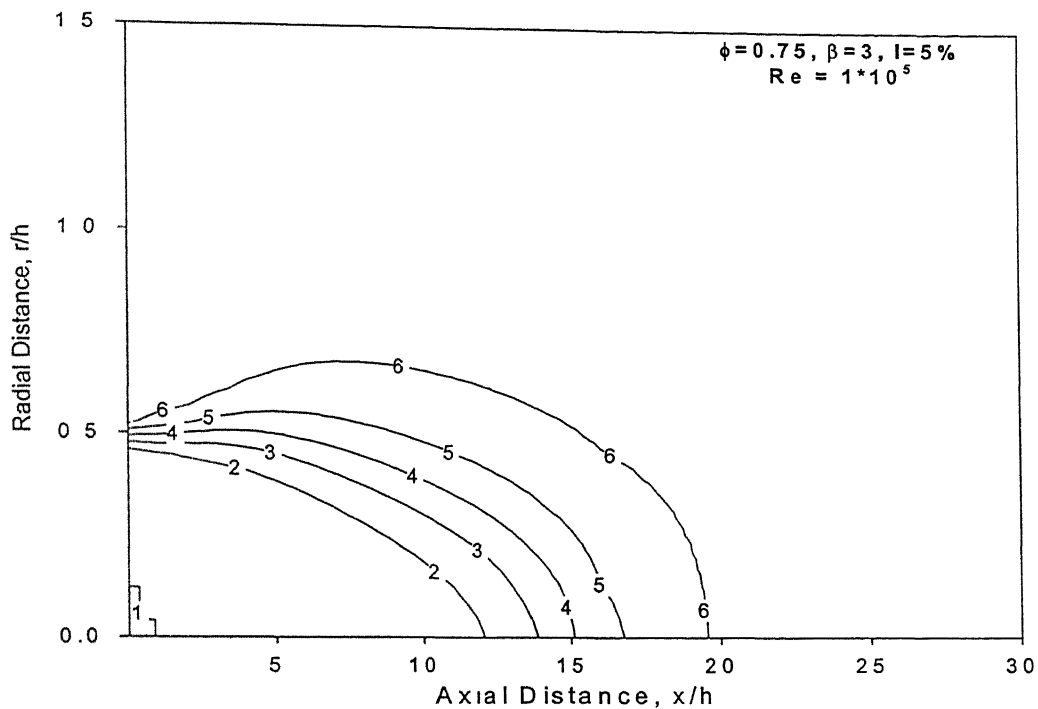
Fig. 5.29 Static Temperature contours for Expansion Ratio = 3, Equivalence Ratio = 0.75, Reynolds Number = 1×10^5, Turbulence Intensity = 5%
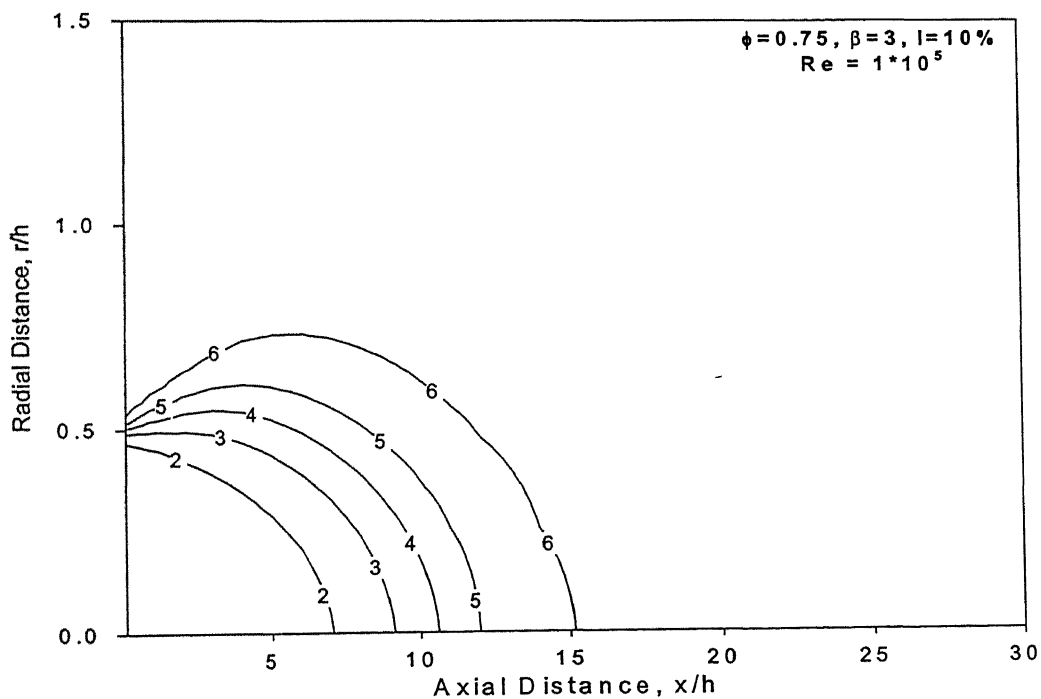
Fig. 5.30 Static Temperature contours for Expansion Ratio = 3, Equivalence Ratio = 0.75, Reynolds Number = 1×10^5, Turbulence Intensity = 10%
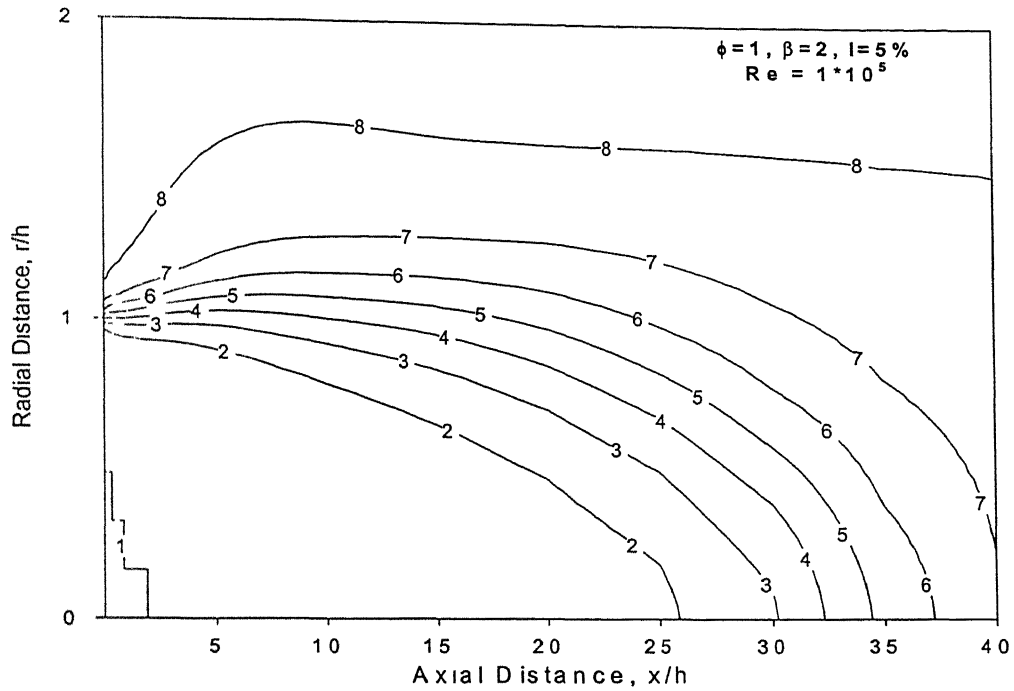
Fig. 5.31 Static Temperature contours for Expansion Ratio = 2, Equivalence Ratio = 1.00, Reynolds Number = 1×10^5, Turbulence Intensity = 5%

Fig. 5.32 Static Temperature contours for Expansion Ratio = 2, Equivalence Ratio = 1.00, Reynolds Number = 1×10^5, Turbulence Intensity = 10%

Fig. 5.33 Static Temperature contours for Expansion Ratio = 3, Equivalence Ratio = 1.00, Reynolds Number = 1×10^5, Turbulence Intensity = 5%
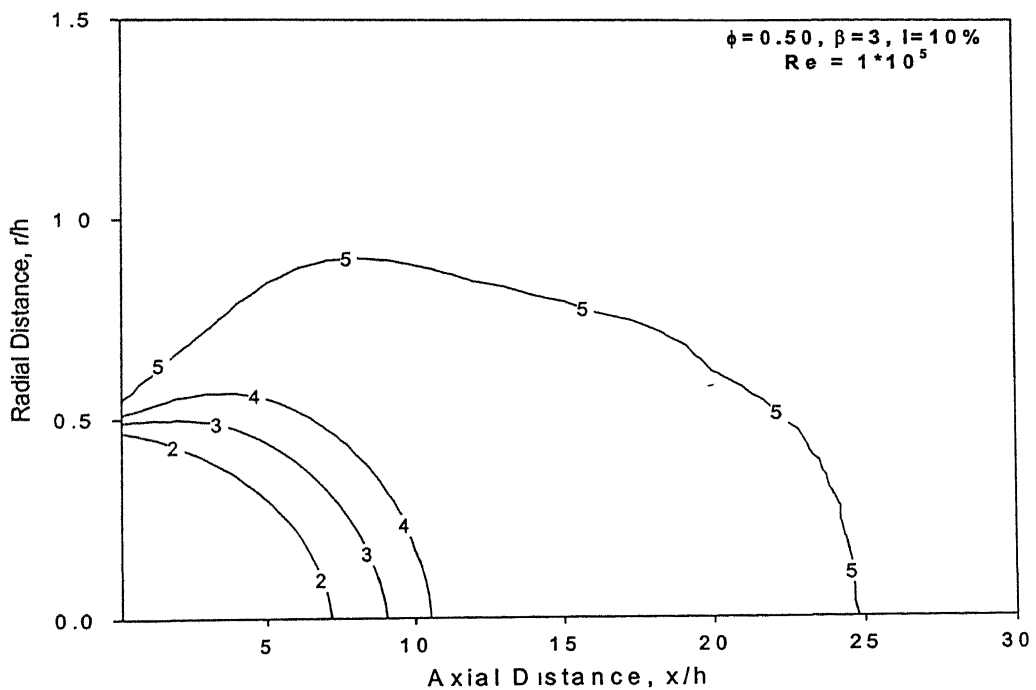

Fig. 5.34 Static Temperature contours for Expansion Ratio = 3, Equivalence Ratio = 1.00, Reynolds Number = 1×10^5, Turbulence Intensity = 10%
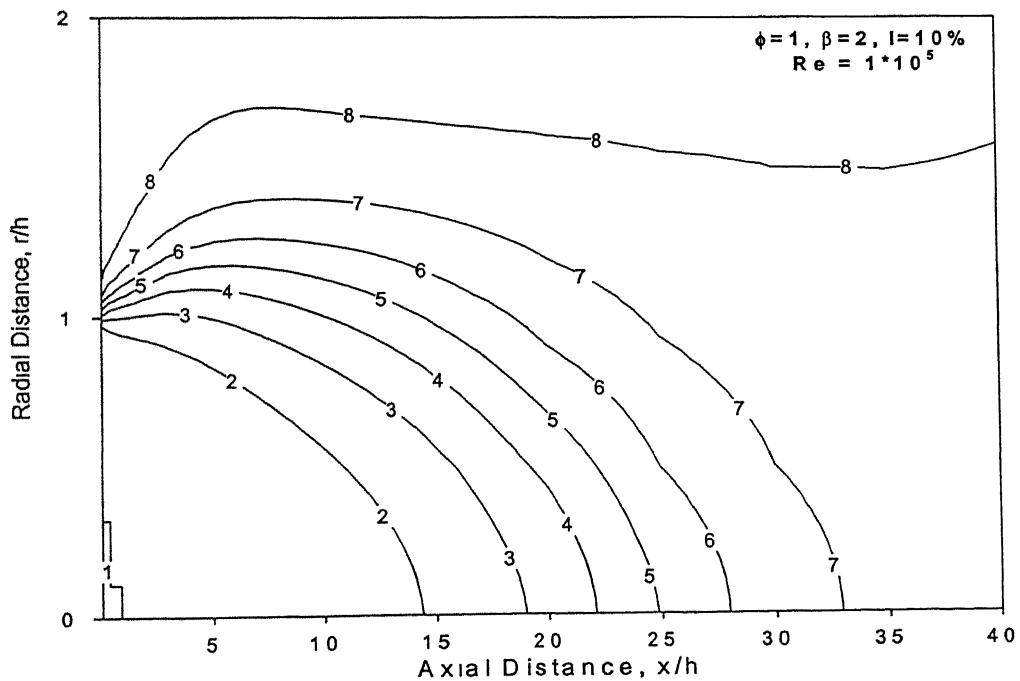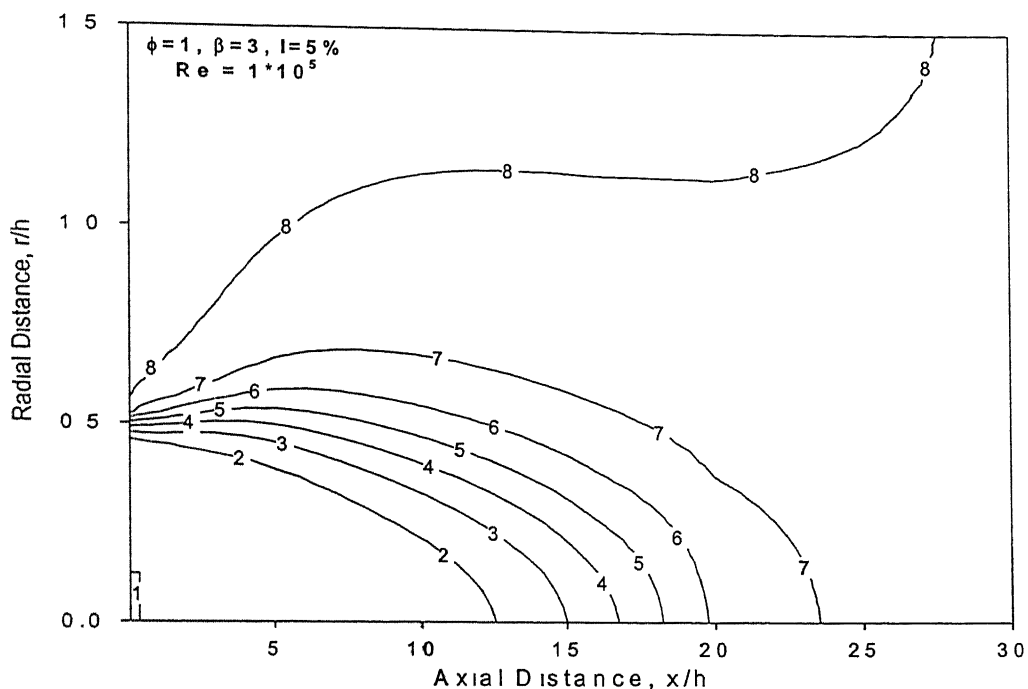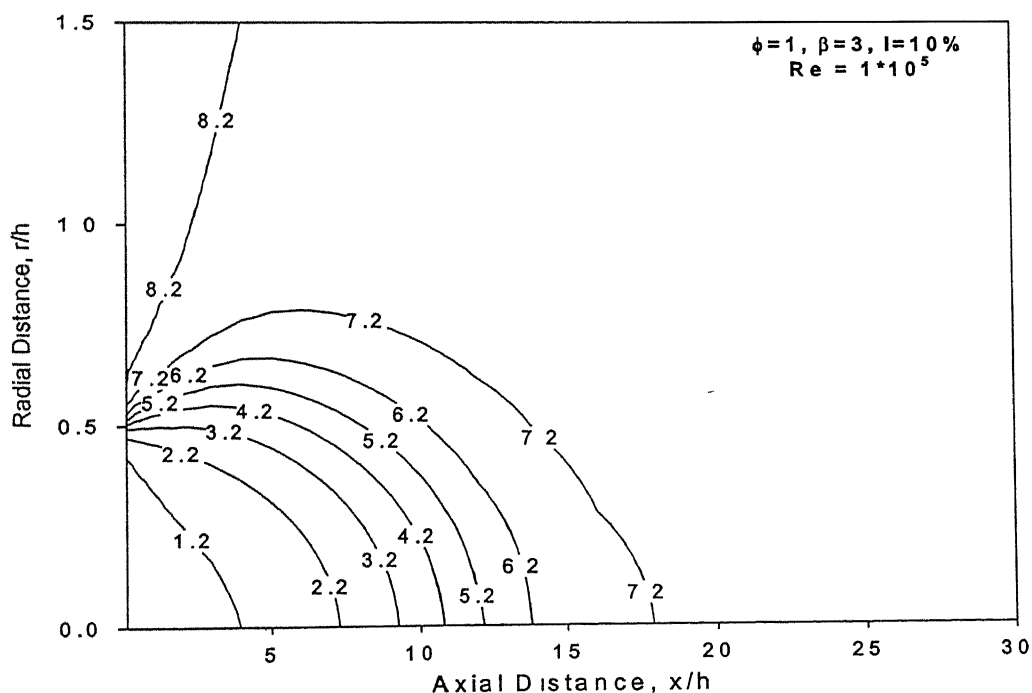
5.2.5 Flame Length and Size

Variation of flame length and size is discussed in this section. The various zones in the temperature profile for a typical premixed flame as found from the experimental studies are (i) Luminous zone, (ii) Shadow image and (iii) Schlieren image. In the present study luminous zone is chosen as the surface of the flame, which divides the reactant species from the product species. The temperature distribution of the luminous zone, given in the work of Mishra, D. P. (1994) as

$$\text{Luminous Zone Temperature} = \frac{\frac{T_f + T_u}{2} + T_f}{2} \tag{5.1}$$

Where, T_f = Adiabatic Flame Temperature

T_u = Reactant Temperature

Fig.5.35 and Fig.5.36 shows the flame front (as solid line) for expansion ratio 2 at Reynolds number 1×10^5 for two different intensities 5% and 10% respectively at stoichiometric air-fuel ratio. It can be noticed that the flame length is considerably reduced with the increase in the intensity level at the inlet. The same trend with more strength can be seen in Fig.5.37 and 5.38 for expansion ratio 3, for intensities 5% and 10% respectively. Table.5.1 summarises these observations. It is clear that with the increase in the expansion ratio, the length of the flame is considerably reduced. It is advantageous to have a shorter flame so as to have a compact combustor. It also seems that for the same expansion ratio, with the increase in the inlet turbulence level, the width of the flame increases. The axial distance at which the maximum flame width is achieved moves little upstream for the higher turbulence intensities and for higher expansion ratios. It can be observed that, for the same turbulence level, increasing the expansion ratio from 2 to 3 reduces the axial distance at which maximum flame width is obtained to half the initial value.

100

Fig. 5.35 Temperature contour showing Flame front for Expansion Ratio = 2, Equivalence Ratio = 1.00, Reynolds Number = 1×10^5, Turbulence Intensity = 5%

Fig. 5.36 Temperature contour showing Flame front for Expansion Ratio = 2, Equivalence Ratio = 1.00, Reynolds Number = 1×10^5, Turbulence Intensity = 10%

101

Fig. 5.37 Temperature contour showing Flame front for Expansion Ratio = 3, Equivalence Ratio = 1.00, Reynolds Number = 1×10^5, Turbulence Intensity = 5%

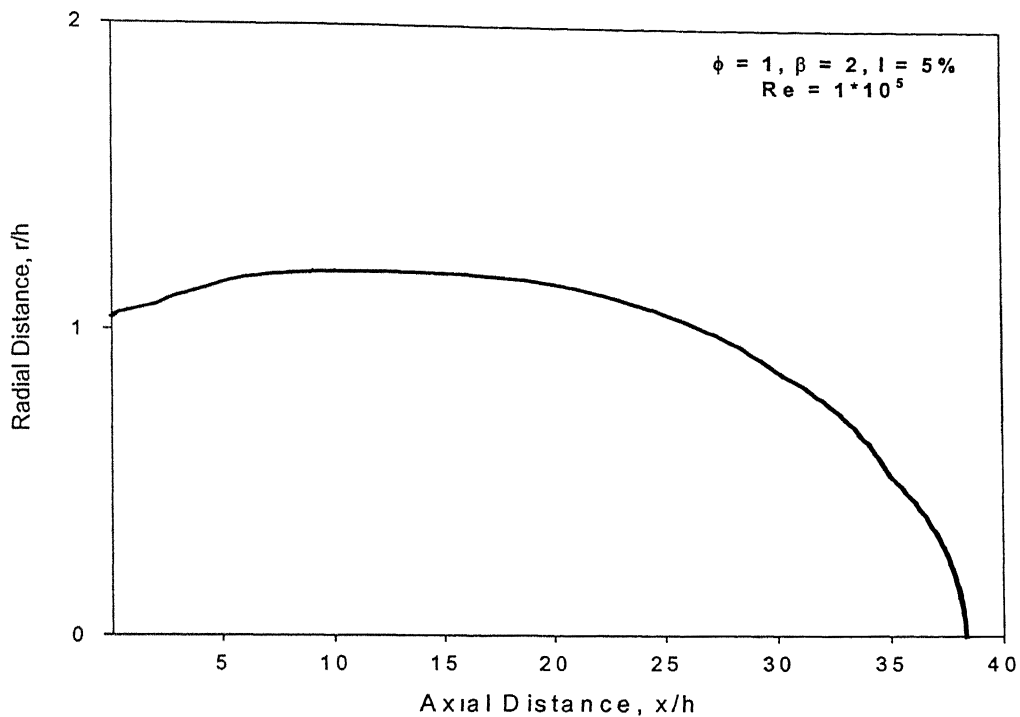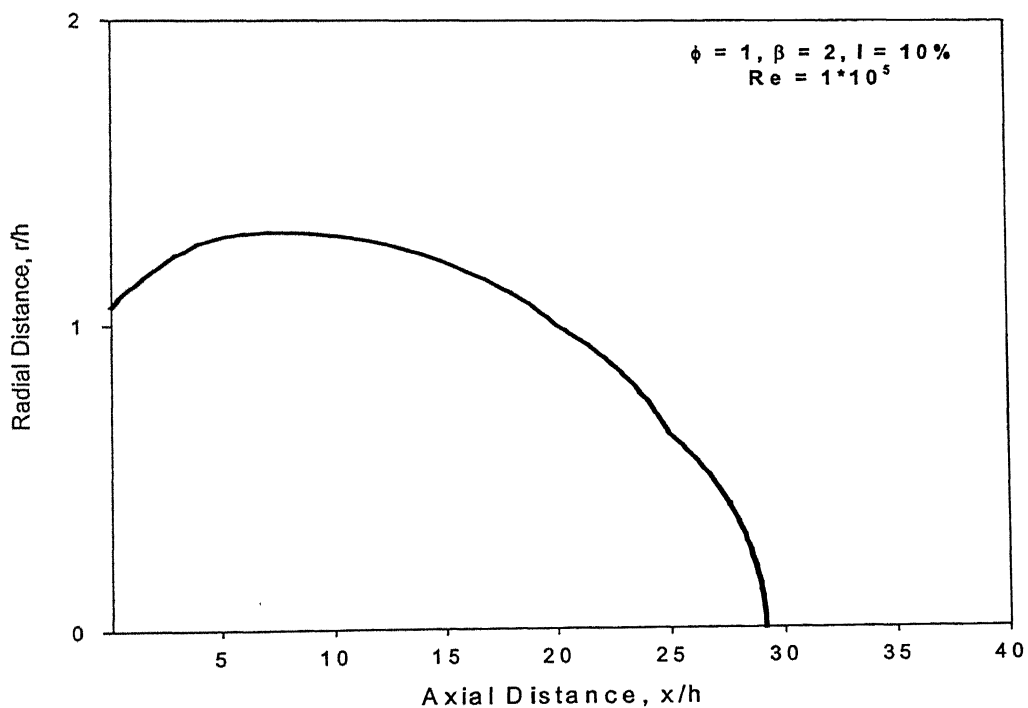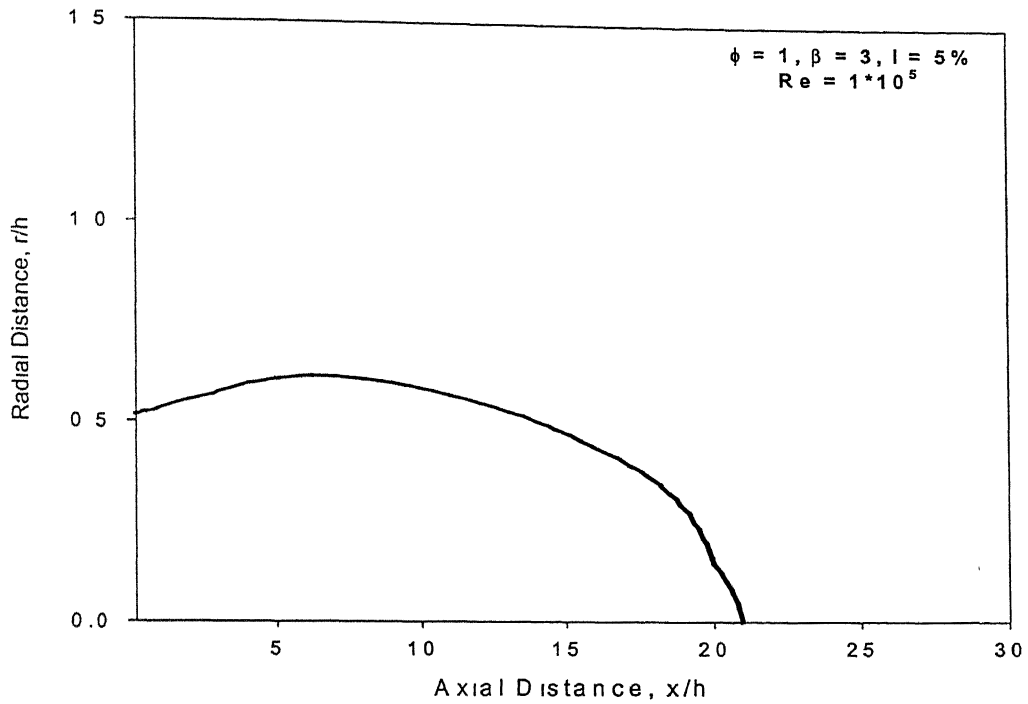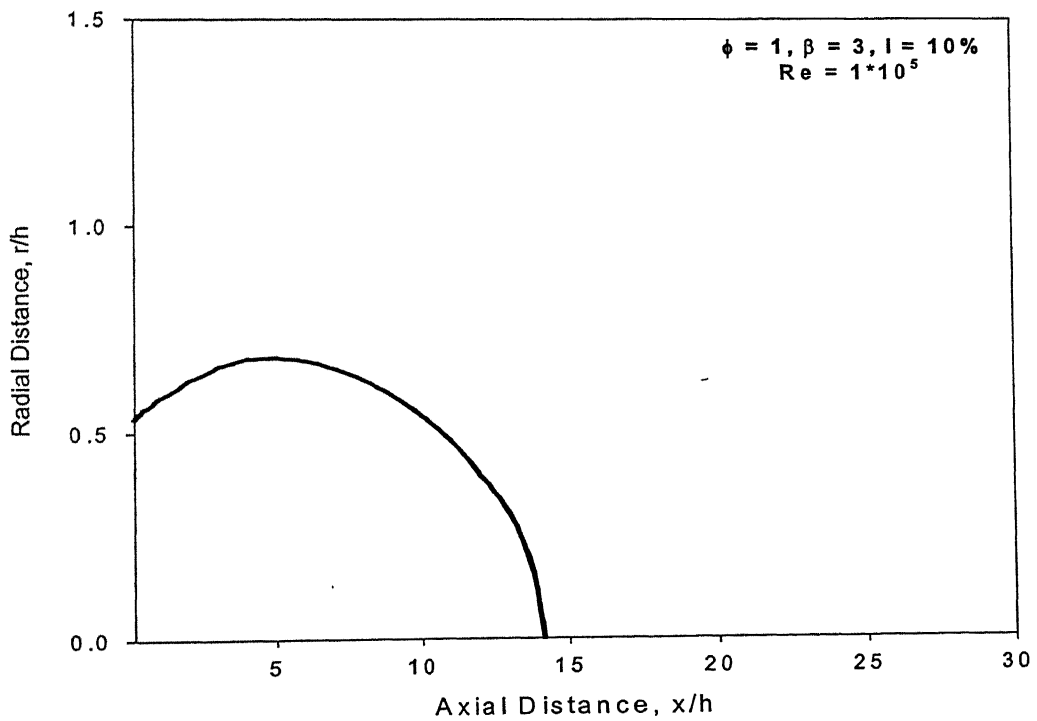**Fig. 5.38 Temperature contour showing Flame front for Expansion Ratio = 3, Equivalence Ratio = 1.00, Reynolds Number = 1×10^5, Turbulence Intensity = 10%**

Table.5.4 Variation in shape of the Flame with the Expansion Ratio and Turbulence Intensity for stoichiometric air-fuel ratio and Re = 1×10^5

Expansion Ratio, β	Turbulence Intensity, I (%)	Flame Length, x/h	Maximum Width of the Flame, r/h	Axial Distance of Maximum Width of the Flame, x/h
2	5	38.0	1.2	12.0
2	10	28.5	1.3	7 5
3	5	21.0	0.61	6.0
3	10	14.0	0.68	4.5

5.2.6 Turbulent Kinetic Energy

The turbulent kinetic energy variation for different equivalence ratios is studied in this section. Turbulent kinetic energy has been normalised by maximum kinetic energy encountered in the corresponding flow field. Only expansion ratio of 2 is considered for the analysis. Fig.5.39 and Fig.5.40 show the variation in turbulent kinetic energy for equivalence ratio of 0.50 at turbulent intensities 5% and 10% respectively. It is observed that maximum kinetic energy is in the shear layer region as in the cold flow case. Also in the reacting flow case, a high value of turbulent kinetic energy is observed through out the length of the combustor. Fig.5.41 and Fig.5.42 show the variation in turbulent kinetic energy for equivalence ratio of 0.75 at turbulent intensities 5% and 10% respectively. Fig.5.43 and Fig.5.44 show the variation in turbulent kinetic energy for equivalence ratio of 1.00 at turbulent intensities 5% and 10% respectively. A clear difference can be seen in the case of equivalence ratios 0.75 and 1.00 with equivalence ratio 0.50, that maximum kinetic energy is observed near the exit rather than in the shear layer. This may be due to, the high-energy supply to the fluid from the hotter combustion products at higher equivalence ratios.

Fig. 5.39 Normalised Turbulent Kinetic Energy contours for Expansion Ratio = 2, Equivalence Ratio = 0.50, Reynolds Number = 1×10⁵, Turbulence Intensity = 5%

Fig. 5.40 Normalised Turbulent Kinetic Energy contours for Expansion Ratio = 2, Equivalence Ratio = 0.50, Reynolds Number = 1×10⁵, Turbulence Intensity = 10%
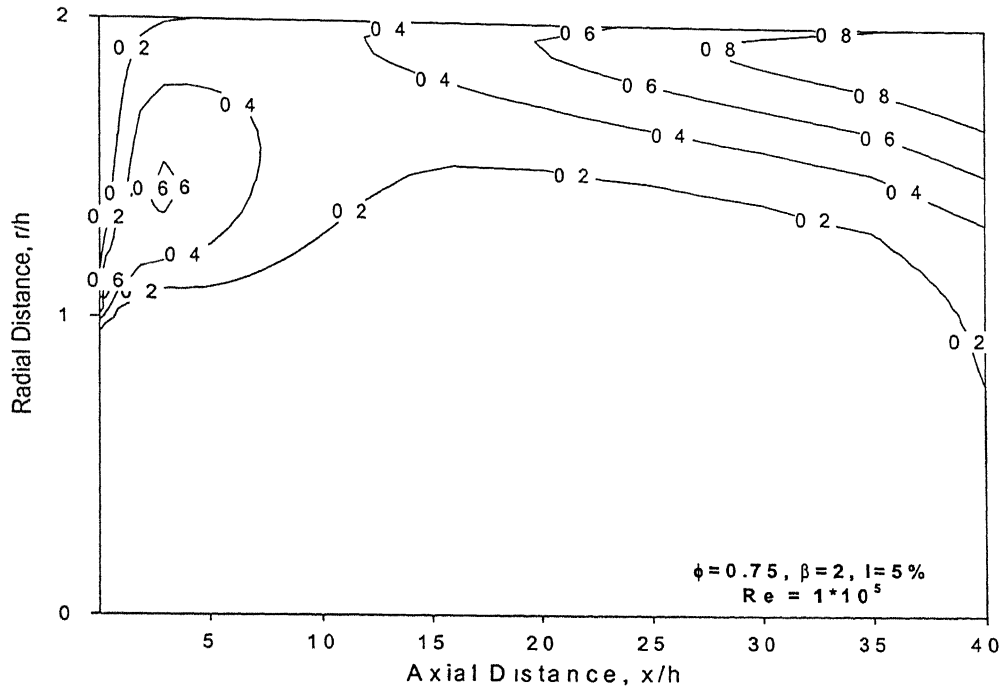
Fig. 5.41 Normalised Turbulent Kinetic Energy contours for Expansion Ratio = 2, Equivalence Ratio = 0.75, Reynolds Number = 1×10⁵, Turbulence Intensity = 5%

Fig. 5.42 Normalised Turbulent Kinetic Energy contours for Expansion Ratio = 2, Equivalence Ratio = 0.75, Reynolds number = 1×10⁵, Turbulence Intensity = 10%

Fig. 5.43 Normalised Turbulent Kinetic Energy contours for Expansion Ratio = 2, Equivalence Ratio = 1.00, Reynolds Number = 1×10⁵, Turbulence Intensity = 5%

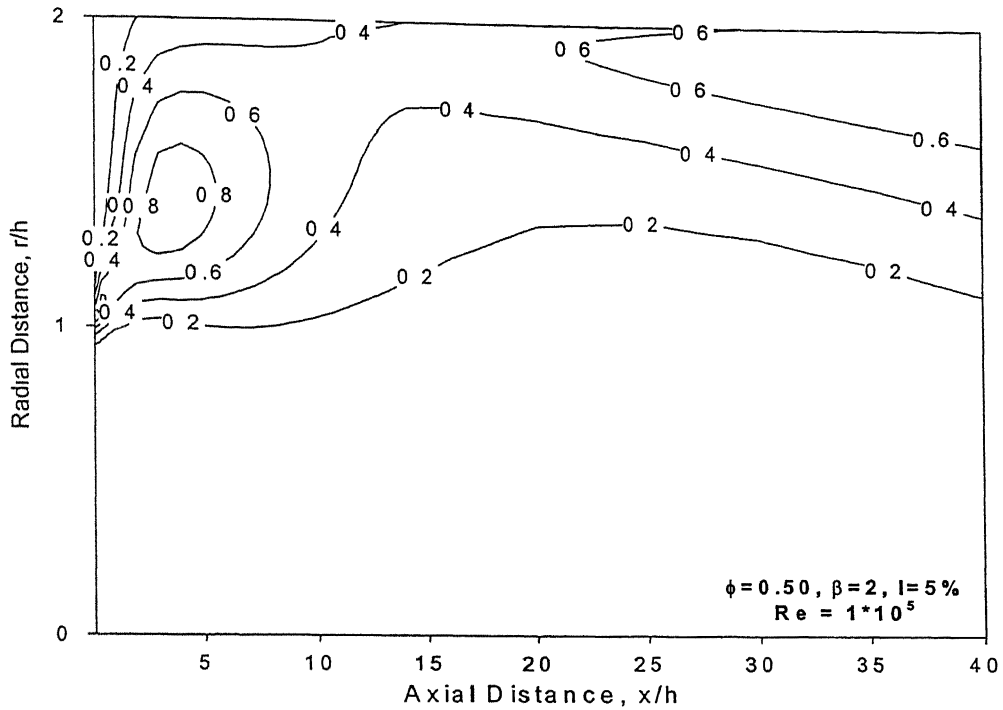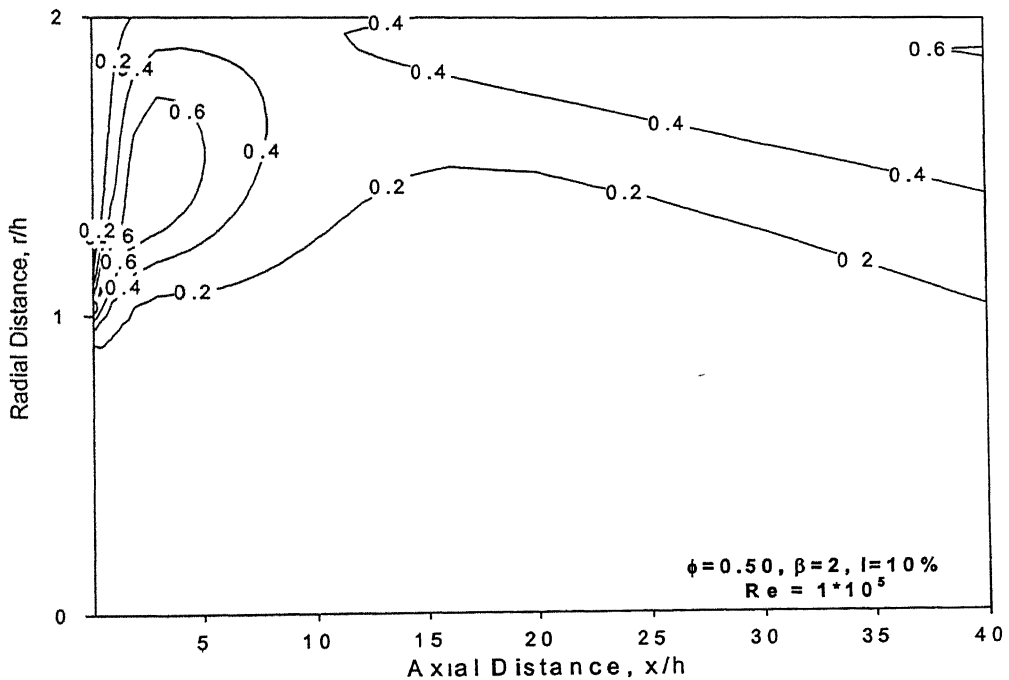**Fig. 5.44 Normalised Turbulent Kinetic Energy contours for Expansion ratio = 2, Equivalence Ratio = 1.00, Reynolds Number = 1×10⁵, Turbulence Intensity = 10%**
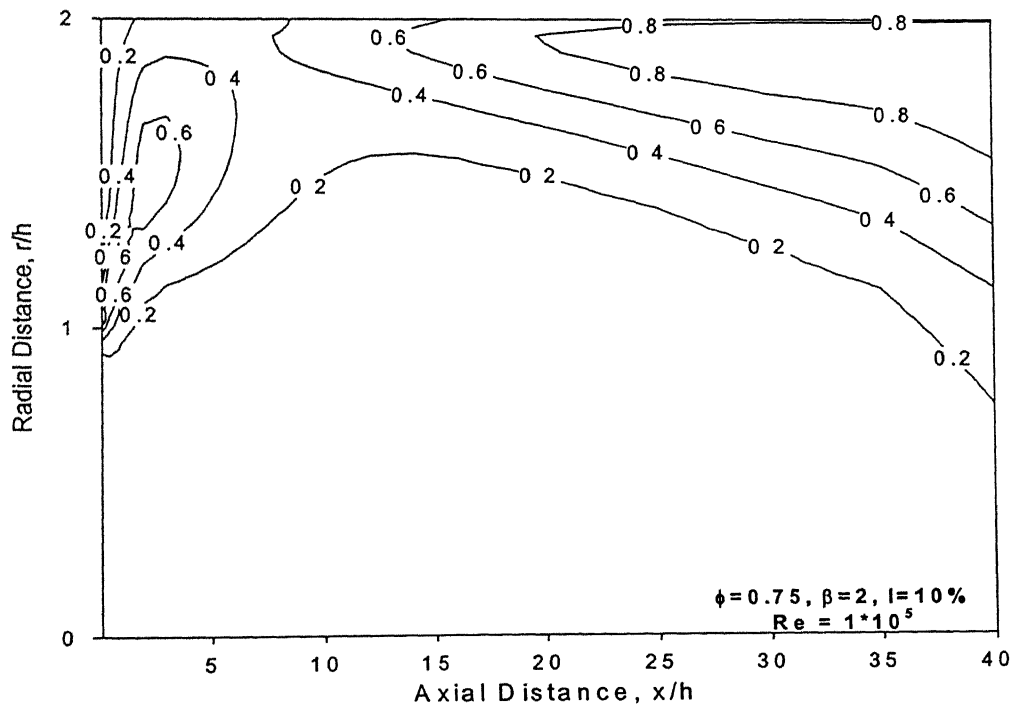
5.2.7 Turbulent Dissipation Rate

The turbulent dissipation rate at different equivalence ratios is investigated. Turbulent dissipation has been normalised by maximum turbulent dissipation rate encountered in the corresponding flow field. The maximum turbulent diffusion occurs in the shear layer as in the cold flow case. The same amount of significant turbulent diffusion occurs also near the wall, particularly near the exit of the combustor. This phenomenon is quite clear from Fig.5.45 and Fig.5 46, which show the turbulent dissipation rate for an equivalence ratio of 0.50 at turbulent intensities 5% and 10% respectively. Fig.5.47 and Fig.5.48 show the variation in turbulent diffusion rate for equivalence ratio of 0.75 at turbulent intensities 5% and 10% respectively. Fig.5.49 and Fig.5.50 show the variation in turbulent diffusion rate for equivalence ratio of 1.00 at turbulent intensities 5% and 10% respectively.

Fig. 5.45 Normalised Turbulent Dissipation Rate contours for Expansion Ratio = 2, Equivalence Ratio = 0.50, Reynolds Number = 1×10^5, Turbulence Intensity = 5%
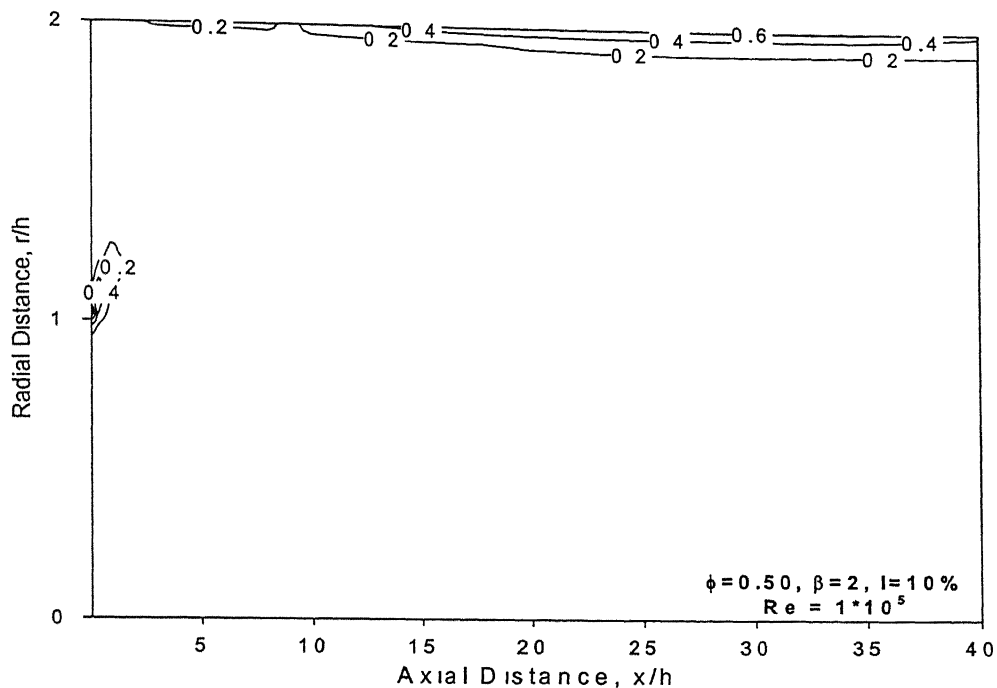
Fig. 5.46 Normalised Turbulent Dissipation Rate contours for Expansion Ratio = 2, Equivalence Ratio = 0.50, Reynolds Number = 1×10^5, Turbulence Intensity = 10%
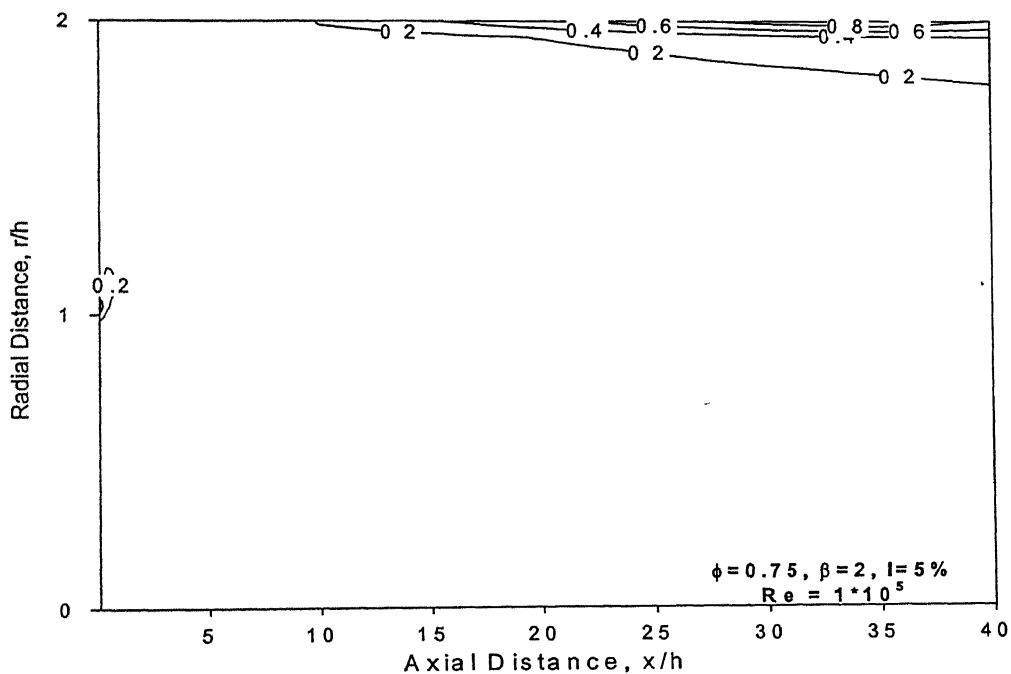
Fig. 5.47 Normalised Turbulent Dissipation Rate contours for Expansion Ratio = 2, Equivalence Ratio = 0.75, Reynolds Number = 1×10^5, Turbulence Intensity = 5%
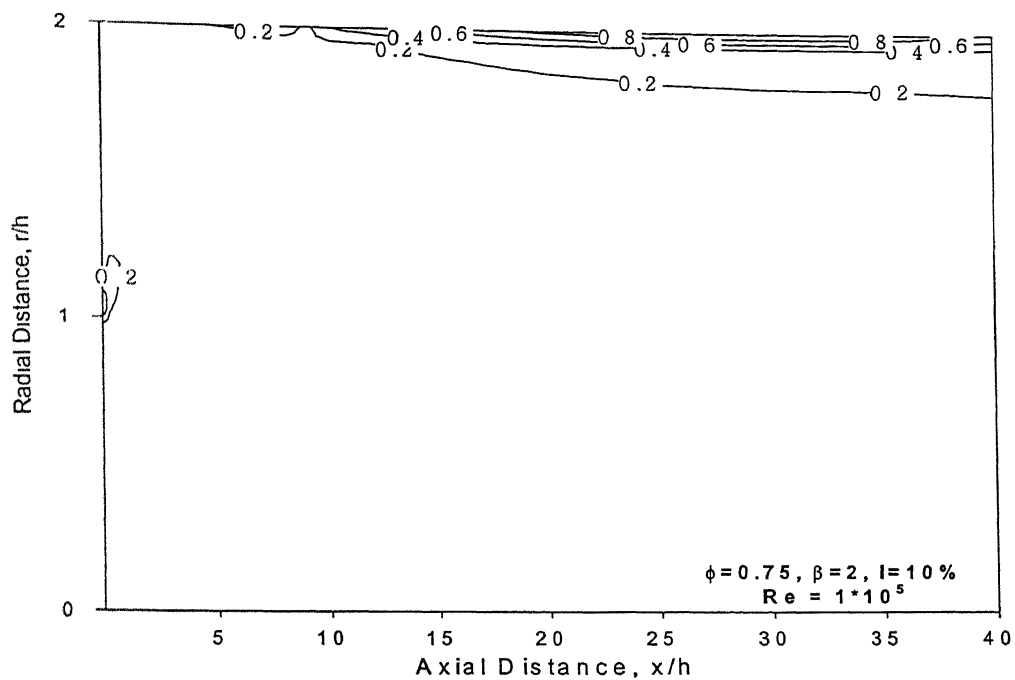
Fig. 5.48 Normalised Turbulent Dissipation Rate contours for Expansion Ratio = 2, Equivalence Ratio = 0.75, Reynolds Number = 1×10⁵, Turbulence Intensity = 10%
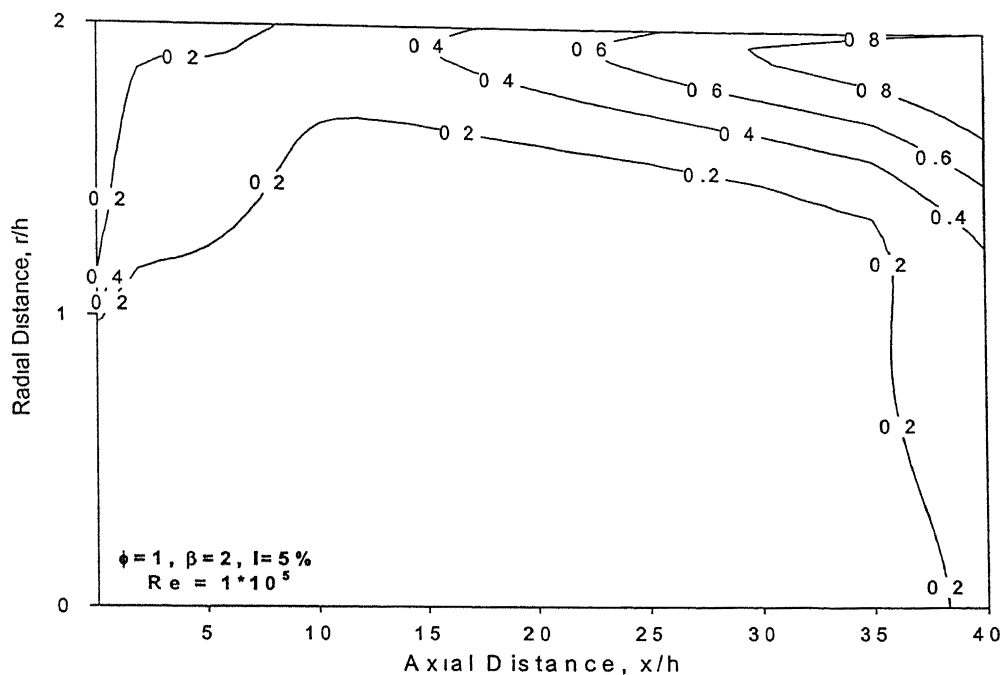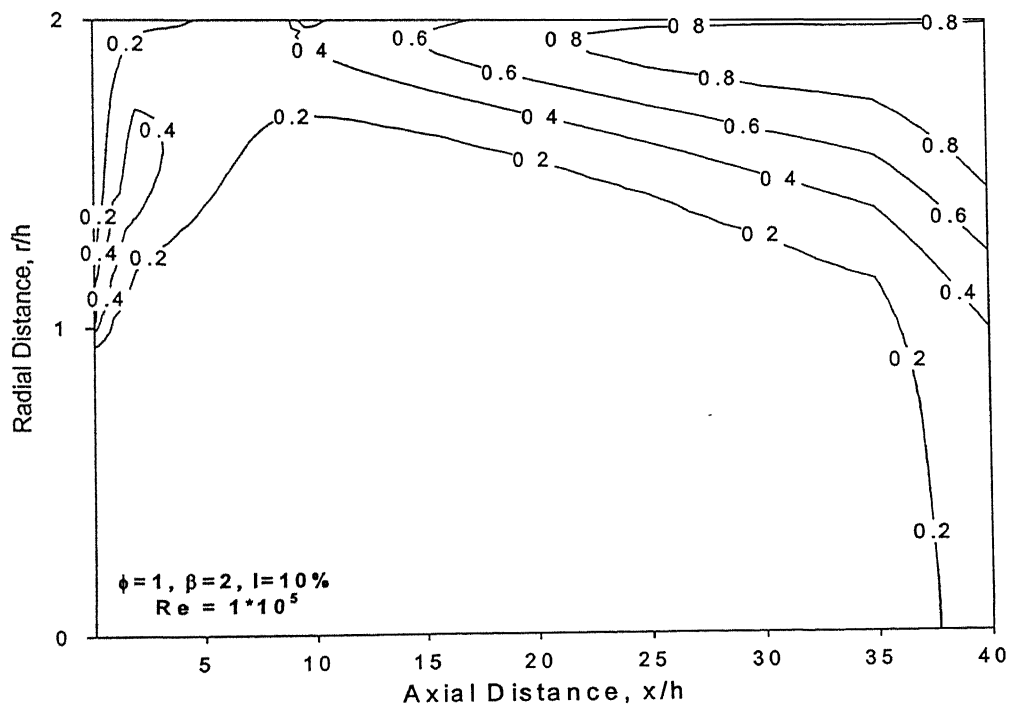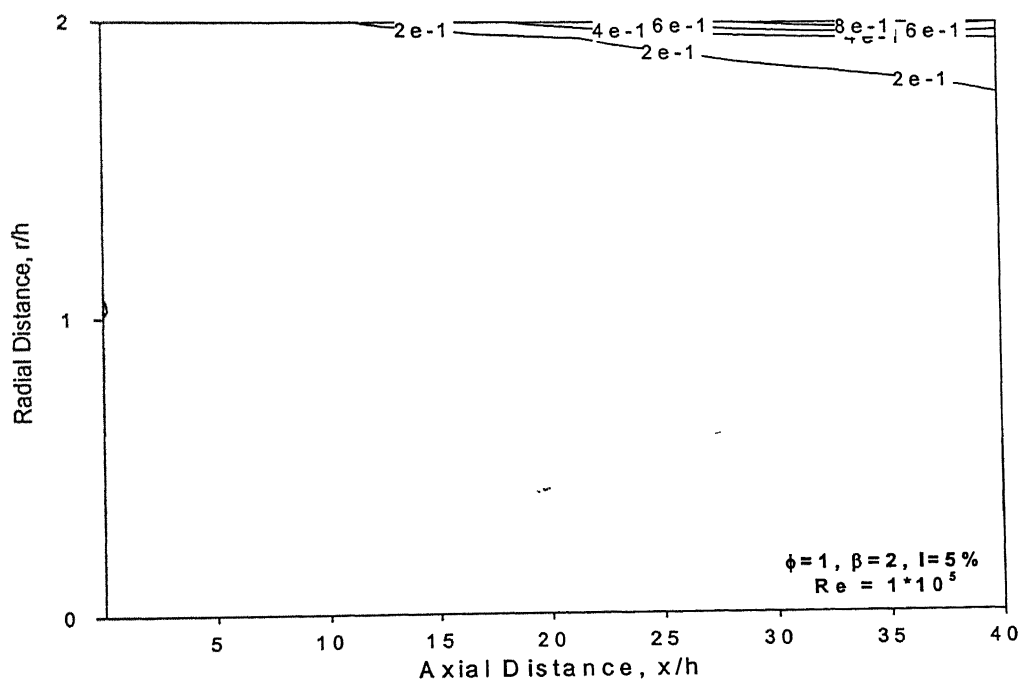

Fig. 5.49 Normalised Turbulent Dissipation Rate contours for Expansion Ratio = 2, Equivalence Ratio = 1.00, Reynolds Number = 1×10⁵, Turbulence Intensity = 5%
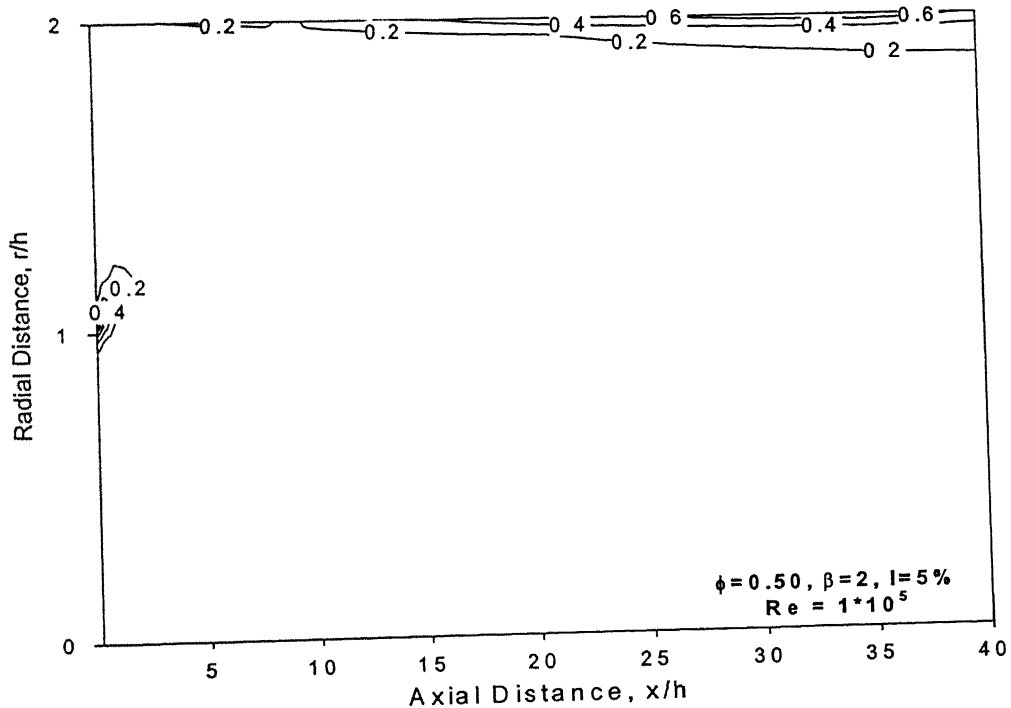
109
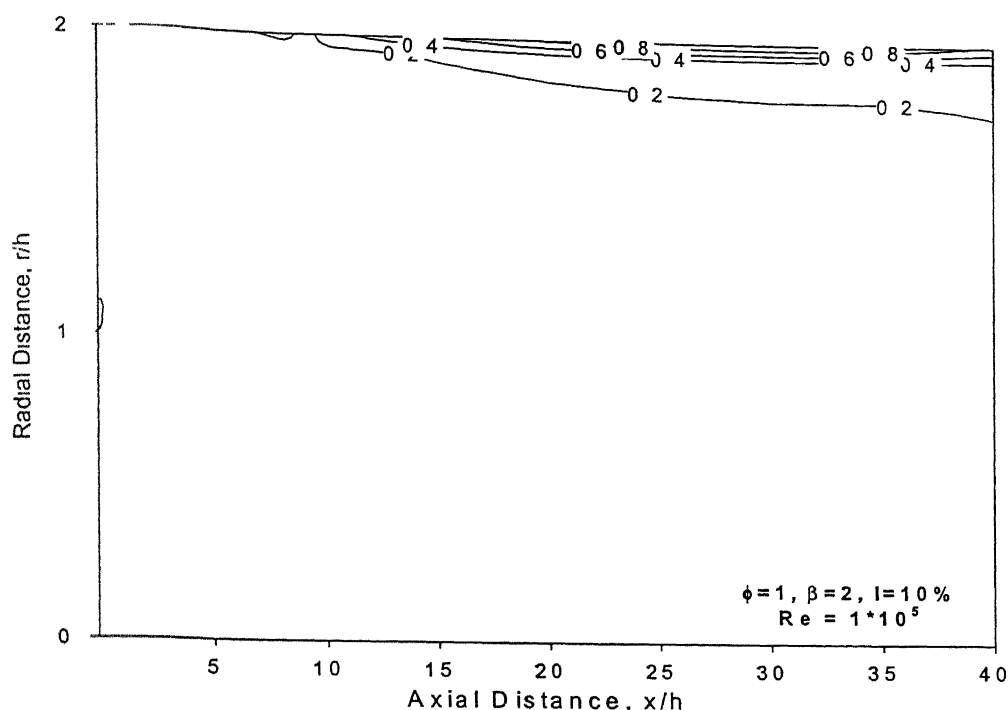
Fig. 5.50 Normalised Turbulent Dissipation Rate contours for Expansion Ratio = 2, Equivalence Ratio = 1.00, Reynolds Number = 1×10^5, Turbulence Intensity = 10%

5.2.8 Species Mass Fraction

In this section, the variation in species mass concentration within the flowfield with the equivalence ratio is investigated. Three species namely C_3H_8, O_2 and CO_2 are considered for the analysis. Fig.4.51 and 4.52 shows the mass fraction contours of C_3H_8 for equivalence ratio 0.50 and 1.00 respectively. It is found that as the distance from the dump plane increases, the mass fraction of C_3H_8 decreases. Also a decrease is found in the radial direction near the dump plane. Maximum mass concentration is found in the potential core due to the lack of combustion, where the same concentration of reactants at the inlet is almost maintained. The same trend is observed in the contours of mass fraction of O_2, in Fig.4.53 and Fig.4.54 for equivalence ratio 0.50 and 1.00 respectively. Exactly opposite trend is found in the case of CO_2 mass fraction, with a minimum in the non-burning potential core and maximum in the regions where the products are already formed. This can be noted from Fig.4.55 and Fig.4.56, which show the contours of mass fraction of CO_2 for equivalence ratio 0.50 and 1.00 respectively.

110
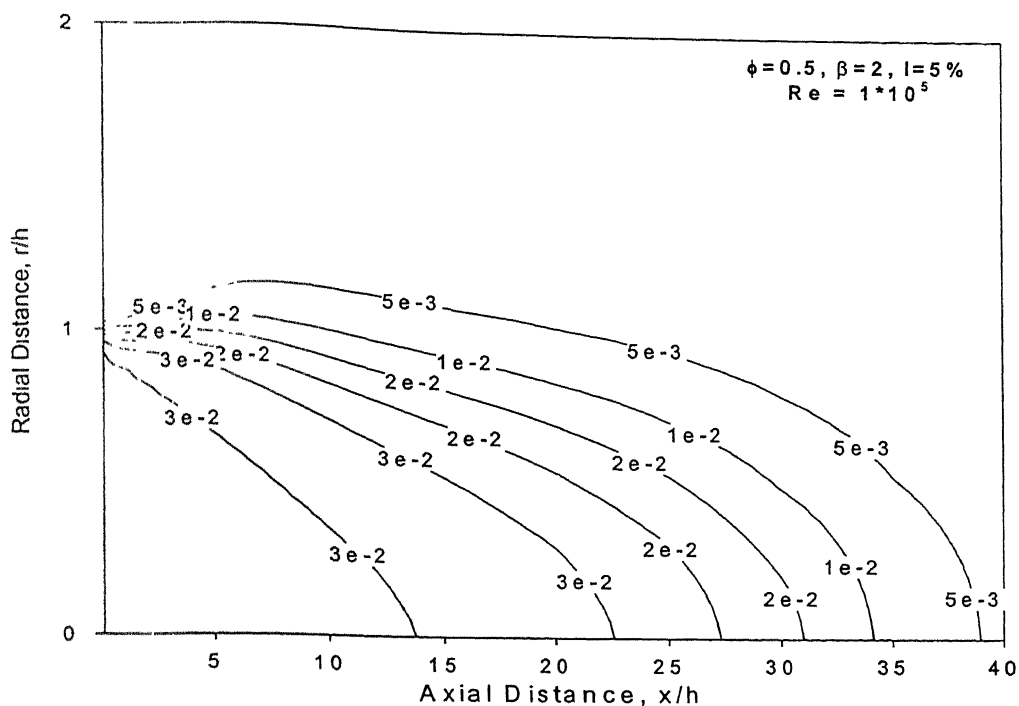
Fig. 5.51 Mass Fraction contours of C₃H₈ for Expansion Ratio = 2, Equivalence Ratio = 0.50, Reynolds Number = 1×10⁵, Turbulence Intensity = 5%
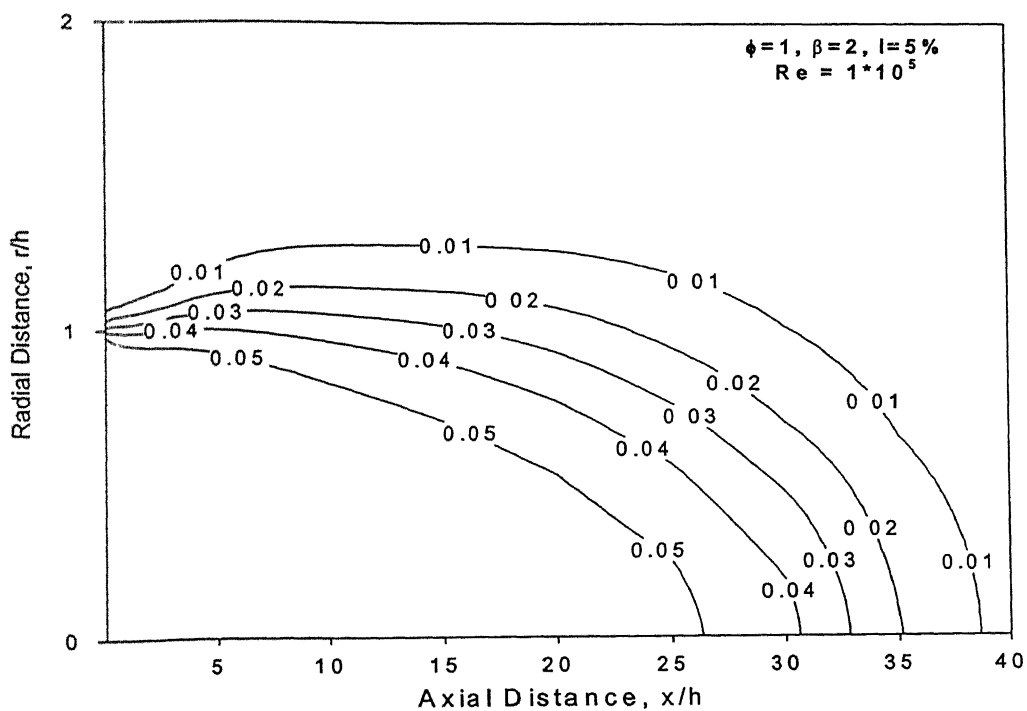
Fig. 5.52 Mass Fraction contours of C₃H₈ for Expansion Ratio = 2, Equivalence Ratio = 1.0, Reynolds Number = 1×10⁵, Turbulence Intensity = 5%

111
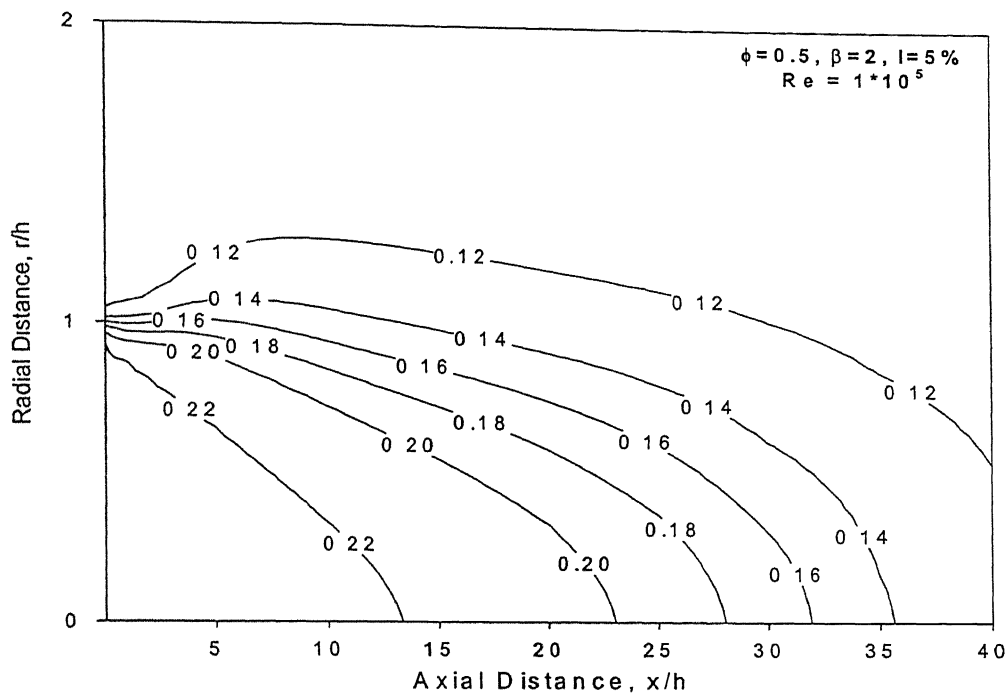
Fig. 5.53 Mass Fraction contours of O_2 for Expansion Ratio = 2, Equivalence Ratio = 0.50, Reynolds Number = 1×10^5, Turbulence Intensity = 5%
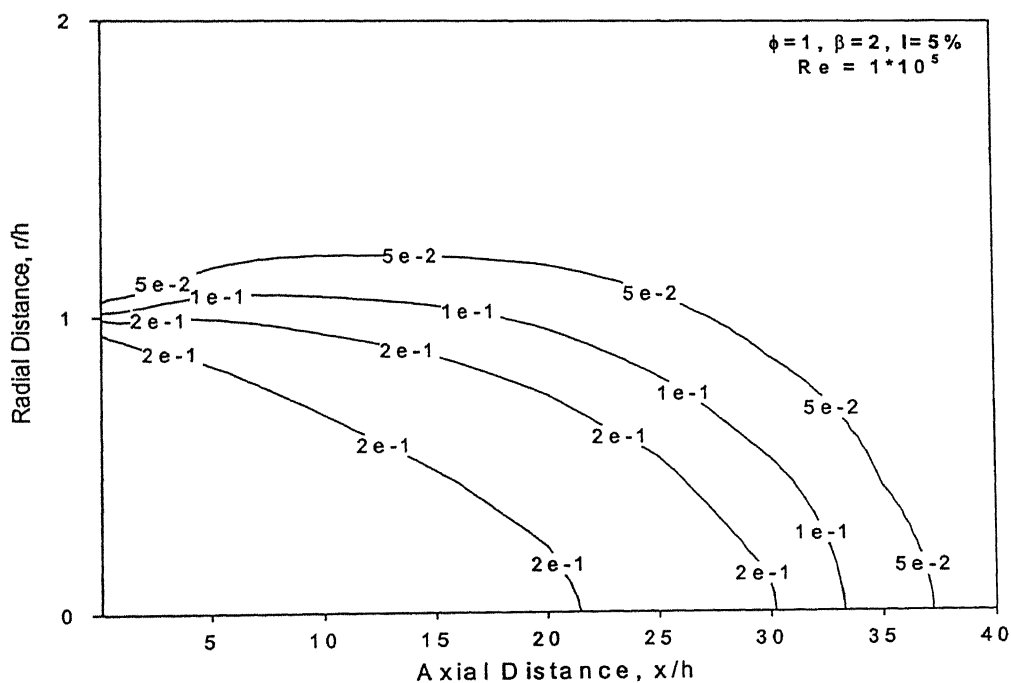
Fig. 5.54 Mass Fraction contours of O_2 for Expansion Ratio = 2, Equivalence Ratio = 1.0, Reynolds Number = 1×10^5, Turbulence Intensity = 5%
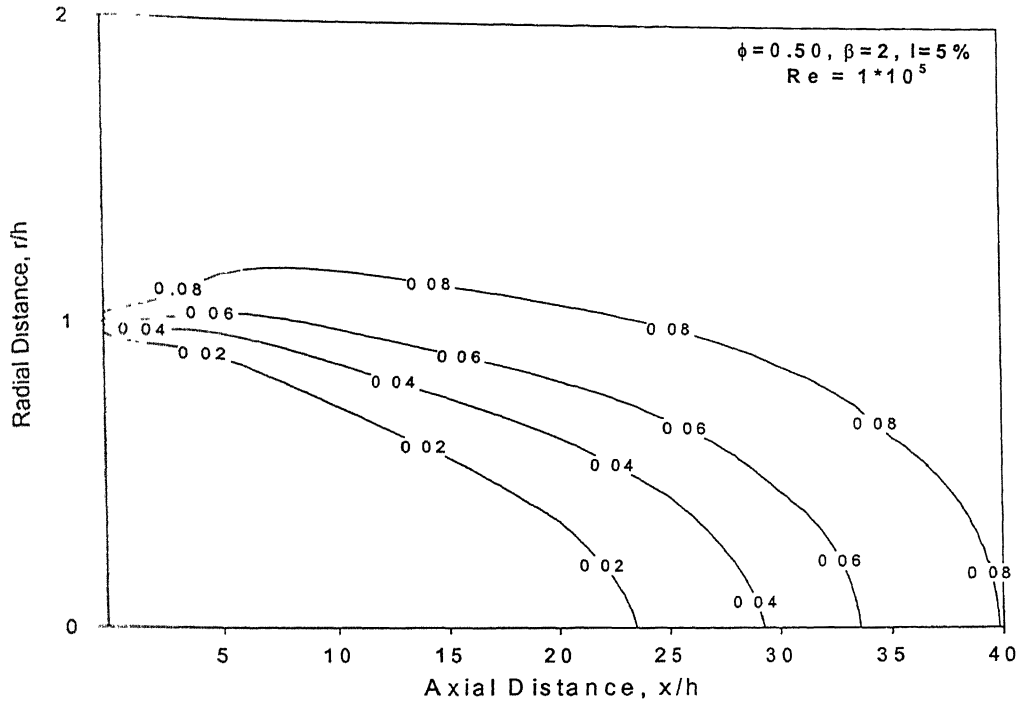
Fig. 5.55 Mass Fraction contours of CO_2 for Expansion Ratio = 2, Equivalence Ratio = 0.50, Reynolds Number = 1×10^5, Turbulence Intensity = 5%
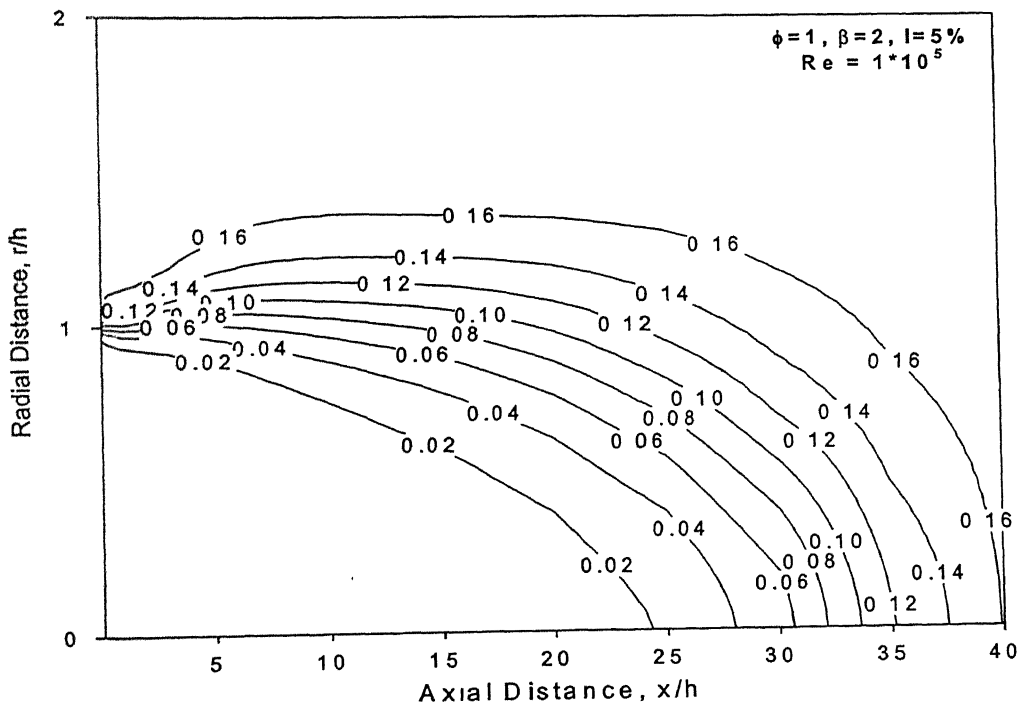
Fig. 5.56 Mass Fraction contours of CO_2 for Expansion Ratio = 2, Equivalence Ratio = 1.0, Reynolds Number = 1×10^5, Turbulence Intensity = 5%

5.3 Comparison of Cold and Reacting Flow

In this section a comparison between cold and reacting flowfield is made. Fig.5.57 shows the variation in centerline axial velocity for cold and reacting flow case for expansion ratio 2 at Reynolds number 1×10^5. Within the potential core, the axial velocities of both the cold and reacting flow are same due to the lack of combustion in the high-speed region. Hence the inlet temperature is maintained within this region. After the potential core there is a sudden increase in the centerline axial velocity of the reacting flow due to the energy supply from the combustion products, and a sudden decrease in cold flow centerline velocity. Fig.5.58 shows the variation in reattachment length, RL, for cold and reacting flow case for expansion ratio 2 at Reynolds number 1×10^5.
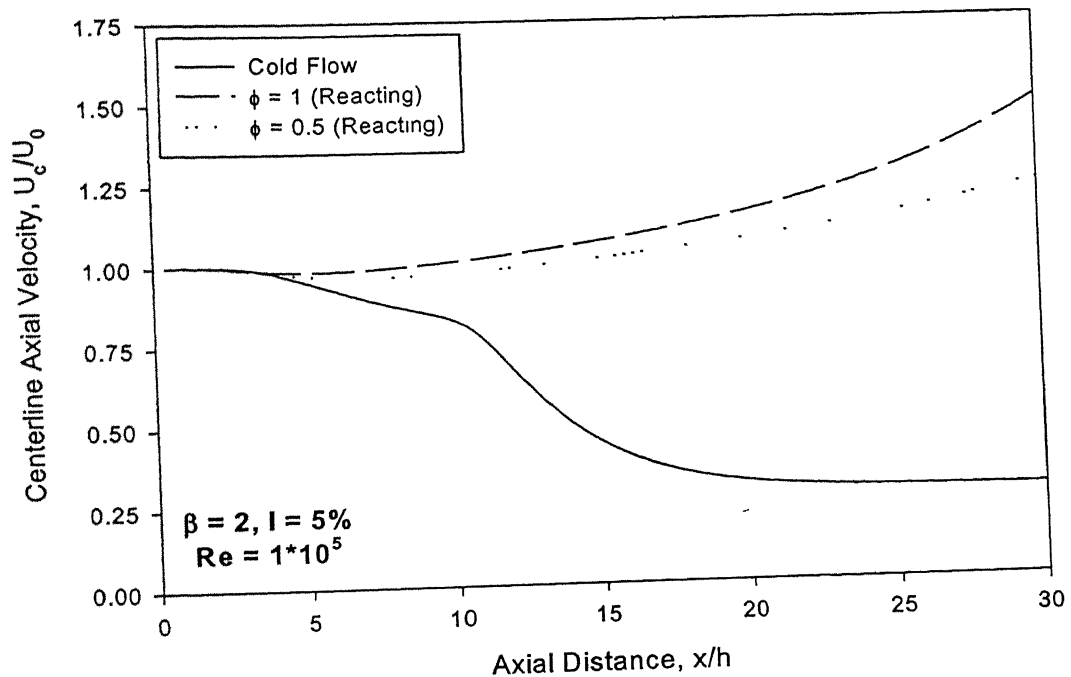
Fig.5.57 Comparison between Cold and Reacting flow Centerline Axial Velocity at Expansion Ratio = 2, Reynolds Number = 1×10^5, Turbulence Intensity = 5%

114
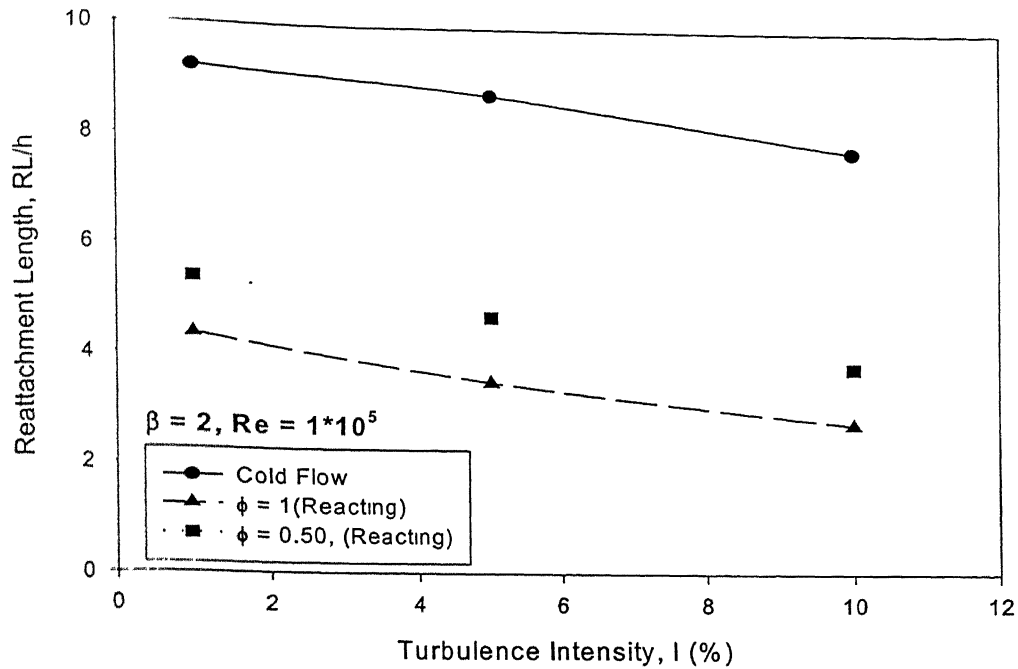
Fig.5.58 Comparison between Cold and Reacting flow Reattachment length at Expansion Ratio = 2, Reynolds Number = 1×10^5

Table.5.5 Comparison between Cold and Reacting flow reattachment Length at Expansion ratio =2, Reynolds Number = 1×10^5

Type of flow	Reattachment Length					
	I = 1%		I = 5%		I = 10%	
	x / h	% Reduction with Cold Flow	x / h	% Reduction with Cold Flow	x / h	% Reduction with Cold Flow
Cold	9.22	-	8.79	-	7.80	-
ϕ = 1.00	4.36	52.7	3.52	59.9	2.76	64.6
ϕ = 0.75	4.80	47.9	4.05	53.9	3.15	59.6
ϕ = 0.50	5.39	41.51	4.71	46.3	3.81	51.1

115

The reattachment lengths for Reynolds number 1×10^5 and expansion ratio 2, obtained from the present calculation have presented in Table.5.5. There is a huge reduction in reattachment length in the reacting flow case as compared to the cold flow case. This reduction is quite significant at higher inlet turbulence intensities and at higher equivalence ratios. A maximum reduction of 64.6% is observed in the case of I=10%, ϕ=1.00 with an expansion ratio of 2, where as a minimum of 41.51% reduction is observed in the case of I=1%, ϕ=0.50 for the same expansion ratio.

Comparing Table.4.2 and Table.5.1, it is found that the reacting flow has not much influence on the negative axial velocity within the recirculation region. However comparing Table.4.3 and Table.5.2, for radial velocity, it can be noted that reacting flow has a significant influence on the radial velocity both in the shear layer and the recirculation zone. Compared to the cold flow case, both the maximum and minimum radial velocities are almost twice the magnitude for the reacting flow. This will make the resultant velocity within the recirculation zone much higher than that of cold flow case, which might be the reason for the shorter reattachment length in the reacting flow case.

Observing the turbulent kinetic energy contours for both the cold and reacting flow, it is found that for the reacting flow, the maximum kinetic energy is in the shear layer region as in the cold flow case. However, in the cold flow case the turbulent kinetic energy almost disappeared halfway through the combustor. But in the reacting flow case, a high value of turbulent kinetic energy is observed through out the length of the combustor. Observing the turbulent dissipation rate contours for both the cold and reacting flow, the maximum turbulent diffusion for the reacting flow occurs in the shear layer as in the cold flow case. But a noticeable difference observed in the reacting flow case compared to cold flow case is that same amount of significant turbulent diffusion occurs also near the wall, particularly near the exit of the combustor.

5.4 Concluding Remarks

An extensive numerical study on the reacting flow inside a dump combustor, used in ramjet combustors has been made in this chapter. Highly turbulent flow field inside the combustor is solved using k-ε turbulence model. The reacting flow has been modelled

using fast chemistry Eddy Dissipation Concept (EDC). Results were compared with experimental results for the validation of the code. Several flow quantities governing the overall flowfield such as axial velocity, radial velocity, static temperature, turbulent kinetic energy and turbulent dissipation rate have been considered in this reacting flow study. A brief study on species mass fraction within the flowfield is also made. Various flow parameter such as inlet turbulence intensity and geometrical parameter such as expansion ratio along with the overall equivalence ratio have been varied to find out the influence of each on the above said flow quantities. Effect of each of these parameters on recirculation size, which is an important parameter determining the flowfield, is also investigated. It is found out that the axial velocities and the radial velocities within the flowfield are many times as compared to the cold flow case due to the heat release and volumetric expansion. The reattachment length for the reacting case is found to be lower than that of the cold flow cases due to higher recirculation velocities. A maximum reduction of 64.6% compared to the cold flow reattachment length is observed in the case of I=10%, ϕ=1.00 with an expansion ratio of 2, where as a minimum of 41.51% reduction is observed in the case of I=1%, ϕ=0.50 for the same expansion ratio. This reduction is quite significant at higher inlet turbulence intensities and at higher equivalence ratios. In the cold flow case only the turbulence intensity is the major factor governing the flowfield, but in the reacting flow case, overall equivalence ratio also plays a dominant role. The turbulent kinetic energy and turbulent dissipation rate are found maximum in the shear layer. However, a high value of turbulent kinetic energy is observed through out the length of the combustor. Also it is found that significant turbulent diffusion occurs also near the wall, particularly near the exit of the combustor.

5.5 Suggestions For Future Work

The following investigations may be suggested for the future work.

1. The predictions can be done using the Reynolds Stress Model (RSM) for modelling the turbulence.
2. Wall function approach used to solve near wall viscous sublayer, can be replaced with Near-Wall model approach, where the near wall viscous sublayer is resolved all the way down to the wall.

117

3. Eddy Dissipation Concept used in the present study to model reacting flow can be substituted with Arrhenius rate expressions.
4. Bluff body can be incorporated in the domain for better flame stability.
5. The effect of emission level can be explored.
6. The realistic heat transfer model can be incorporated.
7. The reacting flow needs more attention.

REFERENCES

1. Anderson, D. A., Tannehill, J. C. and Pletcher, R. H., *Computational Fluid Mechanics and Heat Transfer*, Hemisphere Publishing Corporation, 1984

2. Back, L. H. and Roschke, E. J., "Shear-Layer Flow Regimes and Wave Instabilities and Reattachment Length Downstream of an Abrupt Circular Channel Expansion", *Journal of Applied mechanics*, Transactions of the ASME, September 1972, pp. 677-681

3. Bird, R. B., Stewart, W. E. and Lightfoot, E. N., *Transport Phenomena*, John Wiley & Sons, 1994

4. De Zilwa, S. R. N., Khezzar, L. and Whitelaw, L. H., "Flows Through Plane Sudden-expansions", *International Journal for Numerical methods in Fluids*, 32, 2000, pp. 313-329

5. Drewry, J. E., "Fluid Dynamic Characterization of Sudden Expansion Ramjet Combustor Flow Fields", *AIAA Journal*, Vol. 16, No. 4, April 1978, pp. 313-319

6. Durret, R. P., Stevenson, W. H. and Thompson, H. D., "Radial and Axial Turbulent Flow Measurements With an LDV in an Axisymmetric Sudden Expansion Air Flow", *Journal of Fluids Engineering*, Transactions of the ASME, Vol. 110, December 1988, pp. 367-372

7. FLUENT 5 Users Guide, Fluent Incorporated, 1998

8. Freitas, C. J., "Perspective: Selected Benchmarks From Commercial CFD Codes", *Journal of Fluids Engineering*, Transactions of the ASME, Vol.117, June 1995, pp. 208-218

9. Gabruk, R. S. and Roe, L. A., "Velocity Characteristics of Reacting and Non Reacting Flows in a Dump Combustor", *Journal of propulsion and power*, Vol. 10, No. 2, March- April 1994, pp. 148-154

10. Ghoshdastidar, P. S., *Computer Simulation of Flow and Heat transfer*, Tata McGraw-Hill, 1998

11. Gould, R. D., Stevenson, W. H. and Thompson, H. D., "Investigation of Turbulent Transport in an Axisymmetric Sudden Expansion", *AIAA Journal*, Vol. 28, No. 2, February 1990, pp. 276-283

12. Gould, R. D., Stevenson, W. H. and Thompson, H. D., "Simultaneous Velocity and Temperature Measurements in a Premixed Dump Combustor", *Journal of propulsion and power*, Vol. 10, No. 5, Sept.- Oct. 1994, pp. 639-645

13. Gran, I. R., Ertesvag, I. S. and Magnussen, B. F., "Influence of Turbulence Modelling on Predictions of Turbulent Combustion", *AIAA Journal*, Vol. 35, No. 1, January 1997, pp. 106-110

14. Jang, D. S., "Numerical Calculation of Reattachment Length in Axisymmetric Sudden Expansion Flows", *Fluids Engineering Korea-U. S. Progress*, Hemisphere Publication Corporation, 1991, pp. 143-148

15. Jaw, S. Y. and Chen, C. J., "Present Status of Second Order Closure Models. I: Overview", *Journal of Engineering Mechanics*, Vol.124, No.5, May 1998, pp. 485-501

16. Jaw, S. Y. and Chen, C. J., "Present Status of Second Order Closure Models. II: Applications", *Journal of Engineering Mechanics*, Vol.124, No.5, May 1998, pp. 502-511

17. Kalinske, A. A., "Conversion of Kinetic to Potential Energy in Flow Expansion", *Proceedings of the ASCE*, Vol. 70, 1944, pp. 1545-1564

18. Kangovi, S. and Page, R. H., "Subsonic Turbulent Flow Past a Downstream Facing Annular Step", *Journal of Fluids Engineering*, Transactions of the ASME, Vol. 101, June 1979, pp. 230-236

19. Kuo, K. K., *Principles of Combustion*, John Wiley & Sons, 1986

20. Launder, B. E. and Spalding, D. B., *Lectures in Mathematical Models of Turbulence*, Academic Press, London, England, 1972

21. Lipstein, N. J., *A.S.H.R.A.E. Journal*, Vol. 4, 1962, pp.43-47

22. Lu, C. C., "Measurements of Turbulent Flow Velocity for Sudden Expansion Cylindrical Tube using Laser Doppler Velocimeter (LDV)", *AIChE Journal*, Vol. 26, No. 2, March 1980, pp. 303-305

23. Magnussen, B. F. and Hjertager, B. H., "On Mathematical Models of Turbulent Combustion with Special Emphasis on Soot Formation and Combustion", *Sixteenth Symposium (International) on Combustion*, The Combustion Institute, 1976

24. Mishra, D. P., "Computational Studies of Stretch Effects in Spherical Premixed Flames", PhD Thesis Report, IISc., Bangalore, 1994

25. Moon, L. F. and Rudinger, G., "Velocity Distribution in an Abruptly Expanding Circular Duct", *Journal of Fluids Engineering*, Transactions of the ASME, March 1977, pp. 226-230

26. Natarajan, R., Sundararajan, T. and Ganesan, V., "Investigations of Multi-Phase Jet Mixing and Combustion in a Dump Combustor", Project No. MEE/94-95/095/ARDB/RNAT, Closure Report, IIT Madras, June 2000

27. Patankar, S. V., *Numerical Heat Transfer and Fluid Flow*, Hemisphere Publishing Corporation, 1980

28. Spalding, D. B., "Mixing and Chemical Reaction in Steady Confined Turbulent Flames", *Thirteenth Symposium (International) on Combustion*, The Combustion Institute, 1970

29. So, R. M. C., "Inlet Centerline Turbulence Effects on Reattachment Length in Axisymmetric Sudden Expansion Flows", *Experiments in Fluids*, Volume. 5, 1987, pp.424-430

30. So, R. M. C. and Ahmed, S. A., "Effects on Axisymmetric Sudden Expansion Flows", *Journal of Propulsion and Power*, Volume 4, Number 3, 1988, pp.270-274

31. So, R. M. C. and Ahmed, S. A., "Characteristics of Dump Combustor Flows", *International journal of Heat and Fluid Flow*, Volume 10, No. 1, 1989, pp. 60-64

32. Teyssandier, R. G. and Wilson, M. P., "An Analysis of Flow Through Sudden Enlargements in Pipes", *Journal of Fluid Mechanics*, Vol. 64, Part 1, 1974, pp. 85-95

33. Ward-Smith, A. J., *Internal fluid flow*, Clarendon Press, 1980

34. Yang, B. T. and Yu, M. H., "The Flowfield in a Suddenly Enlarged Combustion Chamber", *AIAA Journal*, Vol. 21, No. 1, January 1983, pp. 92-97

35. Yuan, S. W., *Foundations of Fluid Mechanics*, Prentice-Hall, 1967

36. Zemanick, P. P. and Dougall, R. S., "Local Heat Transfer of Abrupt Circular Channel Expansion", *Journal of Heat Transfer*, Transactions of the ASME, February 1970, pp. 53-60